SMAI-JCM
SMAI Journal of Computational Mathematics

The topological ligament in shape optimization: a connection with thin tubular inhomogeneities

Charles Dapogny

Volume 7 (2021), p. 185-266.

<http://smai-jcm.centre-mersenne.org/item?id=SMAI-JCM_2021__7__185_0>

Publication membre du
Centre Mersenne pour l'édition scientifique ouverte
http://www.centre-mersenne.org/

Soumission sur https://smai-jcm.centre-mersenne.org/ojs/submission

SMAI Journal of Computational Mathematics
Vol. 7, 185-266 (2021)

The topological ligament in shape optimization: a connection with thin tubular inhomogeneities

Charles Dapogny [1]

[1] Univ. Grenoble Alpes, CNRS, Grenoble INP, LJK, 38000 Grenoble, France.
E-mail address: charles.dapogny@univ-grenoble-alpes.fr.

Abstract. In this article, we propose a formal method for evaluating the asymptotic behavior of a shape functional when a thin tubular ligament is added between two distant regions of the boundary of the considered domain. In the contexts of the conductivity equation and the linear elasticity system, we relate this issue to a perhaps more classical problem of thin tubular inhomogeneities: we analyze the solutions to versions of the physical partial differential equations which are posed inside a fixed "background" medium, and whose material coefficients are altered inside a tube with vanishing thickness. Our main contribution from the theoretical point of view is to propose a heuristic energy argument to calculate the limiting behavior of these solutions with a minimum amount of effort. We retrieve known formulas when they are available, and we manage to treat situations which are, to the best of our knowledge, not reported in the literature (including the setting of the 3d linear elasticity system). From the numerical point of view, we propose three different applications of the formal "topological ligament" approach derived from these expansions. At first, it is an original way to account for variations of a domain, and it thereby provides a new type of sensitivity for a shape functional, to be used concurrently with more classical shape and topological derivatives in optimal design frameworks. Besides, it suggests new, interesting algorithms for the design of the scaffold structure sustaining a shape during its fabrication by a 3d printing technique, and for the design of truss-like structures. Several numerical examples are presented in two and three space dimensions to appraise the efficiency of these methods.

2020 Mathematics Subject Classification. 35C20, 49Q10, 65K10, 74B05.

Keywords. Shape and topology optimization, small inhomogeneities, asymptotic analysis, linear elasticity.

1. Introduction

In line with the growing interest raised by shape and topology optimization within the academic and industrial communities, various computational paradigms have emerged, with competing assets and drawbacks; see [95] for an overview. Among them, relaxation-based topology optimization frameworks feature designs as density functions and (possibly) microstructure tensors, describing the local arrangement of material and void at the microscopic scale; see for instance [30, 99] about the SIMP method, and [2] about the homogenization method. Another popular optimal design framework is that of "geometric" shape and topology optimization, where the optimized shape is rather represented as a true "black-and-white" domain. Several mathematical tools are then available to evaluate the sensitivity of the optimized criterion with respect to variations of the design, notably the notions of shape derivative and topological derivative. This article focuses on another, less considered type of sensitivity for functions of the domain which evaluates the effect of gluing a thin tubular ligament to the optimized shape. The proposed approach to address this question relies on a formal connection between this geometric shape and topology optimization setting and the mathematical field of small inhomogeneities asymptotics, which has been the focus of much attention from the inverse problems community, as we shall recall below.

1.1. Foreword: various means to evaluate the sensitivity of a function with respect to the domain

Let us consider a model shape and topology optimization problem of the form:

$$\min_{\Omega \in \mathcal{U}_{\rm ad}} J(\Omega), \tag{1.1}$$

where the objective function $J(\Omega)$ depends on the optimized design Ω, which is sought within a set $\mathcal{U}_{\rm ad}$ of admissible shapes in $\mathbb{R}^d$ ($d = 2, 3$ in applications). A great deal of optimization algorithms dedicated to the resolution of eq. (1.1) (starting from the gradient method) rely on the "sensitivity" of $J(\Omega)$ with respect to "small variations" of Ω. These notions are usually understood from two different, complementary viewpoints:

- Hadamard's boundary variation method is perhaps the most popular framework for geometric shape optimization. It features variations of a shape Ω of the form

  $$\Omega_\theta := (\mathrm{Id} + \theta)(\Omega), \text{ where } \theta : \mathbb{R}^d \to \mathbb{R}^d \text{ is a "small" vector field.}$$

  Intuitively, θ encodes the deformation of Ω (and particulary, its boundary $\partial\Omega$) at each point; see Figure 1.1 (top, right). The *shape derivative* $J'(\Omega)(\theta)$ of J at Ω is accordingly defined as the Fréchet derivative of the underlying mapping $\theta \mapsto J(\Omega_\theta)$ at $\theta = 0$, so that the following expansion holds in the neighborhood of $\theta = 0$:

  $$J(\Omega_\theta) = J(\Omega) + J'(\Omega)(\theta) + \mathrm{o}(\theta), \text{ where } \frac{\mathrm{o}(\theta)}{\|\theta\|} \to 0 \text{ as } \theta \to 0;$$

  see Section 7.2.1 for a little more detailed presentation. We refer generally to e.g. [12, 72, 86, 102] for the mathematical theory underlying Hadamard's boundary variation method, and to [8, 96] for implementation issues.

- The concept of topological derivative is based on variations of Ω of the form

  $$\Omega_{x_0,r} := \Omega \setminus \overline{B(x_0, r)} \text{ where } B(x_0, r) \text{ is the open ball with center } x_0 \text{ and radius } r.$$

  In other terms, $\Omega_{x_0,r}$ is obtained from Ω by nucleation of a hole centered at $x_0 \in \Omega$ with small radius $r > 0$; see Figure 1.1 (bottom, left) for an illustration. The topological derivative $\mathrm{d}J_T(\Omega)(x_0)$ of J at Ω is the first non trivial term in the asymptotic expansion of $J(\Omega_{x_0,r})$ as $r \to 0$; typically:

  $$J(\Omega_{x_0,r}) = J(\Omega) + r^d \mathrm{d}J_T(\Omega)(x_0) + \mathrm{o}(r^d).$$

  We refer to [26, 64, 93, 101] for more details about topological derivatives.

There is also a third notion of sensitivity of $J(\Omega)$ with respect to Ω, seldom considered in the literature, which accounts for the addition to Ω of a ligament $\omega_{\sigma,\varepsilon}$ with "small" thickness ε around a base curve σ; see Figure 1.1 (bottom, right). More precisely, let $\sigma : [0, \ell] \to \mathbb{R}^d$ be a curve, whose endpoints $\sigma(0)$ and $\sigma(\ell)$ belong to $\partial\Omega$, and which otherwise lies completely outside Ω; one considers the variations $\Omega_{\sigma,\varepsilon}$ of Ω defined by:

$$\Omega_{\sigma,\varepsilon} = \Omega \cup \omega_{\sigma,\varepsilon}, \text{ where } \omega_{\sigma,\varepsilon} := \left\{ x \in \mathbb{R}^d, \ d(x, \sigma) < \varepsilon \right\}, \tag{1.2}$$

the thickness $\varepsilon \ll 1$ of the ligament tends to 0, and $d(x, \sigma) = \min_{p \in \sigma} |x - p|$ is the usual Euclidean distance from x to σ. One then looks for an asymptotic expansion of $J(\Omega_{\sigma,\varepsilon})$ of the form:

$$J(\Omega_{\sigma,\varepsilon}) = J(\Omega) + \varepsilon^{d-1} \mathrm{d}J_L(\Omega)(\sigma) + \mathrm{o}(\varepsilon^{d-1}). \tag{1.3}$$

Note that the decay rate ε^{d-1} of the first non trivial term in this expansion is proportional to the measure $|\omega_{\sigma,\varepsilon}|$ of the vanishing ligament as $\varepsilon \to 0$. The sign of the "ligament derivative" $\mathrm{d}J_L(\Omega)(\sigma)$

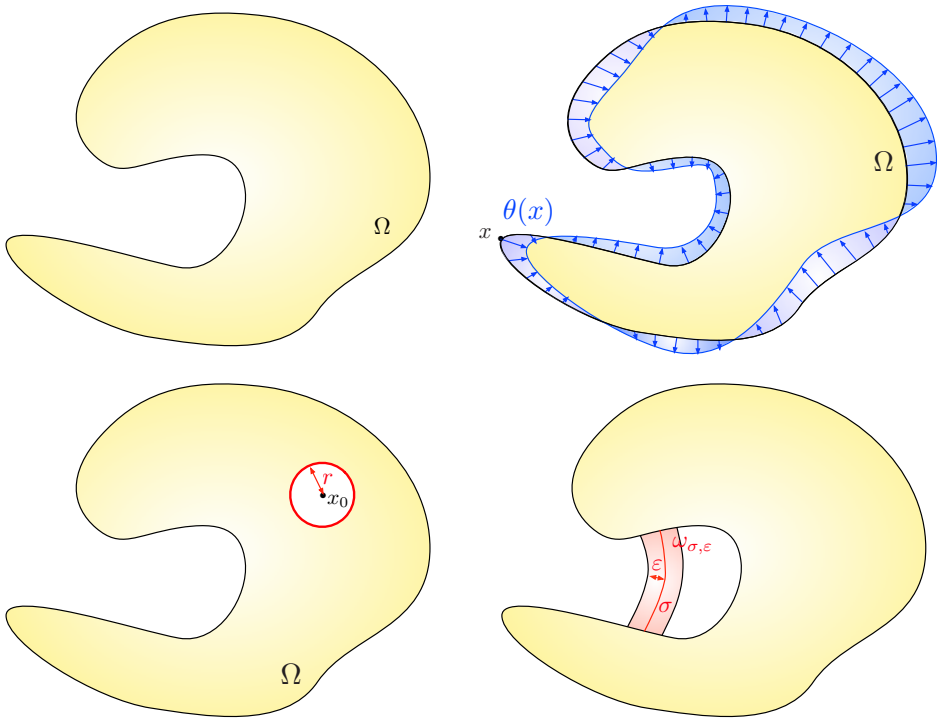

Figure 1.1. (Top, left) One shape $\Omega \subset \mathbb{R}^d$; (top, right) deformation Ω_θ of Ω via the diffeomorphism $(\mathrm{Id}+\theta)$; (bottom, left) variation $\Omega_{x_0,r}$ of Ω by nucleation of a hole with radius r around x_0; (bottom, right) variation $\Omega_{\sigma,\varepsilon}$ of Ω by addition of a thin ligament with base curve σ and thickness ε.

then indicates whether grafting the thin tube $\omega_{\sigma,\varepsilon}$ to Ω is beneficial in terms of the performance criterion $J(\Omega)$.

Variations of a domain of the form eq. (1.2), and the associated asymptotic expansions eq. (1.3) of related shape functionals, have been originally analyzed in the series of articles [87, 88, 89]. Unfortunately, the derivation of an expansion of the form eq. (1.3) is far from being an easy task, especially when the shape optimization problem eq. (1.1) under scrutiny originates from mechanical applications: $J(\Omega)$ then depends on Ω via the solution u_Ω to a partial differential equation posed on Ω (e.g. the conductivity equation, or the linear elasticity system), which characterizes its physical behavior. In this spirit, the asymptotic analysis of partial differential equations posed on domains of the form eq. (1.2) has been considered in the seminal works [87, 88, 89], where expansions of the form eq. (1.3) are proved rigorously. The notion of "exterior topological derivative" constructed in there involves partial differential equations posed on the product set of the shape Ω with the rescaled geometry $\omega_{\sigma,1}$ of the ligament. The mathematical justification of expansions such as eq. (1.3) is intricate; moreover, the resulting formulas do not lend themselves to an easy use in numerical algorithms, as the authors themselves acknowledge in the introduction of [87]; see nevertheless [75] for a recent numerical implementation of related ideas.

1.2. **From topological ligaments to thin tubular inhomogeneities**

In the present article, we propose a formal change in viewpoints about the means to understand variations of a shape of the form eq. (1.2). This paves the way to approximate expansions of a shape

functional when a thin tube is grafted to the considered domain, of the form eq. (1.3). Unlike the rigorous formulas eq. (1.3) established in the aforementioned contributions, our approximate expansions are relatively simple to calculate, and they are also very amenable to use in numerical practice.

In order to enter a little more into specifics, let us slip into the model context of the conductivity equation; the latter is analyzed more thoroughly in Section 2 below and we stay at the formal level for the moment. The considered objective function $J(\Omega)$ of the shape Ω reads:

$$J(\Omega) = \int_\Omega j(u_\Omega)\,\mathrm{d}x, \tag{1.4}$$

where $j : \mathbb{R} \to \mathbb{R}$ is a smooth function, and the physical state u_Ω is the potential, solution to:

$$\begin{cases} -\operatorname{div}(\gamma \nabla u_\Omega) = f & \text{in } \Omega, \\ u_\Omega = 0 & \text{on } \Gamma_D, \\ \gamma \frac{\partial u_\Omega}{\partial n} = g & \text{on } \Gamma_N, \\ \gamma \frac{\partial u_\Omega}{\partial n} = 0 & \text{on } \Gamma, \end{cases} \tag{1.5}$$

and $\gamma(x)$ stands for the inhomogeneous conductivity inside Ω. The parts Γ_D and Γ_N of $\partial\Omega$ bearing homogeneous Dirichlet and inhomogeneous Neumann boundary conditions are non optimizable, and the functions f and g stand for a body source and a heat flux entering Ω through Γ_N, respectively. The remaining, adiabatic subregion Γ of $\partial\Omega$ is therefore the only one subject to optimization. The perturbed version of eq. (1.5) where a thin ligament $\omega_{\sigma,\varepsilon}$ of the form eq. (1.2) is grafted to Ω is described by the system:

$$\begin{cases} -\operatorname{div}(\gamma \nabla u_{\Omega,\varepsilon}) = f & \text{in } \Omega \cup \omega_{\sigma,\varepsilon}, \\ u_{\Omega,\varepsilon} = 0 & \text{on } \Gamma_D, \\ \gamma \frac{\partial u_{\Omega,\varepsilon}}{\partial n} = g & \text{on } \Gamma_N, \\ \gamma \frac{\partial u_{\Omega,\varepsilon}}{\partial n} = 0 & \text{on } \partial(\Omega \cup \omega_{\sigma,\varepsilon}) \setminus (\overline{\Gamma_D} \cup \overline{\Gamma_N}); \end{cases} \tag{1.6}$$

where homogeneous Neumann boundary conditions are imposed on the boundary of the grafted ligament $\omega_{\sigma,\varepsilon}$ defined in eq. (1.2).

In our analysis, we propose to approximate eqs. (1.5) and (1.6); we introduce a large "hold-all" domain $D \subset \mathbb{R}^d$, containing Ω, such that both regions Γ_D and Γ_N of $\partial\Omega$ are also subsets of ∂D, and we replace eq. (1.5) by the following "background" conductivity equation, posed on D as a whole:

$$\begin{cases} -\operatorname{div}(\gamma_0 \nabla u_0) = f & \text{in } D, \\ u_0 = 0 & \text{on } \Gamma_D, \\ \gamma_0 \frac{\partial u_0}{\partial n} = g & \text{on } \Gamma_N, \\ \gamma_0 \frac{\partial u_0}{\partial n} = 0 & \text{on } \partial D \setminus (\overline{\Gamma_D} \cup \overline{\Gamma_N}), \end{cases} \tag{1.7}$$

where $\gamma_0(x)$ is an inhomogeneous conductivity coefficient. Formally, the solution u_0 to eq. (1.7) is a good approximation of that u_Ω to eq. (1.5) when γ_0 is of the form

$$\gamma_0(x) = \begin{cases} \gamma(x) & \text{if } x \in \Omega, \\ \eta\gamma(x) & \text{otherwise,} \end{cases} \tag{1.8}$$

with $\eta \ll 1$, thus mimicking void, or when $\gamma_0(x)$ is a smoothed version of eq. (1.8), as we assume thenceforth for simplicity (see Remark 2.3 below about this point). This is the well-known ersatz material method in shape and topology optimization: see for instance [2, 11, 30, 50] about the consistency of this approach.

As an approximation of eq. (1.6), we then introduce the perturbed version of eq. (1.7) where the thin tube $\omega_{\sigma,\varepsilon} \Subset D$ in eq. (1.2) is filled by a material with conductivity $\gamma_1(x)$; the perturbed potential

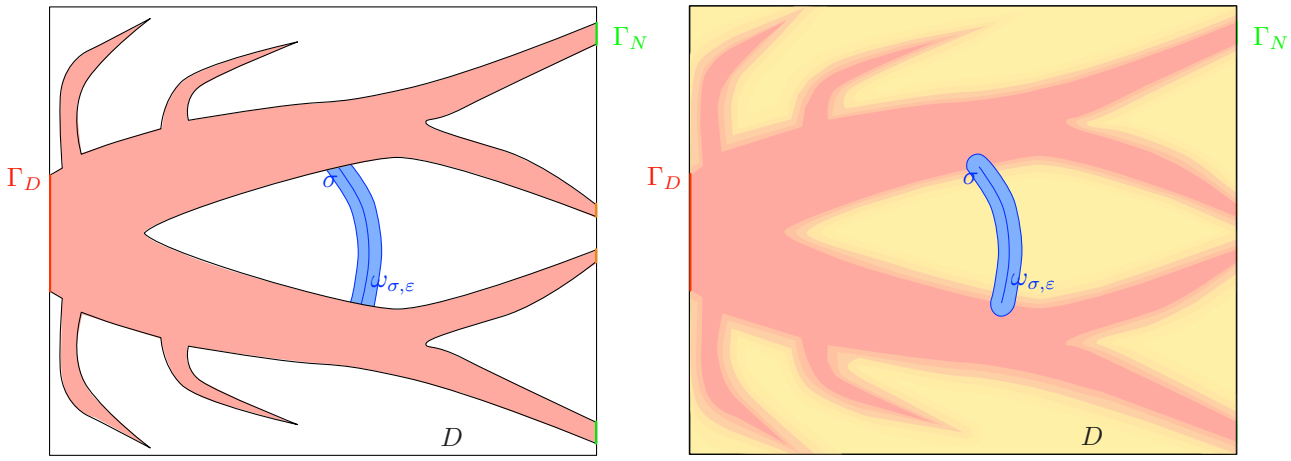

FIGURE 1.2. (Left) Graft of the ligament $\omega_{\sigma,\varepsilon}$ with base curve σ and thickness ε to a shape Ω; (right) corresponding tubular inclusion inside an approximate background medium occupying the hold-all domain D.

u_ε then satisfies:

$$\begin{cases} -\operatorname{div}(\gamma_\varepsilon \nabla u_\varepsilon) = f & \text{in } D, \\ u_\varepsilon = 0 & \text{on } \Gamma_D, \\ \gamma_\varepsilon \frac{\partial u_\varepsilon}{\partial n} = g & \text{on } \Gamma_N, \\ \gamma_\varepsilon \frac{\partial u_\varepsilon}{\partial n} = 0 & \text{on } \partial D, \end{cases} \qquad \text{where } \gamma_\varepsilon(x) = \begin{cases} \gamma_1(x) & \text{if } x \in \omega_{\sigma,\varepsilon}, \\ \gamma_0(x) & \text{otherwise;} \end{cases} \tag{1.9}$$

see Figure 1.2 for an illustration.

Our strategy for calculating approximate topological ligament expansions such as eq. (1.3) now outlines as follows. We investigate the asymptotic behavior of the perturbed, smoothed potential u_ε as $\varepsilon \to 0$, and that of an approximate counterpart $J_\sigma(\varepsilon)$ of the objective $J(\Omega_{\sigma,\varepsilon})$ in eq. (1.4) of the form:

$$J_\sigma(\varepsilon) := \int_D j(u_\varepsilon)\,\mathrm{d}x. \tag{1.10}$$

More precisely, we search for a function $u_1 : D \to \mathbb{R}$ and a real number $J'_\sigma(0)$ such that:

$$u_\varepsilon = u_0 + \varepsilon^{d-1} u_1 + \mathrm{o}(\varepsilon^{d-1}), \text{ and } J_\sigma(\varepsilon) = J_\sigma(0) + \varepsilon^{d-1} J'_\sigma(0) + \mathrm{o}(\varepsilon^{d-1}). \tag{1.11}$$

Note the slight ambiguity in the notation, where the first non trivial term u_1 in the above expansion should not be confused with the solution u_ε to eq. (1.9) for $\varepsilon = 1$. Finally, we retain the value $J'_\sigma(0)$ as an approximation of the ligament derivative $\mathrm{d}J_L(\Omega)(\sigma)$ featured in the exact expansion eq. (1.3).

Interestingly, we could have considered a wide variety of "small" inclusion sets $\omega_\varepsilon \Subset D$ in the formulation of the problem eq. (1.9), beyond thin tubes $\omega_{\sigma,\varepsilon}$ of the form eq. (1.2). For instance, $\omega_{\sigma,\varepsilon}$ could be replaced by a ball with radius ε, or a collection of such.

The general study of the influence of low volume inclusions ω_ε within a smooth background medium has received a considerable attention in the literature. Since the analysis of the approximate asymptotic expansions eq. (1.11) conducted in the next sections relies heavily on results and techniques involved in these investigations, we next present this topic with a little more details.

Remark 1.1. The above strategy for evaluating approximately the sensitivity of a functional with respect to the addition of a thin ligament to the domain is somehow reminiscent of the so-called "Moving Morphable Components" method in structural optimization; see [69], and [73] in the context

of density-based topology optimization. In those works, designs are represented as collections of bars, parametrized by one of their endpoints, their length and orientation. A smooth material coefficient is calculated thanks to the ersatz material method, approximating the mechanical behavior of the design. Finally, the optimal design problem is reformulated and solved in terms of these parameters. This idea could lead to an alternative way to construct a perturbed, smoothed equation such as eq. (1.9), and thereby a smoothed functional eq. (1.10); see also [27] where a similar process is analyzed in connection with shape and topological derivatives.

1.3. **Sensitivity of a problem perturbed by small inhomogeneities**

The effect of low-volume perturbations in the material coefficients of a partial differential equation has been the subject of multiple investigations in the literature. In this section, we mention a few related facts and interesting results, without claiming for exhaustivity.

The general structure of the expansion of the solution u_ε to the conductivity equation eq. (1.9), when the smooth background medium $\gamma_0(x)$ is perturbed by an arbitrary inclusion set ω_ε with vanishing measure $|\omega_\varepsilon| \to 0$ has been identified in the article [44]; it reads:

$$u_\varepsilon(x) = u_0(x) + |\omega_\varepsilon| \int_D \mathcal{M}(y) \nabla u_0(y) \cdot \nabla N(x,y) \, \mathrm{d}\mu(y) + \mathrm{o}(|\omega_\varepsilon|). \tag{1.12}$$

Here, $\mathrm{d}\mu$ is a measure capturing the limiting behavior of the rescaled inclusions $\frac{1}{|\omega_\varepsilon|}\omega_\varepsilon$, $\mathcal{M}(y)$ is a *polarization tensor*, appraising the limiting behavior of the field u_ε inside ω_ε, and $N(x,y)$ is the Green's function of the background conductivity operator in eq. (1.7); see eq. (2.9) below for a precise definition. These conclusions have been extended to various physical contexts, such as those of the linear elasticity system in [31], or the Maxwell's equations in [68].

A few particular instances of the above general question have been thoroughly analyzed, where more specific assumptions about the geometry of the vanishing inclusion set ω_ε make it possible to determine explicitly the limiting measure $\mathrm{d}\mu$ and the polarization tensor $\mathcal{M}(y)$.

- The situation which is best understood is certainly that of *diametrically small* inclusions, where ω_ε is of the form

  $$\omega_\varepsilon = x_0 + \varepsilon\omega, \text{ for some fixed } x_0 \in D \text{ and } \omega \Subset \mathbb{R}^d. \tag{1.13}$$

  The limiting measure $\mathrm{d}\mu$ turns out to be the Dirac distribution δ_{x_0} at the point x_0 where ω_ε shrinks, and the explicit expression of the polarization tensor $\mathcal{M}(x_0)$ involves the solution to an exterior problem posed in $\mathbb{R}^d \backslash \overline{\omega}$; see Section 4 below for more precise statements. Among other contributions in this direction, see [23, 45, 91] in the case of the conductivity equation, [21] as regards the linear elasticity system, and also [97] when, in this context, several diametrically small inclusions are connected via a non local term; see finally [24] when it comes to the Maxwell's equations.

- *Thin* inhomogeneities have also been paid much attention: ω_ε is then a thin sheet of the form

  $$\omega_\varepsilon = \{x \in \mathbb{R}, \ d(x, \mathcal{S}) < \varepsilon\}, \tag{1.14}$$

  around a (open or closed) $(d-1)$ hypersurface $\mathcal{S} \subset \mathbb{R}^d$. In this setting, the limiting measure $\mathrm{d}\mu$ is a Dirac distribution concentrated on the surface $\mathcal{S}$ and for $y \in \mathcal{S}$, the polarization tensor $\mathcal{M}(y)$ is diagonal in a local frame obtained by gathering tangent and normal vectors to $\mathcal{S}$ at y; see Sections 2 and 3 below for a more precise account in two space dimensions. In this context, we refer to [34, 35] for the rigorous calculation of the expansion of the solution u_ε to the conductivity equation based on variational techniques, and to [74] for an alternative method of proof based on layer potentials. Interestingly, asymptotic expansions have been derived in

the thin inhomogeneities context which are *uniform* with respect to the conductivity γ_1 filling ω_ε (the latter may take values arbitrarily close to 0 or ∞): see [54] in the case where $\mathcal{S}$ is closed, and the recent two-part paper [46, 47] dealing with the challenging issue of open curves in 2d. Let us finally refer to [33] about thin inhomogeneities expansions in the context of the linear elasticity equations in 2d.

- One last context of interest in applications is that of *tubular* inhomogeneities $\omega_{\sigma,\varepsilon}$, of the form eq. (1.2). This situation coincides with that of thin inhomogeneities when $d = 2$, but it turns out to be altogether different when $d = 3$. The only rigorous three-dimensional results that we are aware of arise in the context of the conductivity equation, under the assumption that the base curve σ is a straight segment, see [32]. These have been very recently adapted in [43] to the case of the Maxwell's equations, without such a restrictive assumption on the curve σ.

In general, the mathematical analysis of such small inhomogeneities asymptotics can be conducted via different techniques. On the one hand, variational methods rely on precise estimates (in the energy norm, notably) of the field u_ε and the difference between u_ε and u_0 or several intermediate quantities; see the aforementioned works [33, 34, 45, 46, 47, 54, 91]. On the other hand, layer potential techniques are based on a representation of the field u_ε as an integral over the boundary of the vanishing set $\partial\omega_\varepsilon$, and on asymptotic expansion formulas for the Green's function $N(x, y)$ of the background operator involved in this integral; see for instance [19, 22].

From the numerical point of view, asymptotic formulas of the form eq. (1.12) have been widely used for the detection or the reconstruction of small inclusions ω_ε inside a known background medium. Most of these investigations arise in the context of electrical impedance tomography, where a known current g is injected (or a collection of such), and the corresponding potential u_ε, solution to eq. (1.9) is measured either on all, or only one part of the domain D, with the purpose to retrieve some of the features of ω_ε (its diameter, the position of its centroid, etc.).

- The reconstruction of diametrically small inhomogeneities has been extensively addressed in the literature, and we refer to Chapter 5 in [18] for an overview. In a few words, a least-square algorithm was originally proposed in [45] for the reconstruction of the parameters of the inclusion set ω_ε at play in the asymptotic formula eq. (1.12) when the latter is a collection of balls (center, shape). More robust approaches were then devised, using particular input currents g, such as constant [23, 78], linear [18], or exponential functions [22]. The entries of the polarization tensor $\mathcal{M}$ and the locations of the inclusions can then be inferred from the calculation of integral quantities involving the input and measured data, namely, the values of g and the measured potential u_ε on ∂D. Let us also mention the variant of the linear sampling method developed in [39] to deal with the identification of diametrically small inhomogeneities.

- The reconstruction of thin inhomogeneities has been considered in [16] in the context of the 2d conductivity equation; the authors use the knowledge of the first non trivial term in the expansion of the potential u_ε to infer first the polarization tensor, thus the direction of the base curve, assumed to be a line segment, then the endpoints of the curve, from the datum of two boundary measurements. This idea is generalized in [17] to handle inclusions made from multiple segments in 2d.

- To the best of our knowledge, the identification of tubular inhomogeneities inside a three-dimensional medium has only been addressed in [32] and [67], in the context of the conductivity equation and in [43] in the context of Maxwell's equations. In [32], the asymptotic expansion of u_ε is rigorously calculated and used, in the particular case where σ is a straight segment; on the contrary, in [67], the author relies solely on the general structure eq. (1.12) of this

expansion in order to construct an indicator $W(x, n)$ which vanishes on D, except at points $x \in D$ which are close to the sought curve σ and in the directions n which are orthogonal to σ at x. In [43], a regularized least-square algorithm is proposed, which consists in finding the curve σ minimizing the error between the measured far-field and that predicted by the asymptotic formula eq. (1.12).

1.4. **Main contributions and outline of the article**

The findings of the present article were partly announced in the preliminary note [51]; our purpose is twofold.

From the theoretical point of view, our main aim is to calculate the sensitivity of the solution u_ε to certain partial differential equations—namely the conductivity equation and the linearized elasticity system— with respect to perturbations of the background material properties inside tubular inclusions $\omega_{\sigma,\varepsilon}$, of the form eq. (1.2). As we have mentioned, these expansions have already been computed in a variety of situations, mainly in 2d; their proof is however quite intricate, and we propose a formal method to achieve this, inspired by the former works in [54, 85, 91]. With a minimum amount of technicality, the presented argument allows us to retrieve asymptotic expansions for thin tubular inhomogeneities in situations where rigorous proofs are already available in the literature (the cases of the 2d conductivity and linear elasticity equations, and that of the 3d conductivity equation when σ is a straight segment); moreover, it allows for a formal calculation of such expansions in situations which are, to the best of our knowledge, not reported in the literature (such as that of the 3d linear elasticity system). Furthermore, we show that the expansions of u_ε obtained in these different contexts make it possible to calculate the asymptotic behavior of related observables $J_\sigma(\varepsilon)$ (see e.g. eq. (1.10)) in a convenient adjoint-based framework which is familiar in shape and topology optimization.

From the numerical point of view, we explore several applications in shape and topology optimization of our asymptotic formulas for thin tubular inhomogeneities. We have indeed exemplified in Section 1.2 that they make it possible to approximate the sensitivity of a function of the domain when a thin ligament is grafted to the latter. We show how this strategy can be used to fulfill multiple purposes in the shape and topology optimization context, such as:

- to add bars to structures in the course of a "classical" shape optimization process driven by shape derivatives, thereby making the final design less sensitive to the initial guess;
- to calculate an optimized support structure for a shape showing overhang features, in readiness for its construction by additive manufacturing;
- to predict a "clever" initial guess, made of bars, for the optimization of a truss-like structure (i.e. whose outline resembles a collection of bars).

The remainder of this article is organized as follows. In Section 2, we discuss the problem of thin tubular inclusions in the physical context of the two-dimensional conductivity equation. The main result, Theorem 2.1, describes the first non trivial term in the asymptotic expansion of the perturbed state u_ε. Although this situation is well-understood in the literature, we take advantage of its technical simplicity to explain carefully how a simple and heuristic energy argument allows to retrieve the correct expression. The derivative with respect to the vanishing thickness ε of a functional depending on u_ε is then calculated in Section 2.3 by means of a suitable adjoint method. In Section 3, we adapt these developments to the case of the 2d linear elasticity system. Our next task is to obtain similar results in three-dimensional situations. It turns out that this question shares much similarity with the treatment of diametrically small inhomogeneities. For this reason, we expose in Section 4 how our heuristic energy argument also allows to handle this well-known case in the literature. We are then in

position to address the calculation of the asymptotic expansion of the field u_ε in the case of tubular inhomogeneities in 3d, first in the case of the conductivity equation in Section 5, then in the context of the linear elasticity system in Section 6. As we have mentioned, the ideas introduced in this article give rise to various numerical algorithms in connection with the field of shape and topology optimization. These are presented in Section 7, and illustrated with concrete physical examples. Eventually, several theoretical perspectives of our work are outlined in Section 8, as well as promising applications.

2. Asymptotic expansion of the solution to the conductivity equation in 2d

The analyses of this section take place in the setting of the 2d conductivity equation which we have already encountered in Section 1.2, where the salient points of this article can be conveniently exposed, with a minimum level of technicality.

2.1. Presentation of the model setting and statement of the results

Let $D \subset \mathbb{R}^2$ be a bounded Lipschitz domain, filled by a material whose conductivity $\gamma_0 \in \mathcal{C}^\infty(\overline{D})$ satisfies:

$$\forall x \in D, \quad \gamma_- \leq \gamma_0(x) \leq \gamma_+, \tag{2.1}$$

for some fixed constants $0 < \gamma_- \leq \gamma_+$. The boundary ∂D is composed of three disjoint, open subsets: the voltage potential is kept at constant value 0 on Γ_D, while a smooth heat flux $g \in \mathcal{C}^\infty(\overline{\Gamma_N})$ is entering D via the subset Γ_N; the domain D is insulated from the outside on the remaining part $\partial D \setminus (\overline{\Gamma_D} \cup \overline{\Gamma_N})$. Denoting by $f \in \mathcal{C}^\infty(\overline{D})$ a source acting in the medium, the voltage potential u_0 inside D is the unique solution in the space

$$H^1_{\Gamma_D}(D) := \Big\{ u \in H^1(D), \quad u = 0 \text{ on } \Gamma_D \Big\}$$

to the following "background" conductivity equation:

$$\begin{cases} -\operatorname{div}(\gamma_0 \nabla u_0) = f & \text{in } D, \\ u_0 = 0 & \text{on } \Gamma_D, \\ \gamma_0 \frac{\partial u_0}{\partial n} = g & \text{on } \Gamma_N, \\ \gamma_0 \frac{\partial u_0}{\partial n} = 0 & \text{on } \partial D \setminus (\overline{\Gamma_D} \cup \overline{\Gamma_N}). \end{cases} \tag{2.2}$$

Let us already notice that the classical regularity theory for elliptic equations predicts that the solution u_0 to eq. (2.2) is smooth in the interior of D; see e.g. [38, §9.6].

We now consider a version of the above situation where D is perturbed by a "thin" tubular inclusion $\omega_{\sigma,\varepsilon}$ with width $\varepsilon > 0$ around a base curve σ:

$$\omega_{\sigma,\varepsilon} = \Big\{ x \in \mathbb{R}^2, \ \operatorname{dist}(x, \sigma) < \varepsilon \Big\}; \tag{2.3}$$

see Figure 2.1 for an illustration. Here, we assume that $\sigma : [0, \ell] \to D$ is a smooth (open or closed) connected curve, parametrized by arc length (so that ℓ is the length $|\sigma|$ of the curve), which does not intersect ∂D, and is not self-intersecting. Throughout the article, with a slight abuse of notation, we identify the geometric curve σ with its parametrization $s \mapsto \sigma(s)$. The inclusion $\omega_{\sigma,\varepsilon}$ is filled with another material with smooth conductivity $\gamma_1 \in \mathcal{C}^\infty(\overline{D})$, which also satisfies eq. (2.1) (up to modifying the values γ_- and γ_+). The potential u_ε in this perturbed situation is the unique solution in $H^1_{\Gamma_D}(D)$

to the following equation:

$$\begin{cases} -\operatorname{div}(\gamma_\varepsilon \nabla u_\varepsilon) = f & \text{in } D, \\ u_\varepsilon = 0 & \text{on } \Gamma_D, \\ \gamma_0 \frac{\partial u_\varepsilon}{\partial n} = g & \text{on } \Gamma_N, \\ \gamma_0 \frac{\partial u_\varepsilon}{\partial n} = 0 & \text{on } \partial D \setminus (\Gamma_D \cup \Gamma_N), \end{cases} \qquad \text{where } \gamma_\varepsilon(x) = \begin{cases} \gamma_1(x) & \text{if } x \in \omega_{\sigma,\varepsilon} \\ \gamma_0(x) & \text{otherwise.} \end{cases} \tag{2.4}$$

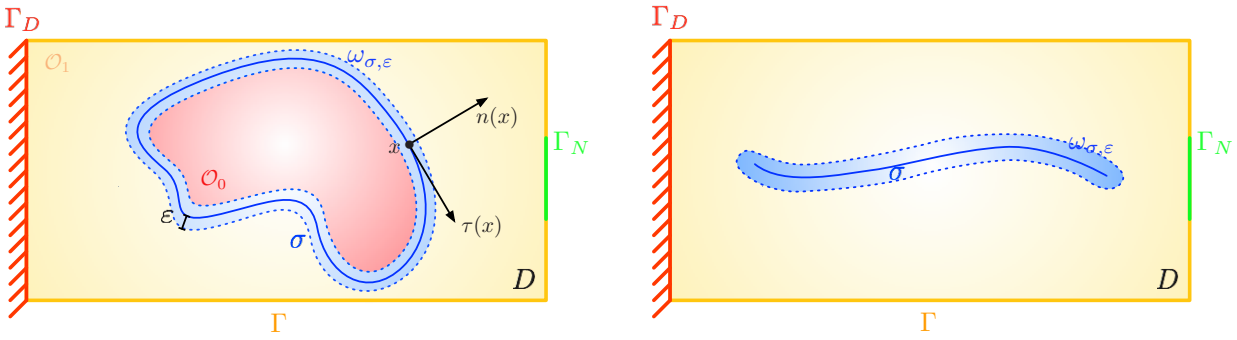

FIGURE 2.1. Setting of the perturbed conductivity problem eq. (2.4) in the case of (left) a closed base curve σ and (right) an open base curve σ.

We aim to understand the behavior of u_ε as the thickness ε of the inclusion vanishes. In this direction, a fairly classical analysis yields the natural convergence result (see Lemma B.1 for a proof):

$$u_\varepsilon \xrightarrow{\varepsilon \to 0} u_0 \text{ strongly in } H^1_{\Gamma_D}(D).$$

We then wish to identify the next term in the asymptotic expansion of u_ε as $\varepsilon \to 0$; the main result of interest is the following. It has been proved independently in [34] owing to a variational method and in [74] by layer potential techniques.

Theorem 2.1. *The following expansion holds at any point $x \in D \setminus \sigma$:*

$$u_\varepsilon(x) = u_0(x) + \varepsilon u_1(x) + \mathrm{o}(\varepsilon), \text{ where } u_1(x) := \int_\sigma \mathcal{M}(y) \nabla u_0(y) \cdot \nabla_y N(x,y) \, \mathrm{d}\ell(y), \tag{2.5}$$

and the remainder $\mathrm{o}(\varepsilon)$ is uniform when x belongs to a fixed compact subset of $D \setminus \sigma$. Here, $N(x,y)$ is the Green's function of the background operator eq. (2.2) (see Section 2.2.1 below), and for any point $y \in \sigma$, the polarization tensor $\mathcal{M}(y)$ is a symmetric 2×2 matrix. Its expression reads, in the local orthonormal frame $(\tau(y), n(y))$ of $\mathbb{R}^2$ made of a unit tangent vector $\tau(y)$ to σ at y and its 90° counterclockwise rotate $n(y)$:

$$\mathcal{M}(y) = \begin{pmatrix} 2(\gamma_1(y) - \gamma_0(y)) & 0 \\ 0 & 2\gamma_0(y)\left(1 - \frac{\gamma_0(y)}{\gamma_1(y)}\right) \end{pmatrix}. \tag{2.6}$$

Remark 2.2. In the above expression, and throughout this article, we have denoted by $\mathrm{d}\ell$ the line measure on a (smooth enough) one-dimensional subset of $\mathbb{R}^d$, $d = 2, 3$. This measure coincides with the surface measure $\mathrm{d}s$ on a $(d-1)$-dimensional hypersurface of $\mathbb{R}^d$ when $d = 2$, and we shall use interchangeably either notation in this situation.

The conclusion of Theorem 2.1 holds regardless of whether σ be closed or open. While the latter situation is the most interesting for our applications, its rigorous mathematical treatment is significantly more involved. Briefly, one has to prove that the contribution of the endpoints of σ to the

asymptotic behavior of u_ε is of order higher than ε. This fact is observed in all the situations handled in the literature, to the best of our knowledge: see [34] for the case of the 2d conductivity equation, [33] for the case of the 2d elasticity system, and [32] in the context of the 3d conductivity equation, under some technical assumptions, and [43] for the case of the 3d Maxwell's equations. It even holds true when, in the 2d conductivity case, the conductivity inside the inclusion is allowed to degenerate to 0 or ∞; see [46, 47, 54].

In Section 2.2.3 below, we propose a formal method, which can be made rigorous in some cases, leading to the correct expansion eq. (2.5) obtained in [34, 74] from intuitive considerations. According to the previous discussion, for simplicity, the presentation of our formal argument proceeds under the simplifying assumption that the curve σ is closed.

Our second topic of attention in Sections 2.2 and 2.3 concerns the behavior as $\varepsilon \to 0$ of a quantity of interest $J_\sigma(\varepsilon)$ involving the perturbed potential u_ε. To set ideas, we consider a function of the form:

$$J_\sigma(\varepsilon) = \int_D j(u_\varepsilon)\,\mathrm{d}x, \tag{2.7}$$

where $j \in \mathcal{C}^\infty(\mathbb{R})$ satisfies the growth assumptions:

$$\forall u \in \mathbb{R}, \quad |j(u)| \le C(1+|u|^2), \quad |j'(u)| \le C(1+|u|), \text{ and } |j''(u)| \le C, \tag{2.8}$$

for some constant $C > 0$. Using Theorem 2.1, we prove in Section 2.3 that $J_\sigma(\varepsilon)$ is differentiable at $\varepsilon = 0$, with derivative

$$J'_\sigma(0) = \int_D j'(u_0)u_1\,\mathrm{d}x.$$

This expression is somewhat awkward, since it involves the term u_1 in eq. (2.5), which depends on σ in a very non trivial way. This makes difficult the identification of a curve σ such that $J'_\sigma(0)$ be as negative as possible. To overcome this drawback, we show that, thanks to the introduction of a suitable adjoint state $p_0 \in H^1_{\Gamma_D}(D)$, this derivative has the alternative form:

$$J'_\sigma(0) = \int_\sigma \mathcal{M}(x)\nabla u_0 \cdot \nabla p_0\,\mathrm{d}\ell(x),$$

which is much more suitable for our purpose.

Remark 2.3. We believe that the aforementioned results, and notably Theorem 2.1, still hold true in the case where the background conductivity γ_0 is only piecewise smooth, with jumps not aligned with the curve σ, and also in the case where σ does intersect ∂D in a non tangential way. Although we have no proof of these facts, we shall see in the examples of Section 7.3 that the use of our asymptotic formulas when σ intersects ∂D yields coherent numerical results.

2.2. **Asymptotic behavior of the potential** u_ε

Our purpose in this section is to retrieve the conclusion of Theorem 2.1 thanks to a simple formal argument based on energy considerations, in the particular case where σ is a closed curve. To this end, we first recall in Section 2.2.1 some elementary facts about the Green's function associated to eq. (2.2) and we say a few words about the signed distance function to a closed curve σ in Section 2.2.2.

2.2.1. *Preliminaries about the Green's function to the background conductivity equation eq.* (2.2) *in 2d*

Let $N(x,y)$ be the Green's function of the mixed boundary value problem in eq. (2.2), that is, for a given point $x \in D$, the function $y \mapsto N(x,y)$ satisfies:

$$\begin{cases} \mathrm{div}_y(\gamma_0(y)\nabla_y N(x,y)) = \delta_{y=x} & \text{in } D, \\ \gamma_0(y)\frac{\partial N}{\partial n_y}(x,y) = 0 & \text{on } \partial D \setminus \overline{\Gamma_D}, \\ N(x,y) = 0 & \text{on } \Gamma_D, \end{cases} \tag{2.9}$$

where $\delta_{y=x}$ is the Dirac distribution at $y = x$. A simple adaptation of the proof of Lemma 2.36 in [62] reveals that the function $N(x,y)$ is symmetric in its arguments: $N(x,y) = N(y,x)$. Moreover, it has essentially the same singularities as the (modified) fundamental solution of the Laplace operator in the free space

$$G(x,y) = \frac{1}{2\pi\gamma_0(x)} \log|x-y|. \tag{2.10}$$

More precisely, the following decomposition holds:

$$N(x,y) = G(x,y) + R(x,y), \tag{2.11}$$

where for $x \in D$, the remainder $y \mapsto R(x,y)$ satisfies:

$$\begin{cases} \mathrm{div}_y(\gamma_0(y)\nabla_y R(x,y)) = \frac{1}{2\pi\gamma_0(x)}\frac{x-y}{|x-y|^2}\cdot\nabla\gamma_0(y) & \text{in } D, \\ \gamma_0(y)\frac{\partial R}{\partial n_y}(x,y) = \frac{\gamma_0(y)}{2\pi\gamma_0(x)}\frac{(x-y)\cdot n(y)}{|x-y|^2} & \text{on } \partial D \setminus \overline{\Gamma_D}, \\ R(x,y) = -\frac{1}{2\pi\gamma_0(x)}\log|x-y| & \text{on } \Gamma_D. \end{cases}$$

Since the right-hand side of the above equation belongs to $L^p(D)$ for $1 \le p < 2$ and is smooth for $y \neq x$, it follows from classical elliptic regularity that, for a given point $x \in D$, the functions $y \mapsto R(x,y)$ and $y \mapsto N(x,y)$ are smooth on $D \setminus \{x\}$; moreover, for any compact subsets $K, K' \Subset D$, there exists a constant C such that:

$$\sup_{x\in K} \|R(x,\cdot)\|_{W^{2,p}(K')} + \sup_{x\in K} \|R(x,\cdot)\|_{H^1(D)} \le C; \tag{2.12}$$

see [38, 66], and also [63] for a more thorough analysis of such Green's functions.

Let now $\sigma \Subset D$ be a smooth, connected, open or closed simple curve (i.e. σ does not present self-intersections); we denote by $n(x)$ a smooth unit normal vector field to σ, whose orientation may be arbitrary for the purpose of this section. When $a(x)$ is a discontinuous quantity across σ which is sufficiently smooth from either side of σ, we denote by

$$a^{\pm}(x) := \lim_{\substack{t\to 0 \\ t>0}} a(x \pm tn(x))$$

the one-sided limits of a at $x \in \sigma$. Accordingly,

$$[a](x) := a^+(x) - a^-(x) \quad \text{and} \quad \{a\}(x) := a^+(x) + a^-(x)$$

are respectively the jump and the mean value of a across σ; see again Figure 2.1.

In the following, we shall require information about the following integrals, involving the GReen's function $N(x,y)$ to eq. (2.2) and a smooth enough density function φ, say $\varphi \in \mathcal{C}^{0,l}(\sigma)$ for some $0 < l < 1$:

$$\forall x \in D \setminus \sigma, \quad \mathcal{S}_\sigma\varphi(x) = \int_\sigma N(x,y)\varphi(y)\,\mathrm{ds}(y),$$
$$\forall x \in D \setminus \sigma, \quad \mathcal{D}_\sigma\varphi(x) = \int_\sigma \gamma_0(y)\frac{\partial N}{\partial n_y}(x,y)\varphi(y)\,\mathrm{ds}(y),$$

These quantities are respectively the well-known *single* and *double layer potentials* associated to φ; see [19, 62, 83] and references therein for related material, and also [76, 77] when σ is open.

The single and double layer potentials $\mathcal{S}_\sigma\varphi$ and $\mathcal{D}_\sigma\varphi$ satisfy the following jump relations on σ:

$$[\mathcal{S}_\sigma\varphi] = 0, \quad \left[\gamma_0 \frac{\partial}{\partial n}(\mathcal{S}_\sigma\varphi)\right] = \varphi, \tag{2.13}$$

and

$$[\mathcal{D}_\sigma\varphi] = -\varphi, \quad \left[\gamma_0 \frac{\partial}{\partial n}(\mathcal{D}_\sigma\varphi)\right] = 0, \tag{2.14}$$

both formulas being obviously independent of the chosen orientation for the normal vector n.

A straightforward calculation based on eqs. (2.13) and (2.14) reveals that the first-order term u_1 in the expansion eq. (2.5) of the perturbed potential u_ε satisfies the following partial differential equation:

$$\begin{cases} -\operatorname{div}(\gamma_0 \nabla u_1) = 0 & \text{in } D \setminus \sigma, \\ u_1 = 0 & \text{on } \Gamma_D, \\ \gamma_0 \frac{\partial u_1}{\partial n} = 0 & \text{on } \partial D \setminus \overline{\Gamma_D}, \\ [u_1] = -2\left(1 - \frac{\gamma_0}{\gamma_1}\right) \frac{\partial u_0}{\partial n} & \text{on } \sigma, \\ \left[\gamma_0 \frac{\partial u_1}{\partial n}\right] = -2 \frac{\partial}{\partial \tau}\left((\gamma_1 - \gamma_0) \frac{\partial u_0}{\partial \tau}\right) & \text{on } \sigma. \end{cases} \tag{2.15}$$

The function u_1 is equivalently characterized by the integral representation eq. (2.5) or as the solution to eq. (2.15). Note however that the functional setting for eq. (2.15) differs, depending on the nature of σ. When σ is closed, u_1 is the unique solution in the space $H^1_{\Gamma_D}(D \setminus \sigma)$ to this equation. Moreover, this function is "variational" in the sense that it is equivalently characterized as the minimizer of an energy functional whose Euler–Lagrange equations precisely yield eq. (2.15). The case where σ is open is more subtle; see [76] for related issues. The function u_1 is no longer variational; it satisfies the various components of eq. (2.15) in the sense that it belongs to $\mathcal{C}^2(D \setminus \overline{\sigma})$, that it has one-sided limits $u_1^\pm(x)$ at every point x in the interior of σ, and that it has logarithmic singularities at the endpoints; see [16] for precise statements and proofs.

Remark 2.4. The exact counterparts of the above properties hold in the case of three space dimensions, up to the fact that the (modified) fundamental solution $G(x, y)$ in eq. (2.10) then reads:

$$G(x, y) = -\frac{1}{4\pi\gamma_0(x)|x - y|}.$$

2.2.2. *Preliminaries about the signed distance function to a closed curve in 2d*

As we have mentioned, our formal calculation of the first-order asymptotic expansion of Theorem 2.1 is considerably simpler when σ is a closed curve. This situation can indeed be treated with the help of the notion of signed distance function, whose main properties we recall for the convenience of the reader, referring to e.g. [42, 55, 66] for details.

Let $\sigma \subset \mathbb{R}^2$ be a smooth, connected, closed simple curve, delimiting an interior and an exterior domain, $\mathcal{O}^0$ and $\mathcal{O}^1$ respectively; see Figure 2.1 (left). We denote by $n = (n_1, n_2) : \sigma \to \mathbb{R}^2$ the unit normal vector to σ, pointing outward $\mathcal{O}^0$, and by $\tau = (n_2, -n_1)$ the corresponding tangent vector, so that for any point $x \in \sigma$, $(\tau(x), n(x))$ is a local orthonormal frame of the plane.

Definition 2.5. • The *signed distance function* d_σ to the interior domain $\mathcal{O}^0$ is defined by:

$$\forall x \in \mathbb{R}^2, \ d_\sigma(x) := \begin{cases} -d(x, \sigma) & \text{if } x \in \mathcal{O}^0, \\ 0 & \text{if } x \in \sigma, \\ d(x, \sigma) & \text{if } x \in \mathcal{O}^1, \end{cases}$$

where

$$d(x, \sigma) = \min_{p \in \sigma} |x - p| \tag{2.16}$$

is the usual Euclidean distance function to σ.

- The points $p \in \sigma$ achieving the minimum in the definition eq. (2.16) are called the *projections* of x onto σ. When there exists a unique such point, it is denoted by $p_\sigma(x)$.
- The skeleton Σ of σ is the set of points $x \in \mathbb{R}^2$ having at least two projections on σ.

Since σ is smooth, there exists $r > 0$ such that the mapping

$$(-r, r) \times \sigma \ni (t, x) \longmapsto x + tn(x) \in \omega_{\sigma,r} \tag{2.17}$$

is a smooth diffeomorphism onto the tubular neighborhood $\omega_{\sigma,r}$ of σ defined in eq. (2.3). Its inverse is:

$$\omega_{\sigma,r} \ni x \longmapsto (d_\sigma(x), p_\sigma(x)) \in (-r, r) \times \sigma;$$

see [14] or [103, Thm. 20, p. 467]. Throughout this article, we assume for notational simplicity and without loss of generality that this property holds for some $r > 1$. As a consequence, the tangential and normal vector fields $\tau(x)$ and $n(x)$ can be extended from σ to the whole set $\omega_{\sigma,1}$ via the formulas

$$\tau(x) \equiv \tau(p_\sigma(x)), \text{ and } n(x) \equiv n(p_\sigma(x)), \quad x \in \omega_{\sigma,1}, \tag{2.18}$$

a notation that we consistently employ in the following. In particular, it is possible to define the normal and tangential derivatives $\frac{\partial u}{\partial n}$ and $\frac{\partial u}{\partial \tau}$ of a (smooth enough) function $u : D \to \mathbb{R}$ on the whole neighborhood $\omega_{\sigma,1}$. Also, when $M : D \to \mathbb{R}^{2\times 2}$ is a matrix-valued function, we denote by

$$M = \begin{pmatrix} M_{\tau\tau} & M_{\tau n} \\ M_{n\tau} & M_{nn} \end{pmatrix}$$

its expression in the local basis (τ, n), that is, for $x \in \omega_{\sigma,1}$: $M_{\tau\tau}(x) = M(x)\tau(x) \cdot \tau(x)$, $M_{\tau n}(x) = M(x)n(x) \cdot \tau(x)$, etc.

The derivatives of the signed distance function d_σ and the projection p_σ read:

$$\forall x \in \omega_{\sigma,1}, \quad \nabla d_\sigma(x) = \frac{x - p_\sigma(x)}{d_\sigma(x)} = n(p_\sigma(x)), \quad \text{and} \quad \nabla p_\sigma(x) = \begin{pmatrix} \frac{1}{1+d_\sigma(x)\kappa(x)} & 0 \\ 0 & 0 \end{pmatrix}, \tag{2.19}$$

where the latter matrix is expressed in the local basis $(\tau(x), n(x))$. Here, $\kappa : \sigma \to \mathbb{R}$ is the mean curvature of σ, oriented in such a way that $\kappa(x)$ is positive when $\mathcal{O}^0$ is locally convex around x, and we take the shortcut $\kappa(x) \equiv \kappa(p_\sigma(x))$ for $x \in \omega_{\sigma,1}$.

In the following, it will also prove useful to recast integrals over the tubular neighborhood $\omega_{\sigma,1}$ as nested integrals over σ and $(-1, 1)$; to this end, applying the coarea formula of Lemma A.1 with the mapping p_σ and using eq. (2.19) yields:

Proposition 2.6. *For any function $\varphi \in L^1(\omega_{\sigma,1})$, it holds:*

$$\int_{\omega_{\sigma,1}} \varphi(x)\,\mathrm{d}x = \int_\sigma \left(\int_{-1}^{1} (1 + t\kappa(p)) f(p + tn(p))\,\mathrm{d}t \right) \mathrm{d}\ell(p).$$

We conclude this section with a few technical formulas involving the extended normal and tangential vector fields $n, \tau : \omega_{\sigma,1} \to \mathbb{R}^2$ in eq. (2.18).

We first calculate the derivatives of n and τ. Differentiating the normalization identities $|\tau|^2 = |n|^2 = 1$ and $\tau \cdot n = 0$, we obtain:

$$\nabla\tau^T\tau = \nabla n^T n = 0, \text{ and } \nabla\tau^T n + \nabla n^T \tau = 0.$$

Besides, the normal vector reads $n = \nabla d_\sigma$, and so the symmetric matrix $\nabla n = \nabla^2 d_\sigma$ is given by:

$$\nabla n = \begin{pmatrix} \frac{\kappa}{1+d_\sigma\kappa} & 0 \\ 0 & 0 \end{pmatrix}. \tag{2.20}$$

in the local basis (τ, n) of the plane; see e.g. [66], §14.6. Now, straightforward calculations yield:

$$\nabla\tau n \cdot \tau = \nabla\tau^T \tau \cdot n = 0, \quad \nabla\tau n \cdot n = \nabla\tau^T n \cdot n = -\nabla n^T \tau \cdot n = 0,$$

as well as:

$$\nabla\tau\tau \cdot \tau = 0 \quad \text{and} \quad \nabla\tau\tau \cdot n = \nabla\tau^T n \cdot \tau = -\nabla n^T \tau \cdot \tau,$$

so that we obtain, in the local basis (τ, n):

$$\nabla\tau = \begin{pmatrix} 0 & 0 \\ -\frac{\kappa}{1+d_\sigma\kappa} & 0 \end{pmatrix}. \tag{2.21}$$

Finally, let $v : \omega_{\sigma,1} \to \mathbb{R}^2$ be a smooth enough vector-valued function; similar calculations based on the previous formulas yield:

$$\nabla(v \cdot n) \cdot n = \nabla v^T n \cdot n + \nabla n^T v \cdot n = \nabla v n \cdot n, \tag{2.22}$$

and

$$\nabla(v \cdot \tau) \cdot n = \nabla v^T \tau \cdot n + \nabla\tau^T v \cdot n = \nabla v n \cdot \tau + \nabla\tau n \cdot v = \nabla v n \cdot \tau. \tag{2.23}$$

Likewise,

$$\nabla(v \cdot n) \cdot \tau = (\nabla n^T v + \nabla v^T n) \cdot \tau = \nabla v\tau \cdot n + \frac{\kappa}{1 + d_\sigma\kappa} v \cdot \tau,$$

and so:

$$\nabla v\tau \cdot n = \nabla(v \cdot n) \cdot \tau - \frac{\kappa}{1 + d_\sigma\kappa} v \cdot \tau. \tag{2.24}$$

Finally,

$$\nabla(v \cdot \tau) \cdot \tau = \nabla\tau^T v \cdot \tau + \nabla v^T \tau \cdot \tau = \nabla v\tau \cdot \tau + \nabla\tau\tau \cdot v = \nabla v\tau \cdot \tau - \frac{\kappa}{1 + d_\sigma\kappa} v \cdot n,$$

which yields:

$$\nabla v\tau \cdot \tau = \nabla(v \cdot \tau) \cdot \tau + \frac{\kappa}{1 + d_\sigma\kappa} v \cdot n. \tag{2.25}$$

Remark 2.7. Most of the above results actually extend to regions outside the tubular neighborhood $\omega_{\sigma,1}$ of σ. More precisely, the mappings d_σ and p_σ turn out to be differentiable on the whole set $D \setminus \overline{\Sigma}$ (see again [42, 55, 66]) and all the formulas in this section hold true in there.

2.2.3. *Formal proof of Theorem 2.1 when σ is a closed curve*

We now describe how the asymptotic behavior of the potential u_ε, solution to eq. (2.4), which has been derived rigorously in [34, 74], can be inferred in a relatively simple manner from heuristic energy considerations. Let us notice that, however formal, this argument can be made rigorous along the lines of our previous work [54], but this goes beyond the scope of the present article. To simplify the presentation, we assume throughout this section that the considered curve σ is closed; see the discussion following Theorem 2.1 about this point.

Introducing the difference $r_\varepsilon := \frac{1}{\varepsilon}(u_\varepsilon - u_0) \in H^1_{\Gamma_D}(D)$, we aim to prove that, as $\varepsilon \to 0$, r_ε converges to the function u_1 defined in eq. (2.5). We proceed in three steps.

Step 1: We represent the error $r_\varepsilon(x)$ at points $x \in D \setminus \sigma$ in terms of the Green's function $N(x, y)$ and the values of r_ε inside $\omega_{\sigma,\varepsilon}$. To this end, a simple calculation reveals that r_ε is the unique solution in $H^1_{\Gamma_D}(D)$ to the following problem:

$$\begin{cases} -\operatorname{div}(\gamma_\varepsilon \nabla r_\varepsilon) = \frac{1}{\varepsilon} \operatorname{div}\left(\mathbb{1}_{\omega_{\sigma,\varepsilon}}(\gamma_1 - \gamma_0)\nabla u_0\right) & \text{in } D, \\ r_\varepsilon = 0 & \text{on } \Gamma_D, \\ \gamma_0 \frac{\partial r_\varepsilon}{\partial n} = 0 & \text{on } \partial D \setminus \overline{\Gamma_D}, \end{cases}$$

where γ_ε is defined in eq. (2.4) and $\mathbb{1}_{\omega_{\sigma,\varepsilon}}$ is the characteristic function of $\omega_{\sigma,\varepsilon}$. The variational form of this equation is:

$$\forall v \in H^1_{\Gamma_D}(D), \quad \int_D \gamma_\varepsilon \nabla r_\varepsilon \cdot \nabla v \, \mathrm{d}x = -\frac{1}{\varepsilon} \int_{\omega_{\sigma,\varepsilon}} (\gamma_1 - \gamma_0) \nabla u_0 \cdot \nabla v \, \mathrm{d}x. \tag{2.26}$$

Let $x \in D \setminus \sigma$ be a fixed point; it follows again from elliptic regularity that r_ε is smooth in a neighborhood of x for $\varepsilon > 0$ small enough. Using the definition eq. (2.9) of the Green's function $N(x, y)$, which holds in the sense of distributions, we obtain:

$$\begin{aligned} r_\varepsilon(x) &= \int_D \mathrm{div}_y(\gamma_0(y) \nabla_y N(x, y)) r_\varepsilon(y) \, \mathrm{d}y, \\ &= -\int_D \gamma_0(y) \nabla r_\varepsilon(y) \cdot \nabla_y N(x, y) \, \mathrm{d}y, \\ &= -\int_D \gamma_\varepsilon(y) \nabla r_\varepsilon(y) \cdot \nabla_y N(x, y) \, \mathrm{d}y + \int_{\omega_{\sigma,\varepsilon}} (\gamma_1 - \gamma_0)(y) \nabla r_\varepsilon(y) \cdot \nabla_y N(x, y) \, \mathrm{d}y. \end{aligned} \tag{2.27}$$

In order to rewrite the first integral in the above right-hand side, we wish to insert $y \mapsto N(x, y)$ as test function in the variational formulation eq. (2.26) for r_ε. Unfortunately, this is not directly possible since $N(x, \cdot)$ is not a function in $H^1_{\Gamma_D}(D)$. More precisely, it follows from eqs. (2.10) to (2.12) that $N(x, y)$ is in $W^{1,1}(D)$ and that it belongs to $H^1(D \setminus \overline{\mathcal{V}})$, where $\mathcal{V}$ is an arbitrary open neighborhood of x. To achieve our purpose nonetheless, we argue as in [44]: since $x \notin \sigma$, for a fixed and small enough ε, there exists an open neighborhood $\mathcal{V} \subset D$ of x such that:

$$\omega_{\sigma,\varepsilon} \Subset D \setminus \overline{\mathcal{V}},$$

and a sequence of functions $v_k \in H^1_{\Gamma_D}(D)$ satisfying:

$$v_k \in H^1_{\Gamma_D}(D), \quad v_k(y) = N(x, y) \text{ for } y \in D \setminus \overline{\mathcal{V}}, \quad \text{and} \quad v_k(y) \xrightarrow{k \to 0} N(x, y) \text{ in } W^{1,1}(D).$$

We may now use $v = v_k$ in eq. (2.26) and take limits in the resulting expression because r_ε is smooth on $\mathcal{V}$. This yields:

$$\int_D \gamma_\varepsilon(y) \nabla r_\varepsilon(y) \cdot \nabla_y N(x, y) \, \mathrm{d}y = -\frac{1}{\varepsilon} \int_{\omega_{\sigma,\varepsilon}} (\gamma_1 - \gamma_0)(y) \nabla u_0(y) \cdot \nabla_y N(x, y) \, \mathrm{d}y;$$

combining this with eq. (2.27) finally results in:

$$r_\varepsilon(x) = \frac{1}{\varepsilon} \int_{\omega_{\sigma,\varepsilon}} (\gamma_1 - \gamma_0)(y) \nabla u_0(y) \cdot \nabla_y N(x, y) \, \mathrm{d}y + \int_{\omega_{\sigma,\varepsilon}} (\gamma_1 - \gamma_0)(y) \nabla r_\varepsilon(y) \cdot \nabla_y N(x, y) \, \mathrm{d}y, \tag{2.28}$$

which is the desired representation formula for $r_\varepsilon(x)$.

Step 2: We identify the behavior of the rescaled error inside the inclusion set $\omega_{\sigma,\varepsilon}$. This is the part where our derivation becomes formal. Let us introduce the mapping $m_\varepsilon : \omega_{\sigma,1} \to \omega_{\sigma,\varepsilon}$ defined by:

$$\forall x \in \omega_{\sigma,1}, \quad m_\varepsilon(x) = p_\sigma(x) + \varepsilon d_\sigma(x) n(p_\sigma(x)). \tag{2.29}$$

Using the material in Section 2.2.2, the derivative of m_ε reads, in the local basis $(\tau(x), n(x))$ of $\mathbb{R}^2$:

$$\nabla m_\varepsilon(x) = \begin{pmatrix} \frac{1 + \varepsilon d_\sigma(x) \kappa(x)}{1 + d_\sigma(x) \kappa(x)} & 0 \\ 0 & \varepsilon \end{pmatrix}. \tag{2.30}$$

We now seek the limiting behavior of the rescaled error $s_\varepsilon := r_\varepsilon \circ m_\varepsilon$ inside the unit inclusion set $\omega_{\sigma,1}$; this quantity will show up in the course of the third step below.

To this end, applying the classical Lax–Milgram theory to the variational problem eq. (2.26) allows to characterize r_ε as the unique solution to the following minimization problem:

$$\min_{u\in H^1_{\Gamma_D}(D)} E_\varepsilon(u), \quad \text{where } E_\varepsilon(u) := \frac{1}{2}\int_D \gamma_\varepsilon|\nabla u|^2\,\mathrm{d}x + \frac{1}{\varepsilon}\int_{\omega_{\sigma,\varepsilon}} (\gamma_1-\gamma_0)\nabla u_0\cdot\nabla u\,\mathrm{d}x. \tag{2.31}$$

Our strategy now outlines as follows: we construct an equivalent minimization problem from eq. (2.31), which involves both scales $(r_\varepsilon, s_\varepsilon)$ of the problem. The minimized objective $F_\varepsilon(u,v)$ depends on functions u which are defined "far" from $\omega_{\sigma,\varepsilon}$ and functions v defined on the rescaled inclusion $\omega_{\sigma,1}$. We then obtain information about the limiting behavior v of s_ε from the intuition that it should minimize the leading order terms of $F_\varepsilon(u,v)$ as $\varepsilon\to 0$.

More precisely, we transform the integrals on $\omega_{\sigma,\varepsilon}$ in eq. (2.31) into integrals posed over $\omega_{\sigma,1}$ by means of a change of variables via the mapping m_ε: the couple $(r_\varepsilon, s_\varepsilon)$ is then the solution to the two-scale minimization problem:

$$\min_{(u,v)\in V_\varepsilon} F_\varepsilon(u,v), \tag{2.32}$$

where the space V_ε is defined by:

$$V_\varepsilon = \left\{ (u,v)\in H^1_{\Gamma_D}(D)\times H^1(\omega_{\sigma,1}),\ \forall x\in\sigma,\ \begin{cases} v(x+n(x)) = u(x+\varepsilon n(x)) \\ v(x-n(x)) = u(x-\varepsilon n(x)) \end{cases} \right\},$$

and the two-scale energy $F_\varepsilon(u,v)$ reads:

$$\begin{aligned} F_\varepsilon(u,v) := \frac{1}{2}\int_{D\setminus\overline{\omega_{\sigma,\varepsilon}}} \gamma_0|\nabla u|^2\,\mathrm{d}x + \frac{1}{2}\int_{\omega_{\sigma,1}} (\gamma_1\circ m_\varepsilon)|\det\nabla m_\varepsilon|(\nabla m_\varepsilon^{-1}\nabla m_\varepsilon^{-T})\nabla v\cdot\nabla v\,\mathrm{d}x \\ + \frac{1}{\varepsilon}\int_{\omega_{\sigma,1}} ((\gamma_1-\gamma_0)\circ m_\varepsilon)|\det\nabla m_\varepsilon|(\nabla u_0)\circ m_\varepsilon\cdot(\nabla m_\varepsilon^{-T}\nabla v)\,\mathrm{d}x. \end{aligned}$$

An elementary calculation based on eq. (2.30) yields:

$$\begin{aligned} F_\varepsilon(u,v) := \frac{1}{2}\int_{D\setminus\overline{\omega_{\sigma,\varepsilon}}} \gamma_0|\nabla u|^2\,\mathrm{d}x + \frac{1}{2\varepsilon}\int_{\omega_{\sigma,1}} (\gamma_1\circ m_\varepsilon)\left(\frac{1+\varepsilon d_\sigma\kappa}{1+d_\sigma\kappa}\right)\left(\frac{\partial v}{\partial n}\right)^2\,\mathrm{d}x \\ + \frac{\varepsilon}{2}\int_{\omega_{\sigma,1}} (\gamma_1\circ m_\varepsilon)\left(\frac{1+d_\sigma\kappa}{1+\varepsilon d_\sigma\kappa}\right)\left(\frac{\partial v}{\partial\tau}\right)^2\,\mathrm{d}x + \int_{\omega_{\sigma,1}} ((\gamma_1-\gamma_0)\circ m_\varepsilon)\left(\frac{\partial u_0}{\partial\tau}\circ m_\varepsilon\right)\frac{\partial v}{\partial\tau}\,\mathrm{d}x \\ + \frac{1}{\varepsilon}\int_{\omega_{\sigma,1}} ((\gamma_1-\gamma_0)\circ m_\varepsilon)\left(\frac{1+\varepsilon d_\sigma\kappa}{1+d_\sigma\kappa}\right)\left(\frac{\partial u_0}{\partial n}\circ m_\varepsilon\right)\frac{\partial v}{\partial n}\,\mathrm{d}x. \end{aligned}$$

We now expect that the limiting behavior of $(r_\varepsilon, s_\varepsilon)$ as $\varepsilon\to 0$, which we denote by (u,v), should minimize in priority the terms weighted by $\frac{1}{\varepsilon}$ in the above expression of $F_\varepsilon(u,v)$. In other terms, the limiting behavior v of s_ε is the solution to the problem:

$$\begin{aligned} \min_{v\in H^1(\omega_{\sigma,1})} \widetilde{F}(v), \quad \text{where } \widetilde{F}(v) := \frac{1}{2}\int_{\omega_{\sigma,1}} (\gamma_1\circ p_\sigma)\left(\frac{1}{1+d_\sigma\kappa}\right)\left(\frac{\partial v}{\partial n}\right)^2\,\mathrm{d}x \\ + \int_{\omega_{\sigma,1}} ((\gamma_1-\gamma_0)\circ p_\sigma)\left(\frac{1}{1+d_\sigma\kappa}\right)\left(\frac{\partial u_0}{\partial n}\circ p_\sigma\right)\frac{\partial v}{\partial n}\,\mathrm{d}x. \end{aligned} \tag{2.33}$$

Writing down the associated Euler–Lagrange equation, we infer that, for any test function $\varphi\in H^1(\omega_{\sigma,1})$:

$$\int_{\omega_{\sigma,1}} (\gamma_1\circ p_\sigma)\left(\frac{1}{1+d_\sigma\kappa}\right)\frac{\partial v}{\partial n}\frac{\partial\varphi}{\partial n}\,\mathrm{d}x + \int_{\omega_{\sigma,1}} ((\gamma_1-\gamma_0)\circ p_\sigma)\left(\frac{1}{1+d_\sigma\kappa}\right)\left(\frac{\partial u_0}{\partial n}\circ p_\sigma\right)\frac{\partial\varphi}{\partial n}\,\mathrm{d}x = 0.$$

We now extract information about the desired limit function v from this equation. Applying the coarea formula of Proposition 2.6 and using test functions of the form

$$\varphi(p+tn(p)) = \psi(p)\zeta(t), \quad p \in \sigma,\ t \in [-1,1],$$

for arbitrary smooth functions $\psi \in \mathcal{C}^\infty(\sigma)$ and $\zeta \in \mathcal{C}^\infty([-1,1])$, we obtain:

$$\int_\sigma \gamma_1(p)\psi(p)\left(\int_{-1}^1 \frac{\mathrm{d}}{\mathrm{d}t}(v(p+tn(p)))\zeta'(t)\,\mathrm{d}t\right)\mathrm{d}\ell(p) \\ + \int_\sigma (\gamma_1(p)-\gamma_0(p))\psi(p)\frac{\partial u_0}{\partial n}(p)\left(\int_{-1}^1 \zeta'(t)\,\mathrm{d}t\right)\mathrm{d}\ell(p) = 0.$$

As a result, for any point $p \in \sigma$, the function $(-1,1) \ni t \mapsto v(p+tn(p))$ is affine (i.e. $\frac{\mathrm{d}^2}{\mathrm{d}t^2}(v(p+tn(p))) = 0$), and $\frac{\mathrm{d}}{\mathrm{d}t}(v(p+tn(p))) = \frac{\partial v}{\partial n}(p+tn(p))$ is the real value given by the relation:

$$\gamma_1(p)\frac{\partial v}{\partial n}(p+tn(p)) + (\gamma_1(p)-\gamma_0(p))\frac{\partial u_0}{\partial n}(p) = 0,$$

that is:

$$\frac{\partial v}{\partial n}(p+tn(p)) = -\frac{1}{\gamma_1(p)}(\gamma_1(p)-\gamma_0(p))\frac{\partial u_0}{\partial n}(p). \tag{2.34}$$

Note that we have not fully characterized the limiting function v for s_ε inside $\omega_{\sigma,1}$, but the above information is all that will be needed for our purpose; see Remark 2.8 and Section 5.4 about this point.

Step 3: We pass to the limit in the representation formula eq. (2.28). A change of variables in eq. (2.28) based on the mapping m_ε immediately brings into play the rescaled function s_ε:

$$\begin{aligned} r_\varepsilon(x) &= \frac{1}{\varepsilon}\int_{\omega_{\sigma,1}} |\det \nabla m_\varepsilon|((\gamma_1-\gamma_0)\circ m_\varepsilon)((\nabla u_0)\circ m_\varepsilon)\cdot\nabla_y N(x,m_\varepsilon(y))\,\mathrm{d}y \\ &\quad + \int_{\omega_{\sigma,1}} |\det \nabla m_\varepsilon|((\gamma_1-\gamma_0)\circ m_\varepsilon)\,\nabla m_\varepsilon^{-T}\nabla s_\varepsilon\cdot\nabla_y N(x,m_\varepsilon(y))\,\mathrm{d}y, \\ &= \int_{\omega_{\sigma,1}} \frac{1+\varepsilon d_\sigma\kappa}{1+d_\sigma\kappa}((\gamma_1-\gamma_0)\circ m_\varepsilon)((\nabla u_0)\circ m_\varepsilon)\cdot\nabla_y N(x,m_\varepsilon(y))\,\mathrm{d}y \\ &\quad + \int_{\omega_{\sigma,1}} (\gamma_1-\gamma_0)\circ m_\varepsilon\left(\varepsilon\frac{\partial s_\varepsilon}{\partial\tau}\frac{\partial N}{\partial\tau_y}(x,m_\varepsilon(y)) + \frac{1+\varepsilon d_\sigma\kappa}{1+d_\sigma\kappa}\frac{\partial s_\varepsilon}{\partial n}\frac{\partial N}{\partial n_y}(x,m_\varepsilon(y))\right)\mathrm{d}y. \end{aligned}$$

Now using the Lebesgue dominated convergence theorem, together with the (formal) convergence of s_ε to the function $v \in H^1(\omega_{\sigma,1})$ partially characterized by eq. (2.34), we obtain:

$$\lim_{\varepsilon\to 0} r_\varepsilon(x) = \int_{\omega_{\sigma,1}} \frac{1}{1+d_\sigma\kappa}((\gamma_1-\gamma_0)\circ p_\sigma)((\nabla u_0)\circ p_\sigma)\cdot\nabla_y N(x,p_\sigma(y))\,\mathrm{d}y \\ + \int_{\omega_{\sigma,1}} (\gamma_1-\gamma_0)\circ p_\sigma\frac{1}{1+d_\sigma\kappa}\frac{\partial v}{\partial n}\frac{\partial N}{\partial n_y}(x,p_\sigma(y))\,\mathrm{d}y, \tag{2.35}$$

where $v \in H^1(\omega_{\sigma,1})$ is the limiting behavior of s_ε derived in the course of the second step. Finally, it follows from the coarea formula of Proposition 2.6 and eq. (2.34) that:

$$\begin{aligned}
&\lim_{\varepsilon\to 0} r_\varepsilon(x) \\
&= 2\int_\sigma (\gamma_1-\gamma_0)(p)\nabla u_0(p)\cdot\nabla_y N(x,p)\,\mathrm{d}\ell(p) + \int_\sigma (\gamma_1-\gamma_0)(p)\left(\int_{-1}^1 \frac{\partial v}{\partial n}(p+tn(p))\,\mathrm{d}t\right)\frac{\partial N}{\partial n_y}(x,p)\,\mathrm{d}\ell(p), \\
&= 2\int_\sigma (\gamma_1-\gamma_0)(p)\nabla u_0(p)\cdot\nabla_y N(x,p)\,\mathrm{d}\ell(p) - 2\int_\sigma (\gamma_1-\gamma_0)(p)\left(1-\frac{\gamma_0(p)}{\gamma_1(p)}\right)\frac{\partial u_0}{\partial n}(p)\frac{\partial N}{\partial n_y}(x,p)\,\mathrm{d}\ell(p), \\
&= 2\int_\sigma (\gamma_1-\gamma_0)(p)\frac{\partial u_0}{\partial \tau}(p)\frac{\partial N}{\partial \tau_y}(x,p)\,\mathrm{d}\ell(p) + 2\int_\sigma \gamma_0(p)\left(1-\frac{\gamma_0(p)}{\gamma_1(p)}\right)\frac{\partial u_0}{\partial n}(p)\frac{\partial N}{\partial n_y}(x,p)\,\mathrm{d}\ell(p),
\end{aligned}$$

which is the desired expression.

Remark 2.8. As we have mentioned, the limiting behavior v of the rescaled error s_ε inside the unit inclusion $\omega_{\sigma,1}$ is not completely determined by our analysis; only the normal derivative eq. (2.34) is. The main reason is that the "near field" v depends on the "far field" u, i.e. the limiting behavior of the error r_ε "far" from σ, in an non trivial way. Actually, injecting the information eq. (2.34) back into the two-scale minimization problem eq. (2.32) and arguing as in [54] (in particular, pursuing the strategy of minimizing only leading order terms as $\varepsilon \to 0$) would provide another minimization problem satisfied by the "far field" u, which is exactly that associated to the equation eq. (2.15) satisfied by the function u_1 in the expansion eq. (2.5). As we shall see in Section 5.4, a completely different phenomenon occurs in 3d, where the "near field" function v can be explicitly characterized, independently of the "far field" u.

2.3. Asymptotic expansion of an observable involving the solution to the conductivity equation

In this section, we investigate more precisely the asymptotic behavior of the quantity of interest $J_\sigma(\varepsilon)$ defined in eq. (2.7) as $\varepsilon \to 0$. Let us start with a preliminary lemma.

Lemma 2.9. *The function $J_\sigma(\varepsilon)$ is differentiable at $\varepsilon = 0$ and its derivative reads:*

$$J'_\sigma(0) = \int_D j'(u_0)u_1\,\mathrm{d}x, \tag{2.36}$$

where u_1 is defined in eq. (2.5).

Proof. Let us first deal with the differentiability of $J_\sigma(\varepsilon)$ at $\varepsilon = 0$; a simple use of Taylor's formula yields:

$$\frac{J_\sigma(\varepsilon)-J_\sigma(0)}{\varepsilon} = \int_D\int_0^1 j'(u_0+t(u_\varepsilon-u_0))\frac{u_\varepsilon-u_0}{\varepsilon}\,\mathrm{d}t\,\mathrm{d}x.$$

The previous Theorem 2.1 shows the pointwise convergence of the sequence of functions $\frac{u_\varepsilon-u_0}{\varepsilon}$. Now invoking the growth condition eq. (2.8) together with the uniform integrability of the sequence of functions supplied by Lemma B.1, the Vitali convergence theorem (see e.g. [36]) allows to pass to the limit $\varepsilon \to 0$ in the above expression. As a result, $J_\sigma(\varepsilon)$ is differentiable at $\varepsilon = 0$, with derivative eq. (2.36). ∎

The formula supplied by Lemma 2.9 is unfortunately difficult to handle, since it involves the function u_1, which depends on σ either via the integral eq. (2.5) involving the Green's function $N(x,y)$, or in an implicit manner, via the solution u_1 to eq. (2.15) where σ plays the role of a "parameter". This difficulty is classical in shape optimization, and in optimal control in general, and it can be overcome

thanks to the introduction of a suitable adjoint state, which allows to make explicit the dependence of $J'_\sigma(0)$ on σ.

Proposition 2.10. *The derivative $J'_\sigma(0)$ rewrites:*

$$\begin{aligned} J'_\sigma(0) &= 2\int_\sigma \gamma_0\left(1-\frac{\gamma_0}{\gamma_1}\right)\frac{\partial u_0}{\partial n}\frac{\partial p_0}{\partial n}\,\mathrm{d}\ell + 2\int_\sigma(\gamma_1-\gamma_0)\frac{\partial u_0}{\partial \tau}\frac{\partial p_0}{\partial \tau}\,\mathrm{d}\ell, \\ &= \int_\sigma \mathcal{M}\nabla u_0\cdot\nabla p_0\,\mathrm{d}\ell, \end{aligned} \tag{2.37}$$

where the polarization tensor $\mathcal{M}$ is that given in eq. (2.6)*, and the adjoint state $p_0 \in H^1_{\Gamma_D}(D)$ is the unique solution to the equation:*

$$\begin{cases} -\operatorname{div}(\gamma_0\nabla p_0) = -j'(u_0) & \text{in } D, \\ p_0 = 0 & \text{on } \Gamma_D, \\ \gamma_0\frac{\partial p_0}{\partial n} = 0 & \text{on } \partial D\setminus\overline{\Gamma_D}. \end{cases} \tag{2.38}$$

Proof. Injecting the integral representation eq. (2.5) for u_1 into the formula eq. (2.36) for $J'_\sigma(0)$, we obtain:

$$\begin{aligned} J'_\sigma(0) &= \int_D\int_\sigma j'(u_0)(x)\left(2(\gamma_1-\gamma_0)(y)\frac{\partial u_0}{\partial \tau_y}(y)\frac{\partial N}{\partial \tau_y}(x,y)+2\left(\frac{\gamma_0}{\gamma_1}(\gamma_1-\gamma_0)\right)(y)\frac{\partial u_0}{\partial n}(y)\frac{\partial N}{\partial n_y}(x,y)\right)\mathrm{d}\ell(y)\,\mathrm{d}x, \\ &= 2\int_\sigma(\gamma_1-\gamma_0)(y)\frac{\partial u_0}{\partial \tau}(y)\frac{\partial}{\partial \tau_y}\left(\int_D \operatorname{div}(\gamma_0\nabla p_0)(x)N(x,y)\,\mathrm{d}x\right)\mathrm{d}\ell(y) \\ &\quad + 2\int_\sigma\left(\frac{\gamma_0}{\gamma_1}(\gamma_1-\gamma_0)\right)(y)\frac{\partial u_0}{\partial n}(y)\frac{\partial}{\partial n_y}\left(\int_D \operatorname{div}(\gamma_0\nabla p_0)(x)N(x,y)\,\mathrm{d}x\right)\mathrm{d}\ell(y), \end{aligned}$$

where the second line follows from the Fubini theorem and the first line in the definition eq. (2.38) of p_0.
On the other hand, using the definition eq. (2.9) of the Green's function $N(x,y)$, and its symmetry with respect to its arguments, it holds, for an arbitrary point $y\in\sigma$,

$$\int_D \operatorname{div}(\gamma_0\nabla p_0)(x)N(x,y)\,\mathrm{d}x = p_0(y).$$

Hence,

$$J'_\sigma(0) = 2\int_\sigma(\gamma_1-\gamma_0)\frac{\partial u_0}{\partial \tau}\frac{\partial p_0}{\partial \tau}\mathrm{d}\ell + 2\int_\sigma\gamma_0\left(1-\frac{\gamma_0}{\gamma_1}\right)\frac{\partial u_0}{\partial n}\frac{\partial p_0}{\partial n}\mathrm{d}\ell.$$

which is the desired formula eq. (2.37). ∎

Remark 2.11. Interestingly, eq. (2.37) can be derived from eq. (2.36) by using the system eq. (2.15) for characterizing u_1, instead of its integral representation eq. (2.5), at least when the curve σ is closed. Indeed, under this assumption, injecting the definition of the adjoint state p_0 into eq. (2.36) and integrating by parts, we obtain:

$$\begin{aligned} J'_\sigma(0) &= \int_{D\setminus\overline{\sigma}} \operatorname{div}(\gamma_0\nabla p_0)u_1\,\mathrm{d}x, \\ &= -\int_\sigma \gamma_0\frac{\partial p_0}{\partial n}[u_1]\,\mathrm{d}\ell - \int_D \gamma_0\nabla p_0\cdot\nabla u_1\,\mathrm{d}x, \\ &= 2\int_\sigma\gamma_0\left(1-\frac{\gamma_0}{\gamma_1}\right)\frac{\partial u_0}{\partial n}\frac{\partial p_0}{\partial n}\,\mathrm{d}\ell - \int_D\gamma_0\nabla p_0\cdot\nabla u_1\,\mathrm{d}x. \end{aligned}$$

Now using the variational formulation attached to eq. (2.15) (and since $p_0 \in H^1_{\Gamma_D}(D) \subset H^1_{\Gamma_D}(D \setminus \sigma)$), we get:

$$\begin{aligned}\int_D \gamma_0 \nabla u_1 \cdot \nabla p_0 \, \mathrm{d}x &= -\int_\sigma \left[\gamma_0 \frac{\partial u_1}{\partial n}\right] p_0 \, \mathrm{d}\ell, \\ &= 2\int_\sigma \frac{\partial}{\partial \tau}\left((\gamma_1 - \gamma_0)\frac{\partial u_0}{\partial \tau}\right) p_0 \, \mathrm{d}\ell.\end{aligned}$$

Combining both expressions, and using integration by parts on σ in the last integral of the above right-hand side, we retrieve eq. (2.37).

Remark 2.12. The particular form eq. (2.7) of functionals $J_\sigma(\varepsilon)$ considered in Proposition 2.10 is only a means to set ideas, and multiple other functionals could be handled in exactly the same way, such as integral quantities involving the trace of the perturbed potential u_ε on a fixed region of ∂D, or "stress-based" criteria based on the gradient ∇u_ε.

With a little anticipation on Section 7, let us finally comment about the practical interest of this result. The quantities u_0 and p_0 only depend on the "background" configuration, and the structure eq. (2.37) makes it easy to identify a curve σ making the derivative $J'_\sigma(0)$ negative, indicating that a tubular inclusion with small enough width ε, filled by a material with conductivity γ_1 "improves" this background configuration, as measured in terms of $J_\sigma(\varepsilon)$. This task is made even easier by the straightforward reformulation of eq. (2.37):

$$J'_\sigma(0) = \int_\sigma P(x, \tau_1(x), \tau_2(x)) \mathrm{d}\ell(x),$$

where $P(x, \cdot, \cdot)$ is the bivariate, homogeneous polynomial of degree two defined for $x \in \sigma$ by:

$$P(x, \tau_1, \tau_2) = \beta_1(x)\tau_1^2 + \beta_2(x)\tau_1\tau_2 + \beta_3(x)\tau_2^2,$$

with the explicit expressions of the coefficients:

$$\beta_1 = 2(\gamma_1 - \gamma_0)\frac{\partial u_0}{\partial x_1}\frac{\partial p_0}{\partial x_1} + 2\gamma_0\left(1 - \frac{\gamma_0}{\gamma_1}\right)\frac{\partial u_0}{\partial x_2}\frac{\partial p_0}{\partial x_2}, \quad \beta_2 = \frac{2}{\gamma_1}(\gamma_1 - \gamma_0)^2\left(\frac{\partial u_0}{\partial x_1}\frac{\partial p_0}{\partial x_2} + \frac{\partial u_0}{\partial x_2}\frac{\partial p_0}{\partial x_1}\right),$$

and

$$\beta_3 = 2\gamma_0\left(1 - \frac{\gamma_0}{\gamma_1}\right)\frac{\partial u_0}{\partial x_1}\frac{\partial p_0}{\partial x_1} + 2(\gamma_1 - \gamma_0)\frac{\partial u_0}{\partial x_2}\frac{\partial p_0}{\partial x_2},$$

where the dependence with respect to x is omitted for brevity.

3. Thin tubular inhomogeneities in the context of the 2d linear elasticity system

In this section, we examine the effect of thin tubular inhomogeneities inside a background elastic medium. Up to an increased level of technicality, our analyses are very close in spirit to those conducted in Section 2, in the context of the 2d conductivity equation. In order to emphasize the parallel between both situations, we reuse the notations in there insofar as possible.

3.1. Presentation of the 2d linear elasticity setting and statement of the main results

3.1.1. *The background and perturbed linearized elasticity systems*

In the present context, the bounded and Lipschitz domain $D \subset \mathbb{R}^2$ represents a structure which is clamped on a subset Γ_D of its boundary ∂D; traction loads $g : \Gamma_N \to \mathbb{R}^2$ are applied on a disjoint subset Γ_N of ∂D, and body forces $f : D \to \mathbb{R}^2$ are assumed. The structure is filled with an isotropic,

linearly elastic material with inhomogeneous, smooth Hooke's tensor $A_0(x)$: for any element e in the set $\mathcal{S}_2(\mathbb{R})$ of symmetric 2×2 matrices,

$$A_0(x)e = 2\mu_0(x)e + \lambda_0(x)\,\mathrm{tr}(e)\mathrm{I}, \tag{3.1}$$

where the Lamé coefficients μ_0 and λ_0 belong to $\mathcal{C}^\infty(\overline{D})$ and satisfy in addition:

$$\forall x \in D, \quad \gamma_- \leq \mu_0(x) \leq \gamma_+, \text{ and } \gamma_- \leq \lambda_0(x) + \mu_0(x) \leq \gamma_+, \tag{3.2}$$

for some positive constants $0 < \gamma_- < \gamma_+$.

The displacement field $u_0 \in H^1_{\Gamma_D}(D)^2$ in the above situation is the unique solution to the system:

$$\begin{cases} -\operatorname{div}(A_0 e(u_0)) = f & \text{in } D, \\ u_0 = 0 & \text{on } \Gamma_D, \\ A_0 e(u_0) n = g & \text{on } \Gamma_N, \\ A_0 e(u_0) n = 0 & \text{on } \partial D \setminus (\overline{\Gamma_D} \cup \overline{\Gamma_N}), \end{cases} \tag{3.3}$$

where $e(u) := \frac{1}{2}(\nabla u + \nabla u^T)$ is the strain tensor associated to a vector field $u : D \to \mathbb{R}^2$. Throughout the sequel, we assume smooth enough data f, g; elliptic regularity then implies that the background displacement u_0 is smooth in the interior of D.

We now consider the situation where the medium A_0 is perturbed by a thin tubular inclusion $\omega_{\sigma,\varepsilon}$ of the form eq. (2.3), filled by another elastic material with smooth, inhomogeneous Hooke's law $A_1(x)$, whose coefficients $\lambda_1, \mu_1 \in \mathcal{C}^\infty(\overline{D})$ also satisfy eq. (3.2). The perturbed elastic displacement $u_\varepsilon \in H^1_{\Gamma_D}(D)^2$ is then characterized by:

$$\begin{cases} -\operatorname{div}(A_\varepsilon e(u_\varepsilon)) = f & \text{in } D, \\ u_\varepsilon = 0 & \text{on } \Gamma_D, \\ A_\varepsilon e(u_\varepsilon) n = g & \text{on } \Gamma_N, \\ A_\varepsilon e(u_\varepsilon) n = 0 & \text{on } \partial D \setminus (\overline{\Gamma_D} \cup \overline{\Gamma_N}), \end{cases} \quad \text{where } A_\varepsilon(x) = \begin{cases} A_1(x) & \text{if } x \in \omega_{\sigma,\varepsilon}, \\ A_0(x) & \text{otherwise.} \end{cases} \tag{3.4}$$

3.1.2. *The Green's function of the linear elasticity system*

Like in Section 2, our goal is to obtain an asymptotic expansion for the perturbed displacement field u_ε (and a related quantity of interest) of the form:

$$u_\varepsilon = u_0 + \varepsilon u_1 + \mathrm{o}(\varepsilon),$$

where the first-order term u_1 has yet to be identified. The precise statement of the result involves, again, the Green's function $N(x, y)$ of the background operator in eq. (3.3). Here, $N(x, y)$ is defined for $x \neq y \in D$ as a 2×2 matrix; for $x \in D$ and $j = 1, 2$, its j^{th} column vector $y \mapsto N_j(x, y)$ is the solution to:

$$\begin{cases} \operatorname{div}_y(A_0(y) e_y(N_j(x,y))) = \delta_{y=x}\xi_j & \text{in } D, \\ A_0(y) e_y(N_j(x,y)) n = 0 & \text{on } \partial D \setminus \overline{\Gamma_D}, \\ N_j(x,y) = 0 & \text{on } \Gamma_D, \end{cases} \tag{3.5}$$

where ξ_j is the j^{th} coordinate vector of $\mathbb{R}^2$.

The Green's function $N(x, y)$ is naturally related to the (modified) fundamental solution of the linearized elasticity operator in the free space – the so-called Kelvin matrix $\Gamma_{ij}(x, y)$, given by:

$$\Gamma_{ij}(x,y) = \frac{\alpha_\Gamma(x)}{2\pi} \log|x-y| \delta_{ij} - \frac{\beta_\Gamma(x)}{2\pi} \frac{(x_i - y_i)(x_j - y_j)}{|x-y|^2}, \quad x \neq y \in \mathbb{R}^2, \quad i, j = 1, 2,$$

where

$$\alpha_\Gamma := \frac{1}{2}\left(\frac{1}{\mu_0} + \frac{1}{2\mu_0 + \lambda_0}\right) \quad \text{and} \quad \beta_\Gamma := \frac{1}{2}\left(\frac{1}{\mu_0} - \frac{1}{2\mu_0 + \lambda_0}\right); \tag{3.6}$$

see [19, 70, 84] for properties of this matrix. More precisely, it holds

$$N(x,y) = \Gamma(x,y) + R(x,y),$$

where the remainder $R(x,y)$ is "smooth enough" – it satisfies eq. (2.12), as in the case of the 2d conductivity equation.

Again, the structure of the sought expansion of the perturbed displacement u_ε (see Theorem 3.2 below) builds upon the layer potential operators associated to the base curve σ. In this context, we introduce the (vector-valued) *single layer potential* $\mathcal{S}_\sigma\varphi$ associated to a (vector-valued) density function $\varphi \in \mathcal{C}^{0,l}(\sigma)^2$ $(0 < l < 1)$:

$$\forall x \in D \setminus \sigma, \quad \mathcal{S}_\sigma\varphi(x) = \int_\sigma N(x,y)\varphi(y)\,\mathrm{ds}(y),$$

and the *double layer potential* $\mathcal{D}_\sigma\varphi$ of φ is:

$$\forall x \in D \setminus \sigma, \quad \mathcal{D}_\sigma\varphi(x) = \int_\sigma (A_0 e_y(N(x,y))n(y))\varphi(y)\,\mathrm{ds}(y).$$

In the above formula, $(A_0 e_y(N(x,y))n(y))$ is by definition the 2×2 matrix where the conormal derivative operator $A_0 e_y(\cdot)n$ is applied *row-wise*. Explicitly, using Cartesian coordinates:

$$(\mathcal{D}_\sigma\varphi(x))_m = \int_\sigma \left(\lambda_0 \left(\sum_{i=1}^d \frac{\partial N_{mi}}{\partial y_i}(x,y)\right)\varphi\cdot n + \mu_0 \sum_{i,j=1}^d \left(\frac{\partial N_{mi}}{\partial y_j}(x,y) + \frac{\partial N_{mj}}{\partial y_i}(x,y)\right) n_i\varphi_j\right)\mathrm{ds}(y);$$

see [19] about these matters.

The jump relations for the single- and double-layer potentials read, in the present context:

$$[\mathcal{S}_\sigma\varphi] = 0, \quad [A_0 e(\mathcal{S}_\sigma\varphi)n] = \varphi, \quad [\mathcal{D}_\sigma\varphi] = -\varphi \quad \text{and} \quad [A_0 e(\mathcal{D}_\sigma\varphi)n] = 0 \text{ on } \sigma. \tag{3.7}$$

Remark 3.1. Again, the above considerations extend to the three-dimensional case, up to the different definition of the Kelvin matrix:

$$\Gamma_{ij}(x,y) = -\frac{\alpha_\Gamma(x)}{4\pi}\frac{1}{|x-y|}\delta_{ij} - \frac{\beta_\Gamma(x)}{4\pi}\frac{(x_i-y_i)(x_j-y_j)}{|x-y|^3}, \quad i,j = 1,2,3,$$

where α_Γ and β_Γ are still given by eq. (3.6).

3.1.3. *Statement of the asymptotic expansion of the displacement u_ε*

The asymptotic behavior of the displacement u_ε as the thickness ε of the ligament $\omega_{\sigma,\varepsilon}$ vanishes is described in the following theorem, whose rigorous proof can be found in [33].

Theorem 3.2. *For an arbitrary point $x \in D \setminus \sigma$, the following asymptotic expansion holds:*

$$u_\varepsilon(x) = u_0(x) + \varepsilon u_1(x) + \mathrm{o}(\varepsilon), \quad \textit{where } u_1(x) = \int_\sigma \mathcal{M}(y)e(u_0) : e_y(N(x,y))\,\mathrm{d}\ell(y), \tag{3.8}$$

and the $\mathrm{o}(\varepsilon)$ is uniform when x is confined to a compact subset $K \subset D \setminus \sigma$. The polarization tensor $\mathcal{M}(y)$ reads, for any symmetric 2×2 matrix $e \in \mathcal{S}_2(\mathbb{R})$:

$$\mathcal{M}(y)e = \alpha_T(y)\,\mathrm{tr}(e)\mathrm{I} + \beta_T(y)e + \gamma_T(y)(e\tau\cdot\tau)\tau\otimes\tau + \delta_T(y)(en\cdot n)n\otimes n,$$

where the coefficients $\alpha_T, \beta_T, \gamma_T$ and δ_T are given by:

$$\alpha_T = 2(\lambda_1-\lambda_0)\frac{\lambda_0+2\mu_0}{\lambda_1+2\mu_1}, \quad \beta_T = 4(\mu_1-\mu_0)\frac{\mu_0}{\mu_1},$$

and

$$\gamma_T = 4(\mu_1-\mu_0)\left(\frac{2\lambda_1+2\mu_1-\lambda_0}{\lambda_1+2\mu_1} - \frac{\mu_0}{\mu_1}\right), \quad \delta_T = 4(\mu_1-\mu_0)\frac{\mu_1\lambda_0-\mu_0\lambda_1}{\mu_1(\lambda_1+2\mu_1)}.$$

One comment is in order about the notation employed in eq. (3.8): $\mathcal{M}(y)e(u_0) : e_y(N(x,y))$ is the vector field with components:

$$(\mathcal{M}(y)e(u_0) : e(N(x,y)))_j = \mathcal{M}(y)e(u_0) : e_y(N_j(x,y)), \quad j = 1,2;$$

i.e. the j^{th} component of $\mathcal{M}(y)e(u_0) : e_y(N(x,y))$ is the Frobenius inner product between the strain tensors of u_0 and the j^{th} column of the Green's function.

Equivalently, using the jump relations eq. (3.7) for the single and double layer potential operators, the first-order term u_1 in the above expansion can be seen as the solution to the system:

$$\begin{cases} -\operatorname{div}(A_0 e(u_1)) = 0 & \text{in } D \setminus \sigma, \\ u_1 = 0 & \text{on } \Gamma_D, \\ A_0 e(u_1) n = 0 & \text{on } \partial D \setminus \overline{\Gamma_D}, \\ [u_1 \cdot \tau] = -4\left(1 - \frac{\mu_0}{\mu_1}\right) e(u_0)_{\tau n}(x) & \text{on } \sigma, \\ [u_1 \cdot n] = -2\left(1 - \frac{2\mu_0+\lambda_0}{2\mu_1+\lambda_1}\right) e(u_0)(x)_{nn} - 2\left(\frac{\lambda_1-\lambda_0}{2\mu_1+\lambda_1}\right) e(u_0)_{\tau\tau}(x) & \text{on } \sigma, \\ [A_0 e(u_1) n] \cdot \tau = -2\frac{\partial a}{\partial \tau}(x) & \text{on } \sigma, \\ [A_0 e(u_1) n] \cdot n = 2\kappa a(x) & \text{on } \sigma, \end{cases} \tag{3.9}$$

where the scalar field $a : \sigma \to \mathbb{R}$ is defined by:

$$a = \left(4\mu_1 \frac{\mu_1 - \mu_0 + \lambda_1}{2\mu_1 + \lambda_1} - 2\frac{\mu_0\lambda_1 - \mu_1\lambda_0}{2\mu_1 + \lambda_1}\right) e(u_0)_{\tau\tau} + 2\left(\frac{\mu_0\lambda_1 - \mu_1\lambda_0}{2\mu_1 + \lambda_1}\right) e(u_0)_{nn}.$$

Again, this solution is "variational" and it belongs to the space $H^1_{\Gamma_D}(D \setminus \sigma)^2$ when σ is a closed curve; when σ is open, the functional setting is a little more involved, and similar to that outlined in Section 2.2.1 in the case of the conductivity equation. We do not elaborate on these issues, since they are not needed in the sequel.

3.2. Formal derivation of the asymptotic expansion of u_ε when σ is a closed curve

In this section, we show how the asymptotic expansion eq. (3.8), which was rigorously established in [33], can be derived from a simple adaptation of the heuristic energy argument exposed in Section 2.2.3. Still under the assumption that σ is closed, we follow the same trail as in there, and for this reason, we only sketch the calculation.

Let us introduce the difference $r_\varepsilon := \frac{1}{\varepsilon}(u_\varepsilon - u_0) \in H^1_{\Gamma_D}(D)^2$, which is the solution to the following variational problem:

$$\forall v \in H^1_{\Gamma_D}(D)^2, \quad \int_D A_\varepsilon e(r_\varepsilon) : e(v)\,\mathrm{d}x = -\frac{1}{\varepsilon}\int_{\omega_{\sigma,\varepsilon}} (A_1 - A_0)e(u_0) : e(v)\,\mathrm{d}x. \tag{3.10}$$

Equivalently, r_ε is the unique solution to the minimization problem:

$$\min_{u \in H^1_{\Gamma_D}(D)^2} E_\varepsilon(u), \quad \text{where } E_\varepsilon(u) := \frac{1}{2}\int_D A_\varepsilon e(u) : e(u)\,\mathrm{d}x + \frac{1}{\varepsilon}\int_{\omega_{\sigma,\varepsilon}} (A_1 - A_0)e(u_0) : e(u)\,\mathrm{d}x. \tag{3.11}$$

Like in Section 2.2.3, we proceed in three steps.

Step 1: We establish a representation formula for the error $r_\varepsilon(x)$ at points $x \in D \setminus \sigma$ in terms of the Green's function $N(x,y)$ in eq. (3.5) and the values of r_ε inside $\omega_{\sigma,\varepsilon}$. A calculation analogous to eq. (2.28) yields, for either component $j = 1, 2$ of the error $r_\varepsilon(x)$:

$$\begin{aligned} r_{\varepsilon,j}(x) &= \int_D \mathrm{div}_y(A_0(y)e_y(N_j(x,y))) \cdot r_\varepsilon(y)\,\mathrm{d}y, \\ &= -\int_D A_0(y)e(r_\varepsilon)(y) : e_y(N_j(x,y)))\,\mathrm{d}y, \\ &= -\int_D A_\varepsilon(y)e(r_\varepsilon)(y) : e_y(N_j(x,y)))\,\mathrm{d}y + \int_{\omega_{\sigma,\varepsilon}} (A_1 - A_0)(y)e(r_\varepsilon)(y) : e_y(N_j(x,y))\,\mathrm{d}y. \end{aligned}$$

Now repeating the argument used in the first step of our derivation in Section 2.2.3, we may "insert" $y \mapsto N_j(x,y)$ as test function in the variational formulation eq. (3.10) for r_ε. The first integral in the above right-hand side then rewrites:

$$\int_D A_\varepsilon(y)e(r_\varepsilon)(y) : e_y(N_j(x,y)))\,\mathrm{d}y = -\frac{1}{\varepsilon}\int_{\omega_{\sigma,\varepsilon}} (A_1 - A_0)(y)e(u_0)(y) : e_y(N_j(x,y)))\,\mathrm{d}y,$$

and so:

$$\begin{aligned} r_{\varepsilon,j}(x) = \frac{1}{\varepsilon}\int_{\omega_{\sigma,\varepsilon}} (A_1 - A_0)(y)e(u_0)(y) : e_y(N_j(x,y)))\,\mathrm{d}y \\ + \int_{\omega_{\sigma,\varepsilon}} (A_1 - A_0)(y)e(r_\varepsilon)(y) : e_y(N_j(x,y))\,\mathrm{d}y, \end{aligned} \quad (3.12)$$

which is the desired representation formula.

Step 2: We examine the limiting behavior of the rescaled error $s_\varepsilon := r_\varepsilon \circ m_\varepsilon$ inside $\omega_{\sigma,\varepsilon}$. To this end, we construct an equivalent two-scale minimization counterpart for the problem eq. (3.15), satisfied by the couple $(r_\varepsilon, s_\varepsilon)$, thanks to a rescaling via the mapping m_ε in eqs. (2.29) and (2.30); we then simplify the involved energy functional by retaining only the leading order terms as $\varepsilon \to 0$.

Before we do so, let us recall the following elementary fact from calculus: if $\varphi : \mathcal{V} \to \mathcal{U}$ is a smooth diffeomorphism between two open sets $\mathcal{V}, \mathcal{U} \subset \mathbb{R}^2$ and $u : \mathcal{U} \to \mathbb{R}^2$ is a smooth vector field, then

$$e(u) \circ \varphi = \frac{1}{2}\left(\nabla(u \circ \varphi)\nabla\varphi^{-1} + \nabla\varphi^{-T}\nabla(u \circ \varphi)^T\right), \text{ and } (\mathrm{div}\, u) \circ \varphi = \mathrm{tr}(\nabla(u \circ \varphi)\nabla\varphi^{-1}).$$

Hence, a change of variables yields, for an arbitrary vector field $u \in H^1_{\Gamma_D}(D)^2$:

$$\begin{aligned} &\int_{\omega_{\sigma,\varepsilon}} A_1 e(u) : e(u)\,\mathrm{d}x \\ &= \int_{\omega_{\sigma,1}} |\det \nabla m_\varepsilon| \left(2\mu_1 \frac{1}{2}\left(\nabla v \nabla m_\varepsilon^{-1} + \nabla m_\varepsilon^{-T}\nabla v^T\right) : \frac{1}{2}\left(\nabla v \nabla m_\varepsilon^{-1} + \nabla m_\varepsilon^{-T}\nabla v^T\right) + \lambda_1\,\mathrm{tr}(\nabla v \nabla m_\varepsilon^{-1})^2\right)\mathrm{d}x, \end{aligned}$$

where we have denoted $v = u \circ m_\varepsilon$. After some calculation, this rewrites:

$$\begin{aligned} \int_{\omega_{\sigma,\varepsilon}} A_1 e(u) : e(u)\,\mathrm{d}x = \int_{\omega_{\sigma,1}} 2\mu_1 \varepsilon \frac{1 + \varepsilon d_\sigma \kappa}{1 + d_\sigma \kappa} \Bigg(\left(\frac{1 + d_\sigma\kappa}{1 + \varepsilon d_\sigma \kappa}\right)^2 (\nabla v\tau \cdot \tau)^2 + \frac{1}{\varepsilon^2}(\nabla v n \cdot n)^2 \\ + \frac{1}{2}\left(\frac{1}{\varepsilon}\nabla v n \cdot \tau + \frac{1 + d_\sigma\kappa}{1 + \varepsilon d_\sigma\kappa}\nabla v\tau \cdot n\right)^2\Bigg)\mathrm{d}x \\ + \int_{\omega_{\sigma,1}} \lambda_1 \varepsilon \frac{1 + \varepsilon d_\sigma\kappa}{1 + d_\sigma\kappa}\left(\frac{1 + d_\sigma\kappa}{1 + \varepsilon d_\sigma\kappa}\nabla v\tau \cdot \tau + \frac{1}{\varepsilon}\nabla v n \cdot n\right)^2 \mathrm{d}x. \end{aligned} \quad (3.13)$$

By the same token, we also get:

$$\begin{aligned}
&\int_{\omega_{\sigma,\varepsilon}} (A_1 - A_0)e(u_0) : e(u)\,\mathrm{d}x \\
&\quad = \int_{\omega_{\sigma,1}} 2(\mu_1-\mu_0)\varepsilon\frac{1+\varepsilon d_\sigma\kappa}{1+d_\sigma\kappa}\left(\frac{1+d_\sigma\kappa}{1+\varepsilon d_\sigma\kappa}((\nabla u_0\circ m_\varepsilon)\tau\cdot\tau)(\nabla v\tau\cdot\tau)\right)\mathrm{d}x, \\
&\qquad + \int_{\omega_{\sigma,1}} 2(\mu_1-\mu_0)\varepsilon\frac{1+\varepsilon d_\sigma\kappa}{1+d_\sigma\kappa}\left(\frac{1}{\varepsilon}((\nabla u_0\circ m_\varepsilon)n\cdot n)(\nabla v n\cdot n)\right)\mathrm{d}x \\
&\qquad + \int_{\omega_{\sigma,1}} 2(\mu_1-\mu_0)\varepsilon\frac{1+\varepsilon d_\sigma\kappa}{1+d_\sigma\kappa}\left((e(u_0)_{\tau n}\circ m_\varepsilon)\,(\frac{1}{\varepsilon}\nabla v n\cdot\tau + \frac{1+d_\sigma\kappa}{1+\varepsilon d_\sigma\kappa}\nabla v\tau\cdot n)\right)\mathrm{d}x \\
&\qquad\quad + \int_{\omega_{\sigma,1}} (\lambda_1-\lambda_0)\varepsilon\frac{1+\varepsilon d_\sigma\kappa}{1+d_\sigma\kappa}((\operatorname{div} u_0)\circ m_\varepsilon)\,\left(\frac{1+d_\sigma\kappa}{1+\varepsilon d_\sigma\kappa}\nabla v\tau\cdot\tau + \frac{1}{\varepsilon}\nabla v n\cdot n\right)\mathrm{d}x. \quad (3.14)
\end{aligned}$$

Collecting eqs. (3.13) and (3.14), the couple $(r_\varepsilon, s_\varepsilon)$ is the solution to the following two-scale minimization problem:

$$\min_{(u,v)\in V_\varepsilon} F_\varepsilon(u,v), \quad \text{where } F_\varepsilon(u,v) = \frac{1}{\varepsilon}F_\varepsilon^1(u,v) + F_\varepsilon^2(u,v), \tag{3.15}$$

and we have denoted

$$\begin{aligned}
F_\varepsilon^1(u,v) := \frac{1}{2}\int_{\omega_{\sigma,1}} &\frac{1+\varepsilon d_\sigma\kappa}{1+d_\sigma\kappa}\left((2\mu_1+\lambda_1)(\nabla v n\cdot n)^2 + \mu_1(\nabla v n\cdot\tau)^2\right)\mathrm{d}x \\
&+ \int_{\omega_{\sigma,1}} 2(\mu_1-\mu_0)\frac{1+\varepsilon d_\sigma\kappa}{1+d_\sigma\kappa}\left(((\nabla u_0\circ m_\varepsilon)n\cdot n)(\nabla v n\cdot n)\right)\mathrm{d}x \\
&+ \int_{\omega_{\sigma,1}} 2(\mu_1-\mu_0)\frac{1+\varepsilon d_\sigma\kappa}{1+d_\sigma\kappa}(e(u_0)_{\tau n}\circ m_\varepsilon)(\nabla v n\cdot\tau)\,\mathrm{d}x \\
&+ \int_{\omega_{\sigma,1}} (\lambda_1-\lambda_0)\frac{1+\varepsilon d_\sigma\kappa}{1+d_\sigma\kappa}((\operatorname{div} u_0)\circ m_\varepsilon)\,(\nabla v n\cdot n)\,\mathrm{d}x. \quad (3.16)
\end{aligned}$$

The quantity $F_\varepsilon^2(u,v)$ in eq. (3.15) is made of terms whose coefficients are of order $\mathcal{O}(1)$ as $\varepsilon\to 0$, and its explicit expression is not needed in the following. The functional space V_ε is defined by:

$$V_\varepsilon := \left\{(u,v)\in H^1_{\Gamma_D}(D)^2\times H^1(\omega_1)^2, \quad \forall x\in\sigma,\ \begin{cases} u(x+\varepsilon n(x)) = v(x+n(x)) \\ u(x-\varepsilon n(x)) = v(x-n(x)) \end{cases}\right\}.$$

We now obtain information about the limiting behavior $v\in H^1(\omega_{\sigma,1})^2$ of s_ε by relying on the intuition that v should minimize the leading order terms in the formulation eq. (3.15), so that it actually solves the problem:

$$\begin{aligned}
\min_{v\in H^1(\omega_{\sigma,1})^2}\widetilde{F}(v), \quad \text{where } \widetilde{F}(v) := \frac{1}{2}\int_{\omega_{\sigma,1}} &\frac{1}{1+d_\sigma\kappa}\left((2\mu_1+\lambda_1)(\nabla v n\cdot n)^2 + \mu_1(\nabla v n\cdot\tau)^2\right)\mathrm{d}x \\
&+ \int_{\omega_{\sigma,1}} 2(\mu_1-\mu_0)\frac{1}{1+d_\sigma\kappa}((\nabla u_0\circ p_\sigma)n\cdot n)(\nabla v n\cdot n)\,\mathrm{d}x \\
&+ \int_{\omega_{\sigma,1}} 2(\mu_1-\mu_0)\frac{1}{1+d_\sigma\kappa}(e(u_0)_{\tau n}\circ p_\sigma)(\nabla v n\cdot\tau)\,\mathrm{d}x \\
&+ \int_{\omega_{\sigma,1}} (\lambda_1-\lambda_0)\frac{1}{1+d_\sigma\kappa}((\operatorname{div} u_0)\circ p_\sigma)\,(\nabla v n\cdot n)\,\mathrm{d}x. \quad (3.17)
\end{aligned}$$

As in Section 2.2.3, we extract the information needed for our purpose about v by writing down the Euler–Lagrange equations for eq. (3.17).

Using at first test functions of the form

$$\forall p \in \sigma,\ t \in (-1,1), \quad \varphi(p+tn(p)) = \zeta(t)\psi(p)\tau(p),$$

where $\psi \in \mathcal{C}^\infty(\sigma)$ and $\zeta \in \mathcal{C}^\infty([-1,1])$ are arbitrary, and the coarea formula of Proposition 2.6, we obtain:

$$\int_\sigma \mu_1 \psi \left(\int_{-1}^1 \frac{\mathrm{d}}{\mathrm{d}t}((v\cdot\tau)(p+tn(p)))z'(t)\,\mathrm{d}t \right) \mathrm{d}\ell(p) + \int_\sigma 2(\mu_1-\mu_0)e(u_0)_{\tau n}\psi \left(\int_{-1}^1 z'(t)\,\mathrm{d}t \right) \mathrm{d}\ell(p) = 0.$$

Here, we recall from eqs. (2.22) to (2.25) that for a sufficiently smooth vector-valued function $v : \mathbb{R}^2 \to \mathbb{R}^2$, it holds:

$$\nabla v n \cdot n = \nabla(v\cdot n)\cdot n \text{ and } \nabla v n \cdot \tau = \nabla(v\cdot\tau)\cdot n. \tag{3.18}$$

Taking now ζ with compact support in $(-1,1)$, we see at once that $t \mapsto (v\cdot\tau)(p+tn(p))$ is an affine function. Using then arbitrary functions $\zeta \in \mathcal{C}^\infty([-1,1])$, it follows that:

$$\mu_1(p)\frac{\mathrm{d}}{\mathrm{d}t}((v\cdot\tau)(p+tn(p))) + 2(\mu_1-\mu_0)e(u_0)(p)_{\tau n} = 0,$$

and so:

$$\frac{\partial}{\partial n}(v\cdot\tau)(p+tn(p)) = \left(-2\left(1-\frac{\mu_0}{\mu_1}\right)e(u_0)_{\tau n} \right)(p). \tag{3.19}$$

Now writing down the Euler–Lagrange equation for eq. (3.17) with test functions $\varphi \in H^1(\omega_{\sigma,1})^2$ of the form

$$\forall p \in \sigma,\ t \in (-1,1), \quad \varphi(p+tn(p)) = \zeta(t)\psi(p)n(p),$$

we obtain similarly:

$$\frac{\partial}{\partial n}(v\cdot n)(p+tn(p)) = \left(-\frac{2(\mu_1-\mu_0)}{2\mu_1+\lambda_1}e(u_0)_{nn} - \frac{\lambda_1-\lambda_0}{2\mu_1+\lambda_1}\left(e(u_0)_{\tau\tau}+e(u_0)_{nn}\right) \right)(p), \tag{3.20}$$

which is the needed information for our purpose.

Step 3: We pass to the limit in the representation formula eq. (3.12). Using again a change of variables via the mapping m_ε in eq. (3.12), we obtain:

$$\begin{aligned} r_{\varepsilon,j}(x) = \frac{1}{\varepsilon}\int_{\omega_{\sigma,1}} &|\det\nabla m_\varepsilon|((A_1-A_0)\circ m_\varepsilon)(e(u_0)\circ m_\varepsilon) : (e_y(N_j)(x,m_\varepsilon(y)))\,\mathrm{d}y \\ &+ \int_{\omega_{\sigma,1}} |\det\nabla m_\varepsilon|\,(2(\mu_1-\mu_0)\circ m_\varepsilon)\,\frac{1}{2}\left(\nabla s_\varepsilon \nabla m_\varepsilon^{-1} + \nabla m_\varepsilon^{-T}\nabla s_\varepsilon^{-T}\right) : (e_y(N_j)(x,m_\varepsilon(y)))\,\mathrm{d}y \\ &+ \int_{\omega_{\sigma,1}} |\det\nabla m_\varepsilon|((\lambda_1-\lambda_0)\circ m_\varepsilon)\ \mathrm{tr}(\nabla s_\varepsilon\nabla m_\varepsilon^{-1})\,(\mathrm{div}_y N_j)(x,m_\varepsilon(y))\,\mathrm{d}y \\ =: I_\varepsilon^1 + I_\varepsilon^2 + I_\varepsilon^3, \end{aligned}$$

with obvious notations.

A simple calculation based on eq. (2.30) now yields:

$$I_\varepsilon^1 = \int_{\omega_{\sigma,1}} \frac{1+\varepsilon d_\sigma\kappa}{1+d_\sigma\kappa}((A_1-A_0)\circ m_\varepsilon)\,(e(u_0)\circ m_\varepsilon) : (e_y(N_j)(x,m_\varepsilon(y)))\,\mathrm{d}y,$$

and so, taking limits and using the coarea formula of Proposition 2.6:

$$\begin{aligned} \lim_{\varepsilon\to 0} I_\varepsilon^1 &= \int_{\omega_{\sigma,1}} \frac{1}{1+d_\sigma\kappa}((A_1-A_0)\circ p_\sigma)\,(e(u_0)\circ p_\sigma) : (e_y(N_j)(x,p_\sigma(y)))\,\mathrm{d}y, \\ &= 2\int_\sigma (A_1-A_0)e(u_0) : e_y(N_j(x,p))\,\mathrm{d}\ell(p). \end{aligned} \tag{3.21}$$

Note that, in the above integrand, as often in the following, we omit the mention to the integration point p when the latter is obvious, to keep expressions simple insofar as possible.

Likewise, it comes:

$$I_\varepsilon^2 = \int_{\omega_{\sigma,1}} 2(\mu_1-\mu_0)\circ m_\varepsilon \Bigg(\varepsilon(\nabla s_\varepsilon \tau\cdot\tau)(e_y(N_j)(x,m_\varepsilon(y))\tau\cdot\tau) \\ + \left(\varepsilon\nabla s_\varepsilon\tau\cdot n + \frac{1+\varepsilon d_\sigma\kappa}{1+d_\sigma\kappa}\nabla s_\varepsilon n\cdot\tau\right)(e_y(N_j)(x,m_\varepsilon(y))\tau\cdot n) \\ + \frac{1+\varepsilon d_\sigma\kappa}{1+d_\sigma\kappa}(\nabla s_\varepsilon n\cdot n)(e_y(N_j)(x,m_\varepsilon(y))n\cdot n)\Bigg)\,\mathrm{d}y,$$

so that, using again eq. (3.18) and the convergence of s_ε to the function v satisfying eqs. (3.19) and (3.20) identified during the second step, we obtain:

$$\lim_{\varepsilon\to 0} I_\varepsilon^2 = \int_{\omega_{\sigma,1}} \frac{2(\mu_1-\mu_0)\circ p_\sigma}{1+d_\sigma\kappa}\left(\frac{\partial}{\partial n}(v\cdot\tau)(e_y(N_j)(x,p_\sigma(y))\tau\cdot n)+\frac{\partial}{\partial n}(v\cdot n)(e_y(N_j)(x,p_\sigma(y))n\cdot n)\right)\mathrm{d}y, \\ = 2\int_\sigma 2(\mu_1-\mu_0)(p)\left(\frac{\partial}{\partial n}(v\cdot\tau)(e_y(N_j(x,p))\tau\cdot n)+\frac{\partial}{\partial n}(v\cdot n)(e_y(N_j(x,p))n\cdot n)\right)\mathrm{d}\ell(p) \quad (3.22)$$

Finally, by the same token,

$$I_\varepsilon^3 = \int_{\omega_{\sigma,1}} (\lambda_1-\lambda_0)\circ m_\varepsilon\left(\varepsilon\nabla s_\varepsilon\tau\cdot\tau+\frac{1+\varepsilon d_\sigma\kappa}{1+d_\sigma\kappa}\nabla s_\varepsilon n\cdot n\right)(\mathrm{div}_y(N_j)(x,m_\varepsilon(y)))\,\mathrm{d}y,$$

and so:

$$\lim_{\varepsilon\to 0} I_\varepsilon^3 = \int_{\omega_{\sigma,1}} \frac{(\lambda_1-\lambda_0)\circ p_\sigma}{1+d_\sigma\kappa}\frac{\partial}{\partial n}(v\cdot n)(\mathrm{div}_y(N_j)(x,p_\sigma(y)))\,\mathrm{d}y, \\ = 2\int_\sigma (\lambda_1-\lambda_0)(p)\frac{\partial}{\partial n}(v\cdot n)(\mathrm{div}_y(N_j(x,p)))\,\mathrm{d}\ell(p) \quad (3.23)$$

Putting eqs. (3.21) to (3.23) together, and using the explicit expressions eqs. (3.19) and (3.20) for the derivatives $\frac{\partial}{\partial n}(v\cdot\tau)$ and $\frac{\partial}{\partial n}(v\cdot n)$, a simple, albeit tedious calculation yields the desired asymptotic expansion eq. (3.8).

3.3. **Derivative of a quantity of interest depending on the perturbed displacement u_ε**

In this section, we use the asymptotic expansion of u_ε obtained in Theorem 3.2 to appraise the limiting behavior of a function $J_\sigma(\varepsilon)$ of the form:

$$J_\sigma(\varepsilon) = \int_D j(u_\varepsilon)\,\mathrm{d}x,$$

where $j:\mathbb{R}^2\to\mathbb{R}$ is a given smooth function, satisfying the growth conditions eq. (2.8).

The result of interest is the next proposition; we omit the proof, since the arguments developed in Section 2.3 in the context of the 2d conductivity equation can be applied in an analogous way.

Proposition 3.3. *The function $J_\sigma(\varepsilon)$ is differentiable at 0, and its derivative reads:*

$$J_\sigma'(0) = \int_\sigma \mathcal{M}e(p_0):e(u_0)\,\mathrm{d}\ell, \\ = \int_\sigma \frac{2}{2\mu_1+\lambda_1}\Big(4\mu_1(\mu_1-\mu_0+\lambda_1)-2(\mu_0\lambda_1+\mu_1\lambda_0)+2\lambda_0(\lambda_1-\lambda_0)\Big)e(p_0)_{\tau\tau}e(u_0)_{\tau\tau}\,\mathrm{d}\ell \\ + \int_\sigma 2(2\mu_0+\lambda_0)\left(\frac{\lambda_1-\lambda_0}{2\mu_1+\lambda_1}\right)\Big(e(p_0)_{\tau\tau}e(u_0)_{nn}+e(p_0)_{nn}e(u_0)_{\tau\tau}\Big)\,\mathrm{d}\ell \\ + \int_\sigma 8\mu_0\left(1-\frac{\mu_0}{\mu_1}\right)e(p_0)_{n\tau}e(u_0)_{n\tau}\,ds + \int_\sigma 2(2\mu_0+\lambda_0)\left(1-\frac{2\mu_0+\lambda_0}{2\mu_1+\lambda_1}\right)e(p_0)_{nn}e(u_0)_{nn}\,\mathrm{d}\ell, \quad (3.24)$$

where $\mathcal{M}$ is the polarization tensor defined in the statement of Theorem 3.2, and the adjoint state p_0 is the unique solution in $H^1_{\Gamma_D}(D)^2$ to the system:

$$\begin{cases} -\operatorname{div}(A_0 e(p_0)) = -j'(u_0) & \text{in } D, \\ p_0 = 0 & \text{on } \Gamma_D, \\ A_0 e(p_0) n = 0 & \text{on } \partial D \setminus \overline{\Gamma_D}. \end{cases} \tag{3.25}$$

As in the conductivity case detailed in Section 2.3, the derivative eq. (3.24) can be rewritten in a way which is easier to exploit in the context of shape and topology optimization:

$$J'_\sigma(0) = \int_\sigma P(x, \tau_1(x), \tau_2(x)) \, \mathrm{d}\ell(x),$$

where, for a given point x, $P(x, \cdot, \cdot)$ is the homogeneous polynomial of degree 4 given by:

$$P(x, \tau_1, \tau_2) = \beta_1(x)\tau_1^4 + \beta_2(x)\tau_1^3\tau_2 + \beta_3(x)\tau_1^2\tau_2^2 + \beta_4(x)\tau_1\tau_2^3 + \beta_5(x)\tau_2^4.$$

Using the shortcuts $e \equiv e(u_0)$ and $f \equiv e(p_0)$ (in which the dependence with respect to the point x is also omitted for brevity), the coefficients β_i, $i = 1, \dots, 5$ read:

$$\beta_1 = \alpha_1 e_{11} f_{11} + \alpha_2(e_{22} f_{11} + e_{11} f_{22}) + \alpha_3 e_{12} f_{12} + \alpha_4 e_{22} f_{22},$$

$$\begin{aligned} \beta_2 = {} & 2\alpha_1(e_{11} f_{12} + e_{12} f_{11}) + 2\alpha_2(-e_{12} f_{11} - e_{11} f_{12} + e_{22} f_{12} + e_{12} f_{22}) \\ & + \alpha_3(e_{12}(f_{22} - f_{11}) + f_{12}(e_{22} - e_{11})) - 2\alpha_4(e_{22} f_{12} + e_{12} f_{22}), \end{aligned}$$

$$\begin{aligned} \beta_3 = {} & \alpha_1(e_{11} f_{22} + 4e_{12} f_{12} + e_{22} f_{11}) + 2\alpha_2(e_{11} f_{11} + e_{22} f_{22} - 4e_{12} f_{12}) \\ & + \alpha_3(-2e_{12} f_{12} + (e_{22} - e_{11})(f_{22} - f_{11})) + \alpha_4(e_{11} f_{22} + e_{22} f_{11} + 4e_{12} f_{12}), \end{aligned}$$

$$\begin{aligned} \beta_4 = {} & 2\alpha_1(e_{12} f_{22} + e_{22} f_{12}) + 2\alpha_2(e_{11} f_{12} + e_{12} f_{11} - e_{12} f_{22} - e_{22} f_{12}) \\ & - \alpha_3(e_{12}(f_{22} - f_{11}) + f_{12}(e_{22} - e_{11})) - 2\alpha_4(e_{11} f_{12} + e_{12} f_{11}), \end{aligned}$$

and

$$\beta_5 = \alpha_1 e_{22} f_{22} + \alpha_2(e_{11} f_{22} + e_{22} f_{11}) + \alpha_3 e_{12} f_{12} + \alpha_4 e_{11} f_{11}.$$

In the above, we have defined:

$$\alpha_1 = \frac{2}{2\mu_1 + \lambda_1}\Big(4\mu_1(\mu_1 - \mu_0 + \lambda_1) - 2(\mu_0\lambda_1 + \mu_1\lambda_0) + 2\lambda_0(\lambda_1 - \lambda_0)\Big),$$

$$\alpha_2 = 2(2\mu_0 + \lambda_0)\left(\frac{\lambda_1 - \lambda_0}{2\mu_1 + \lambda_1}\right), \quad \alpha_3 = 8\mu_0\left(1 - \frac{\mu_0}{\mu_1}\right), \quad \text{and} \quad \alpha_4 = 2(2\mu_0 + \lambda_0)\left(1 - \frac{2\mu_0 + \lambda_0}{2\mu_1 + \lambda_1}\right).$$

4. **Asymptotic expansions in the context of diametrically small inclusions**

As we shall see in more detail from the next Section 5, our mathematical treatment of three-dimensional tubular inclusions $\omega_{\sigma,\varepsilon}$ (the three-dimensional version of eq. (2.3)) somehow boils down to that of a two-dimensional *diametrically small inclusion*, of the form eq. (1.13), a situation which has been extensively studied in the literature, see notably [19, 45, 74, 91]. We shall indeed see that, roughly speaking, the situation of a 3d tubular inhomogeneity amounts to that of a 2d diametrically small inhomogeneity inside each 2d normal plane to the base curve σ. For this reason, we temporarily pause our discussion about tubular inhomogeneities to exemplify how our formal energy argument allows to retrieve the well-known asymptotic expansion formula for the field u_ε when the ambient medium bears a diametrically small inclusion. We focus on the physical context of the conductivity equation in Sections 4.1 to 4.3 and we handle simultaneously the cases where the space dimension equals 2 and 3. The corresponding derivation in the linear elasticity setting entails no additional difficulty, except

that it is a little more involved as far as calculations are concerned. For this reason, we simply state the results of interest in Section 4.4.

4.1. **Diametrically small inclusions in the context of the conductivity equation**

The physical setting of interest is exactly that of Section 2.1: the bounded and Lipschitz domain D is filled by a material with smooth conductivity γ_0 satisfying eq. (2.1), a smooth source term $f : D \to \mathbb{R}$ is acting inside the medium, and a smooth heat flux g is imposed on the region $\Gamma_N \subset \partial D$; the voltage potential u_0 inside D is the unique solution in $H^1_{\Gamma_D}(D)$ to the equation:

$$\begin{cases} -\operatorname{div}(\gamma_0 \nabla u_0) = f & \text{in } D, \\ u_0 = 0 & \text{on } \Gamma_D, \\ \gamma_0 \frac{\partial u_0}{\partial n} = g & \text{on } \Gamma_N, \\ \gamma_0 \frac{\partial u_0}{\partial n} = 0 & \text{on } \partial D \setminus (\overline{\Gamma_D} \cup \overline{\Gamma_N}). \end{cases} \tag{4.1}$$

Assuming that $0 \in D$ for simplicity, a small inclusion $\omega_\varepsilon := \varepsilon\omega \Subset D$ is present inside D, shaped from a smooth bounded domain $\omega \subset \mathbb{R}^d$, and filled by a material with smooth, inhomogeneous conductivity γ_1 which also fulfills eq. (2.1). In this context, the perturbed potential u_ε is the solution in $H^1_{\Gamma_D}(D)$ to the equation:

$$\begin{cases} -\operatorname{div}(\gamma_\varepsilon \nabla u_\varepsilon) = f & \text{in } D \\ u_\varepsilon = 0 & \text{on } \Gamma_D \\ \gamma_0 \frac{\partial u_\varepsilon}{\partial n} = g & \text{on } \Gamma_N, \\ \gamma_0 \frac{\partial u_\varepsilon}{\partial n} = 0 & \text{on } \partial D \setminus (\overline{\Gamma_D} \cup \overline{\Gamma_N}), \end{cases} \qquad \text{where } \gamma_\varepsilon(x) = \begin{cases} \gamma_1(x) & \text{if } x \in \omega_\varepsilon, \\ \gamma_0(x) & \text{otherwise.} \end{cases} \tag{4.2}$$

As we shall see, the main difference between the present situation and that tackled in Section 2 is that the "near field", i.e. the rescaled behavior of u_ε near ω_ε, no longer depends on the "far field", away from ω_ε. This "near field" is a well-defined function, characterized as the solution to a partial differential equation posed on the whole ambient space $\mathbb{R}^d$.

The adapted mathematical setting to deal with such "exterior problems" depends on the space dimension, and we introduce the weighted spaces

$$W^{1,-1}(\mathbb{R}^2) = \left\{ u \in L^2_{\text{loc}}(\mathbb{R}^2),\ \frac{1}{(1+|x|^2)^{\frac{1}{2}} \log(2+|x|^2)} u \in L^2(\mathbb{R}^2),\ \nabla u \in L^2(\mathbb{R}^2) \right\},$$

and

$$W^{1,-1}(\mathbb{R}^3) = \left\{ u \in L^2_{\text{loc}}(\mathbb{R}^3),\ \frac{1}{(1+|x|^2)^{\frac{1}{2}}} u \in L^2(\mathbb{R}^3),\ \nabla u \in L^2(\mathbb{R}^3) \right\}.$$

Let us emphasize that functions $u \in W^{1,-1}(\mathbb{R}^3)$ vanish at infinity, while functions $u \in W^{1,-1}(\mathbb{R}^2)$ do not in general, since the latter space contains constant functions. To harmonize notations, we introduce the space

$$W^{1,-1}_0(\mathbb{R}^d) := \begin{cases} W^{1,-1}(\mathbb{R}^2)/\mathbb{R} & \text{if } d = 2, \\ W^{1,-1}(\mathbb{R}^3) & \text{if } d = 3, \end{cases}$$

of functions in $W^{1,-1}(\mathbb{R}^d)$ vanishing at infinity; see [90, §2.5] for further details about these issues.

4.2. **Asymptotic expansion of the perturbed potential u_ε**

As we have mentioned, the asymptotic behavior of u_ε as $\varepsilon \to 0$ in the context of diametrically small inhomogeneities $\omega_\varepsilon = \varepsilon\omega$ has been extensively studied in the literature, either by variational considerations or by layer potential techniques; see for instance [45, 74, 91] or [19, Ch. 5]. Our purpose

in this section is to sketch how the formal technique exposed in Section 2.2.3 may be adapted to deal with this situation. The result of interest is the following theorem:

Theorem 4.1. *For any point $x \in D \setminus \{0\}$, the following expansion holds:*

$$u_\varepsilon(x) = u_0(x) + \varepsilon^d u_1(x) + \mathrm{o}(\varepsilon^d), \text{ where } u_1(x) := \mathcal{M}\nabla u_0(0) \cdot \nabla_y N(x,0), \tag{4.3}$$

and $N(x,y)$ is the Green's function of the background equation eq. (4.1); see Section 2.2.1. In eq. (4.3), the polarization tensor $\mathcal{M} = (\mathcal{M}_{ij})_{i,j=1,\dots,d}$ is defined by:

$$\forall \xi \in \mathbb{R}^d, \quad \mathcal{M}\xi = (\gamma_1(0) - \gamma_0(0)) \int_\omega (\xi + \nabla \phi_\xi(y))\, \mathrm{d}y, \tag{4.4}$$

where for any $\xi \in \mathbb{R}^d$, ϕ_ξ is the unique solution in $W_0^{1,-1}(\mathbb{R}^d)$ to the exterior problem:

$$\begin{cases} -\Delta \phi_\xi = 0 & \text{in } \omega \cup (\mathbb{R}^d \setminus \overline{\omega}), \\ \gamma_0(0) \frac{\partial \phi_\xi^+}{\partial n} - \gamma_1(0) \frac{\partial \phi_\xi^-}{\partial n} = -(\gamma_0(0) - \gamma_1(0)) \xi \cdot n & \text{on } \partial\omega, \\ |\phi_\xi(y)| \to 0 & \text{when } y \to \infty. \end{cases} \tag{4.5}$$

Formal derivation of eq. (4.3). We aim to analyze the limiting behavior of the remainder $r_\varepsilon := \frac{1}{\varepsilon^d}(u_\varepsilon - u_0) \in H^1_{\Gamma_D}(D)$ "far" from the point 0. Our starting point is again the observation that r_ε is the unique solution to the following variational problem:

$$\forall v \in H^1_{\Gamma_D}(D), \quad \int_D \gamma_\varepsilon \nabla r_\varepsilon \cdot \nabla v \, \mathrm{d}x = -\frac{1}{\varepsilon^d} \int_{\omega_\varepsilon} (\gamma_1 - \gamma_0) \nabla u_0 \cdot \nabla v \, \mathrm{d}x, \tag{4.6}$$

or equivalently to the minimization problem:

$$\min_{u \in H^1_{\Gamma_D}(D)} E_\varepsilon(u), \text{ where } E_\varepsilon(u) := \frac{1}{2} \int_D \gamma_\varepsilon |\nabla u|^2 \, \mathrm{d}x + \frac{1}{\varepsilon^d} \int_{\omega_\varepsilon} (\gamma_1 - \gamma_0) \nabla u_0 \cdot \nabla u \, \mathrm{d}x. \tag{4.7}$$

According to the formal method presented in Sections 2 and 3, we proceed in three steps.

Step 1: We represent the error $r_\varepsilon(x)$ at a given point $x \in D \setminus \{0\}$ in terms of the values of r_ε inside ω_ε. Arguing exactly as in Section 2.2.3 – that is, using the Green's function $N(x,y)$ in eq. (2.9) for the background equation eq. (4.1), integrating by parts, and "injecting" $y \mapsto N(x,y)$ as test function in the formulation eq. (4.6) to transform the resulting expression – we obtain:

$$r_\varepsilon(x) = \frac{1}{\varepsilon^d} \int_{\omega_\varepsilon} (\gamma_1 - \gamma_0)(y) \nabla u_0(y) \cdot \nabla_y N(x,y) \, \mathrm{d}y + \int_{\omega_\varepsilon} (\gamma_1 - \gamma_0)(y) \nabla r_\varepsilon(y) \cdot \nabla_y N(x,y) \, \mathrm{d}y. \tag{4.8}$$

Step 2: We study a rescaled version of r_ε near the inclusion set ω_ε. To this end, let us introduce the rescaled error $s_\varepsilon \in H^1_{\frac{1}{\varepsilon}\Gamma_D}(\frac{1}{\varepsilon}D)$, defined by:

$$s_\varepsilon(z) = \varepsilon^{d-1} r_\varepsilon(\varepsilon z) = \frac{1}{\varepsilon}(u_\varepsilon - u_0)(\varepsilon z), \text{ a.e. } z \in \frac{1}{\varepsilon} D,$$

a quantity which will appear naturally in the course of the third step. The convergence of s_ε as $\varepsilon \to 0$ is the subject of the next lemma, which is exactly Theorem 1 in [45]; we postpone the formal justification of this formula thanks to our heuristic energy argument to the end of the proof of Theorem 4.1.

Lemma 4.2. *The following expansion holds:*

$$\|\nabla(s_\varepsilon - v)\|_{L^2(\frac{1}{\varepsilon}D)} \leq C\varepsilon^{\frac{1}{2}},$$

where $v(y) \in W_0^{1,-1}(\mathbb{R}^d)$ *is the unique solution to the exterior problem:*

$$\begin{cases} -\Delta v = 0 & \text{in } \omega \cup (\mathbb{R}^d \setminus \overline{\omega}), \\ \gamma_0(0)\frac{\partial v^+}{\partial n} - \gamma_1(0)\frac{\partial v^-}{\partial n} = -(\gamma_0(0) - \gamma_1(0))\nabla u_0(0) \cdot n(y) & \text{on } \partial\omega, \\ |v(y)| \to 0 & \text{as } |y| \to \infty. \end{cases} \tag{4.9}$$

Remark 4.3.

- It follows from the theory of exterior problems that eq. (4.9) has a unique solution in $W_0^{1,-1}(\mathbb{R}^d)$; see [90, §2.5.4]. Without entering into details, let us solely mention that when $d = 2$, this fact holds true because the compatibility condition
$$\int_{\partial\omega} \nabla u_0(0) \cdot n(y) \, \mathrm{ds}(y) = 0$$
is obviously satisfied by the right-hand side of the transmission conditions on $\partial\omega$ in eq. (4.9).

- The function $v(y)$ in eq. (4.9) is exactly the function $\phi_{\nabla u_0(0)}$ defined in eq. (4.5).

Step 3: We pass to the limit in the representation formula eq. (4.8). A change of variables in eq. (4.8) brings into play the function s_ε:

$$r_\varepsilon(x) = \int_\omega (\gamma_1 - \gamma_0)(\varepsilon z)\nabla u_0(\varepsilon z) \cdot \nabla_y N(x, \varepsilon z) \, \mathrm{d}z + \int_\omega (\gamma_1 - \gamma_0)(\varepsilon z)\nabla s_\varepsilon(z) \cdot \nabla_y N(x, \varepsilon z) \, \mathrm{d}z.$$

Then, applying Lemma 4.2 yields:

$$\lim_{\varepsilon \to 0} r_\varepsilon(x) = \int_\omega (\gamma_1(0) - \gamma_0(0))(\nabla u_0(0) + \nabla v(z)) \cdot \nabla_y N(x, 0) \, \mathrm{d}z,$$

which is the expected formula eq. (4.3), in view of eq. (4.4). ∎

We eventually provide the missing link in the previous argument.

Formal proof of Lemma 4.2. Using a change of variables in eq. (4.7), the function $s_\varepsilon(z) = \varepsilon^{d-1} r_\varepsilon(\varepsilon z)$ is the unique minimizer in $H^1_{\frac{1}{\varepsilon}\Gamma_D}(\frac{1}{\varepsilon}D)$ of the energy functional defined by:

$$E_\varepsilon(v) = \frac{1}{\varepsilon^d}\left(\frac{1}{2}\int_{\frac{1}{\varepsilon}D\setminus\overline{\omega}} \gamma_0(\varepsilon z)|\nabla v|^2 \, \mathrm{d}z + \frac{1}{2}\int_\omega \gamma_1(\varepsilon z)|\nabla v|^2 \, \mathrm{d}z + \int_\omega (\gamma_1 - \gamma_0)(\varepsilon z)\nabla u_0(\varepsilon z) \cdot \nabla v \, \mathrm{d}z\right).$$

Removing the multiplicative factor, retaining only the leading-order terms in $E_\varepsilon(v)$, and replacing the function space $H^1_{\frac{1}{\varepsilon}\Gamma_D}(\frac{1}{\varepsilon}D)$ by $W_0^{1,-1}(\mathbb{R}^d)$, we expect that s_ε converges to the solution of the approximate minimization problem:

$$\min_{v \in W_0^{1,-1}(\mathbb{R}^d)} \widetilde{E}(v),$$
$$\text{where} \quad \widetilde{E}(v) := \frac{1}{2}\int_{\mathbb{R}^d\setminus\overline{\omega}} \gamma_0(0)|\nabla v|^2 \, \mathrm{d}z + \frac{1}{2}\int_\omega \gamma_1(0)|\nabla v|^2 \, \mathrm{d}z + \int_\omega (\gamma_1(0) - \gamma_0(0))\nabla u_0(0) \cdot \nabla v \, \mathrm{d}z.$$

Writing down the Euler–Lagrange equation associated to this minimization problem, it is easy to see that its unique solution is the function $v(y)$ defined by eq. (4.9), which is the desired conclusion. ∎

4.3. **Asymptotic expansion of a quantity of interest involving u_ε and final comments**

Again, the result of Theorem 4.1 allows to calculate the derivative of a function $J_\omega(\varepsilon)$ depending on the size ε of the inclusion via the perturbed potential u_ε, say:

$$J_\omega(\varepsilon) = \int_D j(u_\varepsilon)\,\mathrm{d}x,$$

where $j : \mathbb{R} \to \mathbb{R}$ is a smooth function, satisfying the growth conditions eq. (2.8). Since the proof is completely analogous to those of Proposition 2.10 and Proposition 3.3, we state the following result without proof.

Proposition 4.4. *The function $J_\omega(\varepsilon)$ has the following expansion at $\varepsilon = 0$:*

$$J_\omega(\varepsilon) = J_\omega(0) + \varepsilon^d J'_\omega(0) + \mathrm{o}(\varepsilon^d), \tag{4.10}$$

where the "derivative" $J'_\omega(0)$ reads:

$$J'_\omega(0) = \mathcal{M}\nabla u_0(0) \cdot \nabla p_0(0).$$

Here, $\mathcal{M}$ is the polarization tensor defined by eq. (4.4), and the adjoint state p_0 is the unique solution in $H^1_{\Gamma_D}(D)$ to:

$$\begin{cases} -\operatorname{div}(\gamma_0 \nabla p_0) = -j'(u_0) & \text{in } D, \\ p_0 = 0 & \text{on } \Gamma_D, \\ \gamma_0 \frac{\partial p_0}{\partial n} = 0 & \text{on } \partial D \setminus \overline{\Gamma_D}. \end{cases}$$

Remark 4.5. When $d = 2$ and ω is the unit disk, one has $|\omega| = \pi$, and a simple calculation based on separation of variables yields, for an arbitrary vector $\xi \in \mathbb{R}^d$:

$$\phi_\xi(y) = \begin{cases} \frac{\gamma_0(0)-\gamma_1(0)}{\gamma_0(0)+\gamma_1(0)} \xi \cdot y & \text{if } y \in \omega, \\ \frac{\gamma_0(0)-\gamma_1(0)}{\gamma_0(0)+\gamma_1(0)} \frac{\xi \cdot y}{|y|^2} & \text{otherwise.} \end{cases}$$

Then, the polarization tensor $\mathcal{M}$ is the isotropic matrix:

$$\mathcal{M} = 2\pi\gamma_0(0)\frac{\gamma_1(0) - \gamma_0(0)}{\gamma_1(0) + \gamma_0(0)}\mathrm{I}, \tag{4.11}$$

and so, eq. (4.10) reads:

$$J_\omega(\varepsilon) = J_\omega(0) + \varepsilon^d 2\pi\gamma_0(0)\frac{\gamma_1(0) - \gamma_0(0)}{\gamma_1(0) + \gamma_0(0)}\nabla u_0(0) \cdot \nabla p_0(0) + \mathrm{o}(\varepsilon^d),$$

which is a well-known topological derivative formula in the context of the two-phase conductivity equation; see e.g. [25].

4.4. **Extension to the linear elasticity case**

The above calculations and conclusions are readily adapted to the case where the scalar conductivity equation eq. (4.1) is replaced by the d-dimensional linear elasticity system eq. (3.3). Along the lines of the previous pages, it can indeed be proved that the following asymptotic expansion holds for the perturbed displacement u_ε:

$$u_{\varepsilon,j}(x) = u_{0,j}(x) + \varepsilon^d u_{1,j}(x) + \mathrm{o}(\varepsilon^d), \quad \text{where } u_{1,j}(x) := \mathcal{M}e(u_0)(0) : e_y(N_j(x,0)), \quad j = 1, \dots, d.$$

The polarization tensor $\mathcal{M}$ is defined by:

$$\forall \xi \in \mathcal{S}(\mathbb{R}^d), \quad \mathcal{M}\xi = (A_1(0) - A_0(0))\left(|\omega|\xi + \int_\omega e(\phi_\xi)(z)\,\mathrm{d}z\right),$$

$N(x,y)$ is the Green's function of the background linear elasticity problem in eq. (3.3) (see Remark 3.1) and ϕ_ξ is now the unique solution in $W_0^{1,-1}(\mathbb{R}^d)^d$ to the exterior problem:

$$\begin{cases} -\operatorname{div}(A_0(0)e(\phi_\xi)) = 0 & \text{in } \mathbb{R}^d \setminus \overline{\omega} \\ -\operatorname{div}(A_1(0)e(\phi_\xi)) = 0 & \text{in } \omega \\ \phi_\xi^+ = \phi_\xi^- & \text{on } \partial\omega \\ A_0(0)e(\phi_\xi)n^+ - A_1(0)e(\phi_\xi)n^- = (A_1(0) - A_0(0))\xi n & \text{on } \partial\omega \\ |\phi_\xi(y)| \to 0 & \text{as } |y| \to \infty. \end{cases} \tag{4.12}$$

This polarization tensor $\mathcal{M}$ can be calculated explicitly when $d = 2$ and ω is the unit disk:

$$\forall e \in \mathcal{S}(\mathbb{R}^d), \quad \mathcal{M}e = \alpha_S \operatorname{tr}(e)\mathrm{I} + \beta_S e;$$

see [19, §10.3] or [20]. In the above formula,

$$\alpha_S = \pi\left(\frac{(\lambda_0+2\mu_0)(\lambda_1+\mu_1-(\lambda_0+\mu_0))}{\mu_0+\lambda_1+\mu_1} - \frac{2\mu_0(\mu_1-\mu_0)(\lambda_0+2\mu_0)}{\mu_1(\lambda_0+3\mu_0)+\mu_0(\lambda_0+\mu_0)}\right)$$
$$\text{and} \quad \beta_S = 4\pi\frac{\mu_0(\lambda_0+2\mu_0)(\mu_1-\mu_0)}{\mu_0(\lambda_0+\mu_0)+\mu_1(\lambda_0+3\mu_0)}, \tag{4.13}$$

and we have denoted $\lambda_i \equiv \lambda_i(0)$, $\mu_i \equiv \mu_i(0)$ for short.

5. Asymptotic expansion of the solution to the conductivity equation in 3d under perturbations by thin tubular inhomogeneities

In this section, we begin our investigations about thin tubular inclusions in 3d. The bounded, Lipschitz domain $D \subset \mathbb{R}^3$ is filled by a material with smooth conductivity $\gamma_0(x)$, fulfilling the ellipticity assumption eq. (2.1), and the potential u_0 is the unique solution in $H^1_{\Gamma_D}(D)$ to the "background" conductivity equation:

$$\begin{cases} -\operatorname{div}(\gamma_0\nabla u_0) = f & \text{in } D, \\ u_0 = 0 & \text{on } \Gamma_D, \\ \gamma_0\frac{\partial u_0}{\partial n} = g & \text{on } \Gamma_N, \\ \gamma_0\frac{\partial u_0}{\partial n} = 0 & \text{on } \partial D \setminus (\overline{\Gamma_D} \cup \overline{\Gamma_N}), \end{cases} \tag{5.1}$$

where the homogeneous Dirichlet boundary conditions are imposed on the region $\Gamma_D \subset \partial D$, and $f : D \to \mathbb{R}$ and $g : \Gamma_N \to \mathbb{R}$ are respectively a smooth source and a smooth flux entering through the region $\Gamma_N \subset \partial D$ which is disjoint from Γ_D.

The constituent material γ_0 in D is perturbed by an inhomogeneity

$$\omega_{\sigma,\varepsilon} = \left\{x \in \mathbb{R}^3, \quad d(x,\sigma) < \varepsilon\right\} \Subset D,$$

taking the shape of a thin tube with width ε around a smooth, simple curve $\sigma : [0,\ell] \to \mathbb{R}^3$, which may be open or closed. The inclusion $\omega_{\sigma,\varepsilon}$ contains a material with smooth conductivity $\gamma_1(x)$ which also satisfies eq. (2.1), so that the perturbed voltage potential u_ε is the unique solution in $H^1_{\Gamma_D}(D)$ to the following equation:

$$\begin{cases} -\operatorname{div}(\gamma_\varepsilon\nabla u_\varepsilon) = f & \text{in } D, \\ u_\varepsilon = 0 & \text{on } \Gamma_D, \\ \gamma_0\frac{\partial u_\varepsilon}{\partial n} = g & \text{on } \Gamma_N, \\ \gamma_0\frac{\partial u_\varepsilon}{\partial n} = 0 & \text{on } \partial D \setminus (\overline{\Gamma_D} \cup \overline{\Gamma_N}), \end{cases} \quad \text{where } \gamma_\varepsilon(x) = \begin{cases} \gamma_1(x) & \text{if } x \in \omega_{\sigma,\varepsilon}, \\ \gamma_0(x) & \text{otherwise.} \end{cases} \tag{5.2}$$

We are interested in the asymptotic expansion of u_ε as ε vanishes. As we have mentioned, to the best of our knowledge, this is still an open question in the literature, although the particular instance where σ is a straight line segment (and not a general curve) has been treated in [32]. In the next sections, we apply our heuristic energy argument to calculate the asymptotic expansion of interest. As in Sections 2 and 3, our presentation is simplified in the case where σ is closed, which we shall assume throughout this section, unless stated otherwise. We are confident that the very same asymptotic formula holds when σ is open (and we shall actually use this formula in this context in the numerical examples of Section 7), since we expect the endpoints of σ to contribute only to higher-order terms in the expansion of u_ε.

We initiate our study by recalling in Section 5.1 a few useful properties about the (unsigned) distance function δ_σ to σ, before turning in Sections 5.2 and 5.3 to the derivation of the sought asymptotic expansions of u_ε and related quantities of interest. We close this study with a few comparisons between the two- and three-dimensional behaviors of tubular inhomogeneities in Section 5.4.

5.1. **The unsigned distance function to a three-dimensional closed curve**

In this section, we collect some facts about the unsigned distance function to a closed curve in 3d; although these are admittedly not new, they are not so easily found under this form in the literature. Throughout this section, $\sigma : [0, \ell] \to \mathbb{R}^3$ is a smooth, closed simple curve. Recall that, without loss of generality, σ is assumed to be parametrized by arc length, that is: $|\sigma'(s)| = 1$ for all $s \in (0, \ell)$.

Definition 5.1.

- The *unsigned* distance function to σ is defined by:
$$\forall x \in \mathbb{R}^3, \quad \delta_\sigma(x) = \inf_{y \in \sigma} |x - y|. \tag{5.3}$$
- The *skeleton* Σ of σ is the set of points $x \in \mathbb{R}^3$ for which the minimum in eq. (5.3) is achieved at least at two distinct points $y_1 \neq y_2 \in \sigma$.
- When $x \notin \Sigma$, the unique minimizer in eq. (5.3), denoted by $p_\sigma(x)$, is called the *projection* of x onto σ.

The skeleton Σ admits the following alternative characterization:

Proposition 5.2. *The skeleton Σ is exactly the set of points $x \in D$ where δ_σ^2 fails to be differentiable. Since δ_σ is a Lipschitz function, Rademacher's theorem implies that Σ has null Lebesgue measure.*

Actually, the smoothness of σ implies that the closure $\overline{\Sigma}$ also has 0 Lebesgue measure.

See [55] for a proof of the first part of the proposition, and [58] about Rademacher's theorem. The final point is delicate, and it is the only one in this statement which requires the smoothness of σ; see [82].

Let us introduce a few additional objects attached to a point $p = \sigma(s_0) \in \sigma$; see Figure 5.1 for an illustration:

- $\tau(p) = \sigma'(s_0)$ is the unit tangent vector to σ at p, with the orientation induced by the parametrization $s \mapsto \sigma(s)$.
- $a(p) := \sigma''(s_0)$ is the acceleration vector of σ at p.
- $N_{\tau(p)} = \{z \in \mathbb{R}^3, \ z \cdot \tau(p) = 0\}$ is the (vector) plane of directions in $\mathbb{R}^3$ which are orthogonal to $\tau(p)$.

- $P_\sigma(p) \subset N_{\tau(p)}$ contains those directions $z \in N_{\tau(p)}$ such that $p+z$ has p as unique projection point:
$$P_\sigma(p) := \left\{ z \in N_{\tau(p)},\ p_\sigma(p+z) = p \right\}.$$
- $B_\sigma(p,r) := B(p,r) \cap \left\{ p+z,\ z \in N_{\tau(p)} \right\}$ is the two-dimensional ball with center p and radius r in the (affine) plane $p + N_{\tau(p)}$.

The next result of interest for our purpose is concerned with the smoothness of δ_σ and p_σ near the curve σ. It is based on an argument using local charts, and a use of the implicit function theorem; see in [14, Thm. 3.1] or [13].

Theorem 5.3. *There exists $\varepsilon_0 > 0$ such that, for $0 < \varepsilon < \varepsilon_0$,*

- *the squared distance function δ_σ^2 is of class $\mathcal{C}^\infty$ on the tubular neighborhood $\omega_{\sigma,\varepsilon}$.*
- *The projection $p_\sigma : \omega_{\sigma,\varepsilon} \to \sigma$ is well-defined and of class $\mathcal{C}^\infty$.*
- *For every point $p \in \sigma$, one has $B_\sigma(p,\varepsilon) \subset P_\sigma(p)$, that is, for any $z \in N_{\tau(p)}$ with $|z| \leq \varepsilon$, $p_\sigma(p+z) = p$.*

For convenience, and without loss of generality, we assume in the following that $\varepsilon_0 > 1$ can be chosen in the above statement. Like in the case of the signed distance function in 2d discussed in Section 2.2.2, the squared distance function δ_σ^2 and the projection p_σ happen to be smooth on the whole set $D \setminus \overline{\Sigma}$; see again [42, 55, 66]. These facts allow, in particular, to define extensions of the tangent vector τ and the acceleration vector a from σ to the neighborhood $\omega_{\sigma,1}$ (and actually $D \setminus \overline{\Sigma}$):
$$\forall x \in \omega_{\sigma,1}, \quad \tau(x) \equiv \tau(p_\sigma(x)), \quad \text{and} \quad a(x) \equiv a(p_\sigma(x)),$$
a convention that we adopt throughout the following.

In the forthcoming sections, we shall need the expressions of the derivatives of δ_σ and p_σ. Our first step toward this goal is the following simple consequence of the first- and second-order optimality conditions for eq. (5.3):

Lemma 5.4. *Let $x \in \mathbb{R}^3 \setminus \overline{\Sigma}$ and $p \in \sigma$ be its projection $p_\sigma(x)$ onto σ; then:*

(i) *The vector $(x-p)$ is normal to σ at p:*
$$\tau(p) \cdot (x-p) = 0.$$

(ii) *The following inequality holds:*
$$1 - a(p) \cdot (x-p) \geq 0.$$

Proof. Let $s_0 \in [0,\ell)$ be the parameter value such that $p = \sigma(s_0)$; by definition, and since the curve σ is closed (and so, $\sigma : [0,\ell] \to \mathbb{R}^3$ can equivalently thought of as an ℓ-periodic mapping $\sigma : \mathbb{R} \to \mathbb{R}^3$), s_0 is the unique solution to:
$$\min_{s \in [0,\ell)} |x - \sigma(s)|^2. \tag{5.4}$$
The first-order necessary condition for optimality then reads:
$$\sigma'(s_0) \cdot (x - \sigma(s_0)) = 0,$$
which is exactly (i).
In a similar fashion, the necessary second-order optimality condition for eq. (5.4) at $s = s_0$ reads:
$$\sigma''(s_0) \cdot (x - \sigma(s_0)) - |\sigma'(s_0)|^2 \leq 0;$$
after rearrangement, this yields (ii). ∎

Let us now proceed with the calculation of the gradient of δ_σ:

Lemma 5.5. *Let $\varepsilon > 0$ be as in Theorem 5.3, x be a point in $\mathbb{R}^3 \setminus (\overline{\Sigma} \cup \sigma)$, and $p = p_\sigma(x)$; then, the gradient $\nabla\delta_\sigma(x)$ reads:*

$$\nabla\delta_\sigma(x) = \frac{x-p}{\delta_\sigma(x)}.$$

Proof. This is a simple consequence of the theorem of differentiation of a minimum value with respect to a parameter, see [55, Ch. 10, Thm. 2.1]. ∎

By analogy with the two-dimensional situation of Section 2.2.2, the unit vector field $\frac{x-p_\sigma(x)}{\delta_\sigma(x)}$, defined on $\mathbb{R}^3 \setminus (\overline{\Sigma} \cup \sigma)$, pointing from σ to x, is denoted by $n(x)$; as a consequence of the definition and Lemma 5.5, it holds:

$$\nabla n(x) = \nabla n^T(x) = \nabla^2\delta_\sigma.$$

We also introduce the unit vector field

$$b : \mathbb{R}^3 \setminus (\overline{\Sigma} \cup \sigma) \to \mathbb{R}^3, \quad b(x) = \tau(p) \times n(x),$$

so that for any point $x \in \mathbb{R}^3 \setminus (\overline{\Sigma} \cup \sigma)$, $(\tau(p), n(x), b(x))$ is a direct orthonormal frame of $\mathbb{R}^3$. Note that $(n(x), b(x))$ is also the vector basis for the polar coordinates in the plane $N_{\tau(p)}$; see again Figure 5.1.

The next result of interest is about the derivative of the projection mapping p_σ:

Proposition 5.6. *Let $x \in \mathbb{R}^3 \setminus \overline{\Sigma}$ and $p = p_\sigma(x)$. Then, the derivative $\nabla p_\sigma(x)$ reads, in any orthonormal basis of $\mathbb{R}^3$ with $\tau(p)$ as first coordinate vector:*

$$\nabla p_\sigma(x) = \begin{pmatrix} \frac{1}{1-\delta_\sigma(x)a(p)\cdot n(x)} & 0 & 0 \\ 0 & 0 & 0 \\ 0 & 0 & 0 \end{pmatrix}.$$

Proof. We already know from Theorem 5.3 and the subsequent remark that the mapping $\mathbb{R}^3 \setminus \overline{\Sigma} \ni x \mapsto p_\sigma(x) \in \sigma$ is smooth; hence, it is enough to calculate $\nabla p_\sigma(x)$ for $x \in R^3 \setminus (\overline{\Sigma} \cup \sigma)$, which we do. Using Lemma 5.5, it holds, for $x \in \mathbb{R}^3 \setminus (\overline{\Sigma} \cup \sigma)$,

$$p_\sigma(x) = x - \delta_\sigma(x)\nabla\delta_\sigma(x),$$

and so:

$$\nabla p_\sigma(x) = \mathrm{I} - \nabla\delta_\sigma(x) \otimes \nabla\delta_\sigma(x) - \delta_\sigma(x)\nabla^2\delta_\sigma(x);$$

in particular, $\nabla p_\sigma(x)$ is a symmetric 3×3 matrix. Also, Theorem 5.3 implies that for any given vector $z \in N_{\tau(p)}$ and for $s > 0$ small enough, $p_\sigma(x + sz) = p_\sigma(x)$, so that, for any such vector:

$$\nabla p_\sigma(x)z = 0.$$

Therefore, the proof of the proposition is complete provided we show the following relation:

$$\forall z \in \mathbb{R}^3, \quad \nabla p_\sigma(x)z \cdot \tau(p) = \frac{z \cdot \tau(p)}{1 - a(p) \cdot (x-p)}, \tag{5.5}$$

which is our next task.

To this end, differentiating the relation

$$\tau(p_\sigma(x)) \cdot (x - p_\sigma(x)) = 0$$

at x, in an arbitrary direction $z \in \mathbb{R}^3$ yields:

$$(\nabla\tau(p)\nabla p_\sigma(x)z) \cdot (x-p) + \tau(p) \cdot (z - \nabla p_\sigma(x)z) = 0, \tag{5.6}$$

in which the directional derivative $\nabla p_\sigma(x)z$ is a tangent vector to σ at p. On the other hand, by definition, for any tangent vector $\tilde{z}$ at σ at p, it holds:

$$\nabla\tau(p)\tilde{z} = \frac{\mathrm{d}}{\mathrm{d}s}\tau(c(s))\Big|_{s=0}$$

where $c : (-l, l) \to \sigma$ is an arbitrary local parametrization of σ with $c(0) = p$ and $c'(0) = \tilde{z} = (\tilde{z} \cdot \tau(p))\tau(p)$. Selecting a curve c with constant velocity $|c'(s)|$ satisfying these properties, it follows from the definition of $a(p)$ that:

$$\nabla\tau(p)\tilde{z} = (\tilde{z} \cdot \tau(p))a(p).$$

In particular, taking $\tilde{z} = \nabla p_\sigma(x)z$ in the above identity, we obtain:

$$\nabla\tau(p)\nabla p_\sigma(x)z = (\nabla p_\sigma(x)z \cdot \tau(p))\, a(p). \tag{5.7}$$

Inserting eq. (5.7) into eq. (5.6) finally yields:

$$((\nabla p_\sigma(x)z) \cdot \tau(p))\, (a(p) \cdot (x - p)) + \tau(p) \cdot (z - \nabla p_\sigma(x)z) = 0,$$

whence eq. (5.5) follows, thus completing the proof of the proposition. ∎

It follows from Proposition 5.6 and the definition of $n(x)$ that the derivative of the mapping $x \mapsto n(x)$ reads, in the local basis $(\tau(p), n(x), b(x))$:

$$\forall x \in \mathbb{R}^3 \setminus (\overline{\Sigma} \cup \sigma), \quad \nabla n(x) = \begin{pmatrix} \frac{-a(p)\cdot n(x)}{1-\delta_\sigma(x)a(p)\cdot n(x)} & 0 & 0 \\ 0 & 0 & 0 \\ 0 & 0 & \frac{1}{\delta_\sigma(x)} \end{pmatrix}. \tag{5.8}$$

Likewise, exploiting the orthonormality relations within the basis (τ, n, b), simple albeit lengthy calculations yield the following formulas (in the same basis):

$$\nabla\tau(x) = \begin{pmatrix} 0 & 0 & 0 \\ \frac{a(p)\cdot n}{1-\delta_\sigma(x)a(p)\cdot n} & 0 & 0 \\ 0 & 0 & 0 \end{pmatrix}, \quad \text{and} \quad \nabla b(x) = \begin{pmatrix} 0 & 0 & 0 \\ 0 & 0 & -\frac{1}{\delta_\sigma(x)} \\ 0 & 0 & 0 \end{pmatrix}. \tag{5.9}$$

Let us now apply the coarea formula of Lemma A.1 to the mapping $p_\sigma : \mathbb{R}^3 \setminus \overline{\Sigma} \to \sigma$:

Proposition 5.7. *Let $\varphi \in L^1(D)$; then,*

$$\int_D \varphi(x)\,\mathrm{d}x = \int_\sigma \left(\int_{D \cap P_\sigma(p)} (1 - |z|a(p) \cdot n(z))\varphi(p + z)\,\mathrm{ds}(z) \right) \mathrm{d}\ell(p).$$

In the above formula, as in the rest of this article, $\mathrm{d}\ell$ stands for the line measure on σ (that is, the restriction to σ of the one-dimensional Hausdorff measure), while ds is the surface measure on each normal plane $N_{\tau(p)}$ (the restriction to $N_{\tau(p)}$ of the two-dimensional Hausdorff measure).

We conclude this section with a few useful notations:

- The *normal component* v_N of a vector field $v : \mathbb{R}^3 \to \mathbb{R}^3$ is given by:
$$\forall x \in \mathbb{R}^3 \setminus \overline{\Sigma}, \quad v_N(x) = v(x) - (v(x) \cdot \tau(x))\tau(x).$$
- Accordingly, the normal component $\nabla_N u$ of the gradient of a smooth enough function $u : \mathbb{R}^3 \to \mathbb{R}$ is defined on $\mathbb{R}^3 \setminus \overline{\Sigma}$ by:
$$\nabla_N u = (\nabla u)_N = \nabla u - \frac{\partial u}{\partial \tau}\tau.$$
- The *normal part* e_N of a symmetric matrix $e \in \mathcal{S}_3(\mathbb{R})$ is:
$$e_N = e - (e\tau) \otimes \tau - \tau \otimes (e\tau) + (e\tau \cdot \tau)\tau \otimes \tau.$$

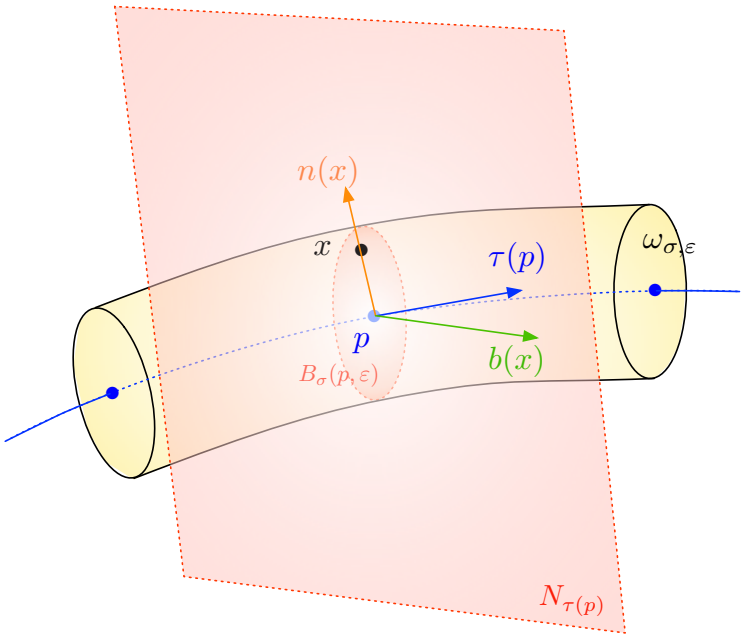

Figure 5.1. Illustration of the main objects attached to the 3d tubular inclusions considered in Section 5.1.

- The *normal derivative* $\nabla_N v$ of a smooth enough vector field $v : \mathbb{R}^3 \to \mathbb{R}^3$ is defined on $\mathbb{R}^3 \setminus \overline{\Sigma}$ by:

$$\nabla_N v = \nabla v - (\nabla v \tau) \otimes \tau,$$

and so the *normal strain tensor* of v is:

$$e_N(v) = \frac{1}{2}(\nabla_N v + (\nabla_N v)^T).$$

This strain tensor can be expressed in the local basis (n, b) of the plane $N_{\tau(p)}$ as:

$$e_N(v) = (e(v)n \cdot n)n \otimes n + (e(v)b \cdot b)b \otimes b + (e(v)n \cdot b)(n \otimes b + b \otimes n),$$

and with a small abuse of notations, we shall either consider $e_N(v)$ as a 3×3 symmetric matrix with 0 entries in the τ indices, or as a 2×2 matrix.

Note that eqs. (5.8) and (5.9) imply immediately:

$$e_N(v) = e_N(v_N).$$

Also, for smooth enough vector fields $v, w : \mathbb{R}^3 \to \mathbb{R}^3$, it holds:

$$e(v) : e(w) = e_N(v) : e_N(w) + 2(e(v)\tau)_N \cdot (e(w)\tau)_N + (\nabla v \tau \cdot \tau)(\nabla w \tau \cdot \tau). \tag{5.10}$$

5.2. **Formal derivation of the asymptotic expansion of u_ε**

In this section, we look for the asymptotic expansion of the perturbed potential u_ε, the solution to eq. (5.2), as the thickness ε of the tubular inclusion $\omega_{\sigma,\varepsilon}$ vanishes. As we have already emphasized, our argument is formal; even though we believe that it could be made rigorous, along the lines of [54, 91], this goes beyond the scope of this article. Since the next result has only been proved rigorously in the literature in a particular case (see again [32]), we state it as a conjecture.

Conjecture 5.8. *The following formula holds, for any point $x \in D \setminus \sigma$:*

$$u_\varepsilon(x) = u_0(x) + \varepsilon^2 u_1(x) + \mathrm{o}(\varepsilon^2), \text{quadwhere } u_1(x) := \int_\sigma \mathcal{M}(p)\nabla u_0(p) \cdot \nabla_y N(x,p)\, \mathrm{d}\ell(p). \tag{5.11}$$

Here, $N(x,y)$ is the Green's function of the background equation eq. (5.1)*; see Section 2.2.1 and notably Remark 2.4. For $p \in \sigma$, the polarization tensor $\mathcal{M}(p)$ is the 3×3 matrix defined by the following formula, expressed in any orthonormal basis of $\mathbb{R}^3$ with $\tau(p)$ as first coordinate vector:*

$$\mathcal{M}(p) = \begin{pmatrix} \pi(\gamma_1 - \gamma_0)(p) & 0 \\ 0 & \mathcal{M}_{NN}(p) \end{pmatrix}, \tag{5.12}$$

where the 2×2 submatrix $\mathcal{M}_{NN}(p)$ is the polarization tensor associated to a disk-shaped, diametrically small inclusion in 2d:

$$\mathcal{M}_{NN}(p) = 2\pi\gamma_0(p)\frac{\gamma_1(p) - \gamma_0(p)}{\gamma_0(p) + \gamma_1(p)}\mathrm{I};$$

see Section 4 and eq. (4.11)*.*

Formal argument. Let us, as usual, consider the error $r_\varepsilon := \frac{1}{\varepsilon^2}(u_\varepsilon - u_0) \in H^1_{\Gamma_D}(D)$, which is the unique solution to the following variational problem:

$$\forall v \in H^1_{\Gamma_D}(D), \quad \int_D \gamma_\varepsilon \nabla r_\varepsilon \cdot \nabla v \,\mathrm{d}x = -\frac{1}{\varepsilon^2}\int_{\omega_{\sigma,\varepsilon}} (\gamma_1 - \gamma_0)\nabla u_0 \cdot \nabla v \,\mathrm{d}x,$$

or equivalently, the solution to the minimization problem:

$$\min_{u \in H^1_{\Gamma_D}(D)} E_\varepsilon(u), \text{ where } E_\varepsilon(u) := \frac{1}{2}\int_D \gamma_\varepsilon |\nabla u|^2 \,\mathrm{d}x + \frac{1}{\varepsilon^2}\int_{\omega_{\sigma,\varepsilon}} (\gamma_1 - \gamma_0)\nabla u_0 \cdot \nabla u \,\mathrm{d}x.$$

We proceed in three steps.

Step 1: We write a representation formula for the error $r_\varepsilon(x)$ "far " from σ, in terms of the Green's function $N(x,y)$ of the background operator eq. (4.1) and the values of r_ε inside $\omega_{\sigma,\varepsilon}$. Considering an arbitrary, fixed point $x \in D \setminus \sigma$, one obtains exactly as in the proof of Theorem 2.1 that, for $\varepsilon > 0$ small enough:

$$r_\varepsilon(x) = \frac{1}{\varepsilon^2}\int_{\omega_{\sigma,\varepsilon}} (\gamma_1 - \gamma_0)(y)\nabla u_0(y) \cdot \nabla_y N(x,y)\,\mathrm{d}y + \int_{\omega_{\sigma,\varepsilon}} (\gamma_1 - \gamma_0)(y)\nabla r_\varepsilon \cdot \nabla_y N(x,y)\,\mathrm{d}y. \tag{5.13}$$

Step 2: We analyze the limiting behavior of a rescaled version of r_ε inside $\omega_{\sigma,\varepsilon}$. In order to carry out this formal part of our argument, let us introduce the mapping $m_\varepsilon : \omega_{\sigma,1} \to \omega_{\sigma,\varepsilon}$ defined by:

$$m_\varepsilon(x) = p_\sigma(x) + \varepsilon\delta_\sigma(x)n(x), \tag{5.14}$$

where we recall the notation $n(x) = \frac{x - p_\sigma(x)}{\delta_\sigma(x)}$ from Section 5.1. According to Lemma 5.5 and Proposition 5.6, the derivative of m_ε reads, at an arbitrary point $x \in \omega_{\sigma,1}$:

$$\nabla m_\varepsilon(x) = \begin{pmatrix} \frac{1 - \varepsilon\delta_\sigma(x)a(x)\cdot n(x)}{1 - \delta_\sigma(x)a(x)\cdot n(x)} & 0 & 0 \\ 0 & \varepsilon & 0 \\ 0 & 0 & \varepsilon \end{pmatrix}, \tag{5.15}$$

in any orthonormal basis of $\mathbb{R}^3$ having $\tau(p)$ as first coordinate vector. What's more, still using the material from Section 5.1, m_ε can be extended to a mapping $\mathbb{R}^3 \setminus \overline{\Sigma} \to \mathbb{R}^3 \setminus \overline{\Sigma}$, and we introduce the rescaled remainder $s_\varepsilon := \varepsilon r_\varepsilon \circ m_\varepsilon$, which will naturally be involved during the calculations of the third step. In order to analyze its behavior near the unit inclusion set $\omega_{\sigma,1}$, we express s_ε as the minimizer of a rescaled version of the energy functional $E_\varepsilon(u)$, which we subsequently simplify by retaining only the leading order terms as $\varepsilon \to 0$.

Using the coarea formula of Proposition 5.7, $E_\varepsilon(u)$ rewrites, for an arbitrary function $u \in H^1_{\Gamma_D}(D)$:

$$E_\varepsilon(u) = \frac{1}{2}\int_\sigma \left(\int_{D\cap P_\sigma(p)} (1-|z|a(p)\cdot n(z))\gamma_\varepsilon(p+z)|\nabla u|^2(p+z)\,\mathrm{ds}(z)\right)\mathrm{d}\ell(p)$$
$$+ \frac{1}{\varepsilon^2}\int_\sigma \left(\int_{B_\sigma(p,\varepsilon)} (1-|z|a(p)\cdot n(z))(\gamma_1-\gamma_0)(p+z)\nabla u_0(p+z)\cdot\nabla u(p+z)\,\mathrm{ds}(z)\right)\mathrm{d}\ell(p).$$

We now rescale both inner integrals in the above expression by means of the mapping m_ε; this yields:

$$E_\varepsilon(u) = \frac{\varepsilon^2}{2}\int_\sigma \left(\int_{\frac{1}{\varepsilon}(D\cap P_\sigma(p))} (1-\varepsilon|z|a(p)\cdot n(z))\gamma_\varepsilon(p+\varepsilon z)|\nabla u\circ m_\varepsilon|^2(p+z)\,\mathrm{ds}(z)\right)\mathrm{d}\ell(p)$$
$$+\int_\sigma \left(\int_{B_\sigma(p,1)} (1-\varepsilon|z|a(p)\cdot n(z))(\gamma_1-\gamma_0)(p+\varepsilon z)\nabla u_0(p+\varepsilon z)\cdot(\nabla u\circ m_\varepsilon)(p+z)\,\mathrm{ds}(z)\right)\mathrm{d}\ell(p).$$

A simple calculation allows to see that the rescaled version $v = \varepsilon u\circ m_\varepsilon$ of an arbitrary function $u\in H^1_{\Gamma_D}(D)$ satisfies:

$$\begin{aligned}(\nabla u)\circ m_\varepsilon &= \frac{1}{\varepsilon}\nabla m_\varepsilon^{-T}\nabla v\\ &= \frac{1}{\varepsilon}\frac{1-\delta_\sigma a\cdot n}{1-\varepsilon\delta_\sigma a\cdot n}\left(\frac{\partial v}{\partial\tau}\right)\tau + \frac{1}{\varepsilon^2}\nabla_N v.\end{aligned}$$

Hence, the energy functional $E_\varepsilon(u)$ rewrites:

$$E_\varepsilon(u) = \frac{1}{\varepsilon^2}F_\varepsilon(v),$$

where we have defined:

$$\begin{aligned}F_\varepsilon(v) := \frac{1}{2}\int_\sigma \Bigg(\int_{\frac{1}{\varepsilon}(D\cap P_\sigma(p))} \gamma_\varepsilon(p+\varepsilon z)\Big(\varepsilon^2\frac{(1-|z|a(z)\cdot n(z))^2}{1-\varepsilon|z|a(z)\cdot n(z)}\left(\frac{\partial v}{\partial\tau}(p+z)\right)^2\\ + (1-\varepsilon|z|a(z)\cdot n(z))|\nabla_N v(p+z)|^2\Big)\,\mathrm{ds}(z)\Bigg)\mathrm{d}\ell(p)\\ + \int_\sigma\Bigg(\int_{B_\sigma(p,1)}(\gamma_1-\gamma_0)(p+\varepsilon z)\Big(\varepsilon(1-\varepsilon|z|a(z)\cdot n(z))\frac{\partial u_0}{\partial\tau}(p+\varepsilon z)\frac{\partial v}{\partial\tau}(p+z)\\ +(1-\varepsilon|z|a(z)\cdot n(z))\nabla_N u_0(p+\varepsilon z)\cdot\nabla_N v(p+z)\Big)\,\mathrm{ds}(z)\Bigg)\mathrm{d}\ell(p). \quad (5.16)\end{aligned}$$

Like in the situations tackled in the previous sections, we expect that the limiting behavior of the rescaled remainder $s_\varepsilon = \varepsilon r_\varepsilon\circ m_\varepsilon$ "near" the rescaled inclusion set $\omega_{\sigma,1}$ can be determined by looking at the solution to the minimization problem

$$\min_v F_\varepsilon(v).$$

Let us emphasize that the above formulation is not mathematically rigorous, and we deliberately do not attempt to provide an adapted functional framework, which seems a difficult task.

According to our methodology, we look after the minimization of the approximate energy functional $\widetilde{F}(v)$ obtained from $F_\varepsilon(v)$ by retaining only leading-order terms:

$$\widetilde{F}(v) = \frac{1}{2}\int_\sigma \int_{N_{\tau(p)}} \widehat{\gamma}(p,z)|\nabla_N v|^2(p+z)\,\mathrm{ds}(z)\,\mathrm{d}\ell(p) + \int_\sigma \int_{B_\sigma(0,1)} (\gamma_1-\gamma_0)(p)\nabla_N u_0(p)\cdot\nabla_N v(p+z)\,\mathrm{ds}(z)\,\mathrm{d}\ell(p), \quad (5.17)$$

where we have defined, for $p\in\sigma$ and $z\in N_{\tau(p)}$:

$$\widehat{\gamma}(p,z) = \begin{cases}\gamma_1(p) & \text{if } z\in B_\sigma(0,1),\\ \gamma_0(p) & \text{otherwise.}\end{cases}$$

Note that the formal simplification eq. (5.17) from eq. (5.16) – and notably the change in domains of integration for the inner integrals, from $\frac{1}{\varepsilon}(D\cap P_\sigma(p))$ to the whole plane $N_{\tau(p)}$ – tacitly relies on the intuition that for a fixed point $p\in\sigma$, the function $N_{\tau(p)}\ni z\mapsto v(p+z)$ vanishes when $|z|\to\infty$.

That the coefficients of the energy $\widetilde{F}(v)$ have a tensorized structure with respect to $\sigma\times B_\sigma(p,1)$ entices us to search for the limiting behavior v of s_ε in the tubular region $\omega_{\sigma,1}$ as $\varepsilon\to 0$ under the form:

$$\forall p\in\sigma,\quad \forall z\in N_{\tau(p)},\quad s_\varepsilon(p+z)\approx v(p,z),$$

for a function $v:\Big\{(p,z)\in\sigma\times\mathbb{R}^3,\ z\in N_{\tau(p)}\Big\}\to\mathbb{R}$ to be determined. To achieve this task, we use the Euler–Lagrange equations for the minimization of eq. (5.17), with test functions of the form

$$\forall p\in\sigma,\quad \forall z\in N_{\tau(p)},\quad w(p+z)=\varphi(p)\psi(z),$$

for arbitrary smooth functions $\varphi\in\mathcal{C}^\infty(\sigma)$, $\psi\in\mathcal{C}^\infty(N_{\tau(p)})$. This immediately yields that for every point $p\in\sigma$, the mapping $N_{\tau(p)}\ni z\mapsto v(p,z)$ is the solution to the following exterior problem posed on the plane $N_{\tau(p)}$:

$$\begin{cases} -\Delta_z v(p,z) = 0 & \text{for } z\in N_{\tau(p)}\setminus\partial B_\sigma(0,1),\\ v(p,z)^+ = v(p,z)^- & \text{for } z\in\partial B_\sigma(0,1),\\ \gamma_0(p)\frac{\partial v^+}{\partial n_z}(p,z)-\gamma_1(p)\frac{\partial v^-}{\partial n_z}(p,z) = -(\gamma_0-\gamma_1)(p)\nabla_N u_0(p)\cdot n(z) & \text{for } z\in\partial B_\sigma(0,1),\\ |v(p,z)|\to 0 & \text{when } z\to\infty. \end{cases} \quad (5.18)$$

In other terms, we recognize that the function $z\mapsto v(p,z)$ is

$$v(p,z)=\phi_{\nabla_N u_0(p)}(z),$$

where for $\xi\in\mathbb{R}^2$, $\phi_\xi\in W_0^{1,-1}(\mathbb{R}^2)$ is the (radial) cell function attached to a 2d diametrically small, disk-shaped inclusion; see eq. (4.5). Note that, in the above formula, (and in eq. (5.18) before that), we have identified the plane $N_{\tau(p)}$ with $\mathbb{R}^2$ (that is, we have identified one orthonormal basis of the former plane with one of the latter). Since both functions $z\mapsto v(p,z)$ and $\phi_{\nabla_N u_0(p)}$ have radial symmetry, this identification can be performed in an arbitrary way, and the forthcoming considerations do not depend on this choice.

To conclude this second step, we note for further reference that the following identity holds:

$$\mathcal{M}_{NN}(p)\nabla_N u_0(p) = (\gamma_1(p)-\gamma_0(p))\int_{B_\sigma(p,1)}\Big(\nabla_N u_0(p)+\nabla_N v(p,z)\Big)\,\mathrm{ds}(z), \quad (5.19)$$

as a consequence of the expression eq. (4.4) of the polarization tensor $\mathcal{M}_{NN}(p)$ and of eqs. (4.5) and (5.18).

Step 3: We pass to the limit in the representation formula eq. (5.13). Rescaling both integrals in the right-hand side of eq. (5.13) by means of the mapping m_ε, we obtain:

$$\begin{aligned}
r_\varepsilon(x) &= \frac{1}{\varepsilon^2}\int_{\omega_{\sigma,1}} |\det(\nabla m_\varepsilon)|(\gamma_1-\gamma_0)(m_\varepsilon(z))(\nabla u_0)(m_\varepsilon(z))\cdot\nabla_y N(x,m_\varepsilon(z))\,\mathrm{d}z \\
&\quad + \int_{\omega_{\sigma,1}} (\gamma_1-\gamma_0)(m_\varepsilon(z))|\det(\nabla m_\varepsilon)|\nabla m_\varepsilon^{-T}\nabla(r_\varepsilon\circ m_\varepsilon)\cdot\nabla_y N(x,m_\varepsilon(z))\,\mathrm{d}z, \\
&= \int_{\omega_{\sigma,1}} \frac{1-\varepsilon\delta_\sigma(z)a(z)\cdot n(z)}{1-\delta_\sigma(z)a(z)\cdot n(z)}(\gamma_1-\gamma_0)(m_\varepsilon(z))(\nabla u_0)(m_\varepsilon(z))\cdot\nabla_y N(x,m_\varepsilon(z))\,\mathrm{d}z \\
&\quad + \int_{\omega_{\sigma,1}} (\gamma_1-\gamma_0)(m_\varepsilon(z))\left(\varepsilon\frac{\partial s_\varepsilon}{\partial\tau}\frac{\partial N}{\partial\tau_y}(x,m_\varepsilon(z)) + \frac{1-\varepsilon\delta_\sigma(z)a(z)\cdot n(z)}{1-\delta_\sigma(z)a(z)\cdot n(z)}\nabla_N s_\varepsilon\cdot\nabla_{N_y}N(x,m_\varepsilon(z))\right)\mathrm{d}z,
\end{aligned}$$

where we have used the expression eq. (5.15) of the derivative of m_ε as well as the definition of s_ε. Now bringing into play the approximation of s_ε by the function v in eq. (5.18) inferred in the course of the second step, then using the coarea formula of Proposition 5.7, it follows:

$$\begin{aligned}
\lim_{\varepsilon\to0} r_\varepsilon(x) &= \int_{\omega_{\sigma,1}} \frac{1}{1-\delta_\sigma(z)a(z)\cdot n(z)}(\gamma_1-\gamma_0)\circ p_\sigma(\nabla u_0\circ p_\sigma)\cdot\nabla_y N(x,p_\sigma(z))\,\mathrm{d}z \\
&\quad + \int_{\omega_{\sigma,1}} \frac{1}{1-\delta_\sigma(z)a(z)\cdot n(z)}(\gamma_1-\gamma_0)\circ p_\sigma\nabla_N v\cdot\nabla_{N_y}N(x,p_\sigma(z))\,\mathrm{d}z, \\
&= \int_\sigma\int_{B_\sigma(p,1)} (\gamma_1-\gamma_0)(p)\nabla u_0(p)\cdot\nabla_y N(x,p)\,\mathrm{d}s(z)\,\mathrm{d}\ell(p) \\
&\quad + \int_\sigma\int_{B_\sigma(p,1)} (\gamma_1-\gamma_0)(p)\nabla_N v(p,z)\cdot\nabla_{N_y}N(x,p)\,\mathrm{d}s(z)\,\mathrm{d}\ell(p), \\
&= \int_\sigma |B_\sigma(p,1)|(\gamma_1-\gamma_0)(p)\frac{\partial u_0}{\partial\tau}(p)\frac{\partial N}{\partial\tau_y}(x,p)\,\mathrm{d}\ell(p) \\
&\quad + \int_\sigma\int_{B_\sigma(p,1)} (\gamma_1-\gamma_0)(p)\Big(\nabla_N u_0(p)+\nabla_N v(p,z)\Big)\cdot\nabla_{N_y}N(x,p)\,\mathrm{d}s(z)\,\mathrm{d}\ell(p).
\end{aligned}$$

Using finally eq. (5.19) to reformulate the second integral in the above right-hand side in terms of the two-dimensional polarization tensor $\mathcal{M}_{NN}$, we finally obtain:

$$\lim_{\varepsilon\to0} r_\varepsilon(x) = \pi\int_\sigma(\gamma_1-\gamma_0)(p)\frac{\partial u_0}{\partial\tau}(p)\frac{\partial N}{\partial\tau_y}(x,p)\,\mathrm{d}\ell(p) + \int_\sigma \mathcal{M}_{NN}\nabla_N u_0(p)\cdot\nabla_{N_y}N(x,p)\,\mathrm{d}\ell(p),$$

which is the desired result. ∎

5.3. **Asymptotic expansion of a quantity of interest involving u_ε**

We now consider the derivative of a functional depending on the small thickness ε via the perturbed potential u_ε in eq. (5.2) of the form:

$$J_\sigma(\varepsilon) = \int_D j(u_\varepsilon)\,\mathrm{d}x,$$

where $j:\mathbb{R}\to\mathbb{R}$ is a smooth function satisfying the growth conditions eq. (2.8). The result of interest is the following proposition, whose proof is again omitted; see the proof of Proposition 2.10 if need be.

Proposition 5.9. *The function $J_\sigma(\varepsilon)$ has the following asymptotic expansion as $\varepsilon\to0$,*

$$J_\sigma(\varepsilon) = J_\sigma(0) + \varepsilon^2 J'_\sigma(0) + \mathrm{o}(\varepsilon^2),$$

where the "derivative" $J'_\sigma(0)$ reads:

$$J'_\sigma(0) = \int_\sigma \mathcal{M}\nabla u_0 \cdot \nabla p_0 \, \mathrm{d}x. \tag{5.20}$$

In the above formula, $\mathcal{M}$ is the polarization tensor defined in eq. (5.12)*, and the adjoint state p_0 is the unique solution in $H^1_{\Gamma_D}(D)$ to the equation:*

$$\begin{cases} -\operatorname{div}(\gamma_0 \nabla p_0) = -j'(u_0) & \text{in } D, \\ p_0 = 0 & \text{on } \Gamma_D, \\ \gamma_0 \frac{\partial p_0}{\partial n} = 0 & \text{on } \partial D \setminus \overline{\Gamma_D}. \end{cases}$$

A more practical version of this result reads:

$$J'_\sigma(0) = \int_\sigma P(x, \tau_1(x), \tau_2(x), \tau_3(x)) \, \mathrm{d}\ell(x),$$

where for $x \in \sigma$, $\tau = (\tau_1, \tau_2, \tau_3) \mapsto P(x, \tau_1, \tau_2, \tau_3)$ is the trivariate polynomial with degree 2:

$$P(x, \tau_1, \tau_2, \tau_3) = 2\pi\gamma_0(x)\frac{\gamma_1(x) - \gamma_0(x)}{\gamma_1(x) + \gamma_0(x)} \nabla u_0(x) \cdot \nabla p_0(x) + \pi \frac{(\gamma_1(x) + \gamma_0(x))^2}{\gamma_1(x) + \gamma_0(x)} \left(\nabla u_0(x) \otimes \nabla p_0(x)\right) \tau \cdot \tau.$$

5.4. **Comparison between the 2d and the 3d cases**

Let us conclude this study of thin tubular inhomogeneities in the context of the three-dimensional conductivity equation with a few remarks about the differences between the 2d case analyzed in Section 2 and the present 3d situation. In order to ease the discussion, we go on assuming that the curve σ is closed.

However similar at first glance, the 2d and 3d asymptotic formulas eq. (2.5) and eq. (5.11) have actually quite different structures. As we have seen indeed, the first non trivial term u_1 in the 2d expansion of u_ε is "variational", insofar as it can be characterized as the solution to a fairly classical boundary value problem (or as the minimizer of the corresponding energy functional) and it belongs to a functional space which is inherited from that associated to u_ε; see the equation eq. (2.15) and the comments thereafter.

On the contrary, in the three-dimensional case, u_1 cannot be characterized in the same fashion: intuitively, curves in 3d are "too small" sets to bear boundary conditions in the context of a "standard" second-order elliptic problem (they have zero harmonic capacity). This difference is reflected by the difference in order (ε^2 rather than ε) at which the correction u_1 comes up in eq. (5.11).

Another interesting manifestation of this phenomenon lies in the study that we carried out during the second step of the proofs of Theorem 2.1 and Conjecture 5.8, about the "far field" u and the "near field" v, as the limiting behaviors of the error $r_\varepsilon = \frac{1}{\varepsilon^{d-1}}(u_\varepsilon - u_0)$ and its rescaled version s_ε, respectively. In our 2d analysis, we have not completely determined the limit v of s_ε inside the unit inclusion set $\omega_{\sigma,1}$ (and we did not need to do so). In this case actually, the complete limiting behavior v would depend on the "far field" u; see Remark 2.8. If we were to try and apply verbatim the methodology used in the context of Conjecture 5.8 in the 2d case, we would have to consider, for each point $p \in \sigma$, an exterior problem posed on the normal line to σ at p, that is, a one-dimensional version of eq. (5.18). This 1d exterior problem has no solution decaying to 0 at infinity, but only solutions tending to constant values at infinity. These constants are exactly the connection between the limiting behaviors of the "near field" v and the "far field" u that we observed in the case of the 2d conductivity equation. On the contrary, we have seen that in 3d, the 2d exterior problem eq. (5.18) characterizing the "near field" v in each normal plane to σ has a solution which goes to 0 at infinity. As a result, it is a completely determined function, independently of the "far field".

6. The linear elasticity case in three space dimensions

In this section, we adapt the previous considerations to analyze the effects of thin tubular inhomogeneities in the context of 3d linearly elastic structures, a situation which has not yet been addressed in the literature, to the best of our knowledge.

The physical setting is the exact three-dimensional counterpart to that described in Section 3.1.1. Inside a bounded, Lipschitz domain D, the "background" and perturbed displacements $u_0, u_\varepsilon : D \to \mathbb{R}^3$ are the solutions to the 3d versions of the systems eq. (3.3) and eq. (3.4), respectively. The two isotropic materials featured in these equations are physically described by Hooke's laws A_0, A_1 of the form eq. (3.1), with respective Lamé parameters λ_0, μ_0 and λ_1, μ_1.

Using our formal energy method, we derive the asymptotic expansion of the perturbed displacement $u_\varepsilon \in H^1_{\Gamma_D}(D)^3$ in terms of u_0 and a suitable polarization tensor $\mathcal{M}$. Since the derivation is analogous to that conducted in the 3d conductivity setting in Section 5 (up to an increased level of technicality), we solely provide the main steps of the argument.

Conjecture 6.1. *The following asymptotic expansion holds at an arbitrary point $x \in D \setminus \sigma$:*

$$u_\varepsilon(x) = u_0(x) + \varepsilon^2 u_1(x) + \mathrm{o}(\varepsilon^2), \text{ where } u_1(x) = \int_\sigma \mathcal{M}(p) e(u_0) : e_y(N(x,p)) \, \mathrm{d}\ell(p),$$

$N(x,y)$ is the Green's function of the background operator in eq. (3.3) *(see Remark 3.1), and the polarization tensor $\mathcal{M}(p)$ is defined at any point $p \in \sigma$ by:*

$$\forall e, \tilde{e} \in \mathcal{S}_d(\mathbb{R}), \quad \mathcal{M}e : \tilde{e} = \mathcal{M}_{NN} e_N : \tilde{e}_N + \frac{\pi(\lambda_1 - \lambda_0)(\lambda_0 + 2\mu_0)}{\mu_0 + \lambda_1 + \mu_1} \Big(\operatorname{tr}(e_N)(\tilde{e}\tau \cdot \tau) + (e\tau \cdot \tau) \operatorname{tr}(\tilde{e}_N) \Big)$$
$$+ 4\mathcal{M}_{\tau N}(e\tau)_N \cdot (\tilde{e}\tau)_N + \pi \left(2(\mu_1 - \mu_0) + (\lambda_1 - \lambda_0) - \frac{(\lambda_1 - \lambda_0)^2}{\mu_1 + \lambda_1 + \mu_0} \right) (e\tau \cdot \tau)(\tilde{e}\tau \cdot \tau). \quad (6.1)$$

Here, we have omitted the mention to the point p under consideration for brevity. We have also introduced the two tensors $\mathcal{M}_{\tau N}(p)$ and $\mathcal{M}_{NN}(p)$, acting on two-dimensional quantities, defined by:

- *$\mathcal{M}_{\tau N}(p)$ is the 2×2 matrix describing the effect of a disk-shaped, diametrically small inclusion in the 2d conductivity setting, where the conductivity coefficients at play equal $\mu_0(p)$ and $\mu_1(p)$, namely:*
$$\mathcal{M}_{\tau N}(p) = 2\pi\mu_0(p) \frac{\mu_1(p) - \mu_0(p)}{\mu_1(p) + \mu_0(p)} \mathrm{I}; \quad (6.2)$$
see eq. (4.11).

- *$\mathcal{M}_{NN}(p)$ is the isotropic fourth-order tensor describing the effect of a disk-shaped diametrically small inclusion in the linear elasticity setting; it is defined for any symmetric 2×2 matrix e by:*
$$\mathcal{M}_{NN}(p)e = \alpha_S(p) \operatorname{tr}(e) \mathrm{I} + \beta_S(p) e, \quad (6.3)$$
where the coefficients $\alpha_S(p)$ and $\beta_S(p)$ are given by eq. (4.13)*; see Section 4.4.*

Formal argument. As usual, let us introduce the error $r_\varepsilon := \frac{1}{\varepsilon^2}(u_\varepsilon - u_0)$, which is the unique solution in $H^1_{\Gamma_D}(D)^3$ to the variational problem

$$\forall v \in H^1_{\Gamma_D}(D)^3, \quad \int_D A_\varepsilon e(r_\varepsilon) : e(v) \, \mathrm{d}x = -\frac{1}{\varepsilon^2} \int_{\omega_{\sigma,\varepsilon}} (A_1 - A_0)(x) e(u_0) : e(v) \, \mathrm{d}x;$$

equivalently, r_ε is the unique solution to the minimization problem

$$\min_{u \in H^1_{\Gamma_D}(D)^3} E_\varepsilon(u), \text{ where } E_\varepsilon(u) := \frac{1}{2} \int_D A_\varepsilon e(u) : e(u) \, \mathrm{d}x + \frac{1}{\varepsilon^2} \int_{\omega_{\sigma,\varepsilon}} (A_1 - A_0) e(u_0) : e(u) \, \mathrm{d}x. \quad (6.4)$$

Step 1: We construct a representation formula for the error $r_\varepsilon(x)$ "far" from $\omega_{\sigma,\varepsilon}$ in terms of the Green's function $N(x,y)$ of the background equation eq. (3.3) and the values of r_ε inside $\omega_{\sigma,\varepsilon}$. Considering a fixed point $x \in D \setminus \sigma$ and arguing exactly as in the proof of Theorem 2.1 (Step 1), we obtain, for $j = 1, 2, 3$ and $\varepsilon > 0$ small enough:

$$r_{\varepsilon,j}(x) = \frac{1}{\varepsilon^2}\int_{\omega_{\sigma,\varepsilon}} (A_1 - A_0)(y)e(u_0)(y) : e_y(N_j(x,y))\,\mathrm{d}y + \int_{\omega_{\sigma,\varepsilon}} (A_1 - A_0)(y)e(r_\varepsilon)(y) : e_y(N_j(x,y))\,\mathrm{d}y. \quad (6.5)$$

Step 2: Asymptotic behavior of a rescaled version of r_ε. To conduct this formal step of our argument, let us introduce the rescaled error $s_\varepsilon := \varepsilon r_\varepsilon \circ m_\varepsilon$, where m_ε is the mapping given by eq. (5.14). We aim to determine the limiting behavior of s_ε near the rescaled inclusion set $\omega_{\sigma,1}$, and to this end, we perform a rescaling and a simplification of the energy functional $E_\varepsilon(u)$ in eq. (6.4).

At first, the coarea formula of Proposition 5.7 yields the following equivalent expression for the energy $E_\varepsilon(u)$ attached to an arbitrary function $u \in H^1_{\Gamma_D}(D)^3$:

$$E_\varepsilon(u) = \frac{1}{2}\int_\sigma \left(\int_{D\cap P_\sigma(p)} (1 - |y|a(p)\cdot n(y))(A_\varepsilon e(u) : e(u))(p+y)\,\mathrm{ds}(y)\right)\mathrm{d}\ell(p) + \frac{1}{\varepsilon^2}\int_\sigma \left(\int_{B_\sigma(p,\varepsilon)} (1 - |y|a(p)\cdot n(y))(A_1 - A_0)(p+y)e(u_0)(p+y) : e(u)(p+y)\,\mathrm{ds}(y)\right)\mathrm{d}\ell(p).$$

We then rescale both inner integrals in the above right-hand side owing to a change of variables involving m_ε; this yields:

$$E_\varepsilon(u) = \frac{\varepsilon^2}{2}\int_\sigma \left(\int_{\frac{1}{\varepsilon}(D\cap P_\sigma(p))} (1 - \varepsilon|z|a(p)\cdot n(z))(A_\varepsilon(e(u)\circ m_\varepsilon) : (e(u)\circ m_\varepsilon))(p+z)\,\mathrm{ds}(z)\right)\mathrm{d}\ell(p) + \int_\sigma \left(\int_{B_\sigma(p,1)} (1 - \varepsilon|z|a(p)\cdot n(z))(A_1 - A_0)(p+\varepsilon z)e(u_0)(p+\varepsilon z) : (e(u)\circ m_\varepsilon)(p+z)\,\mathrm{ds}(z)\right)\mathrm{d}\ell(p).$$

Now, elementary calculations based on eq. (5.14) allow to relate the strain tensor of a smooth enough vector-valued function $u : D \to \mathbb{R}^3$ to the derivatives of $v := \varepsilon u \circ m_\varepsilon$:

$$\begin{aligned} &e(u)\circ m_\varepsilon \\ &= \frac{1}{2}\Big(\nabla(u\circ m_\varepsilon)\nabla m_\varepsilon^{-1} + \nabla m_\varepsilon^{-T}\nabla(u\circ m_\varepsilon)^T\Big), \\ &= \frac{1}{\varepsilon}\begin{pmatrix} \frac{1-\delta_\sigma a\cdot n}{1-\varepsilon\delta_\sigma a\cdot n}e(v)\tau\cdot\tau & \frac{1}{2}\Big(\frac{1-\delta_\sigma a\cdot n}{1-\varepsilon\delta_\sigma a\cdot n}\nabla v\tau\cdot n + \frac{1}{\varepsilon}\nabla v n\cdot\tau\Big) & \frac{1}{2}\Big(\frac{1-\delta_\sigma a\cdot n}{1-\varepsilon\delta_\sigma a\cdot n}\nabla v\tau\cdot b + \frac{1}{\varepsilon}\nabla v b\cdot\tau\Big) \\ \frac{1}{2}\Big(\frac{1-\delta_\sigma a\cdot n}{1-\varepsilon\delta_\sigma a\cdot n}\nabla v\tau\cdot n + \frac{1}{\varepsilon}\nabla v n\cdot\tau\Big) & \frac{1}{\varepsilon}e(v)n\cdot n & \frac{1}{\varepsilon}e(v)n\cdot b \\ \frac{1}{2}\Big(\frac{1-\delta_\sigma a\cdot n}{1-\varepsilon\delta_\sigma a\cdot n}\nabla v\tau\cdot b + \frac{1}{\varepsilon}\nabla v b\cdot\tau\Big) & \frac{1}{\varepsilon}e(v)n\cdot b & \frac{1}{\varepsilon}e(v)b\cdot b \end{pmatrix}, \end{aligned} \quad (6.6)$$

where the above matrix is expressed in the local basis (τ, n, b) of the space. Similarly, it holds:

$$(\operatorname{div} u)\circ m_\varepsilon = \frac{1}{\varepsilon}\frac{1-\delta_\sigma a\cdot n}{1-\varepsilon\delta_\sigma a\cdot n}e(v)\tau\cdot\tau + \frac{1}{\varepsilon^2}\left(e(v)n\cdot n + e(v)b\cdot b\right). \quad (6.7)$$

A series of simple, albeit tedious calculations reveals that:

$$E_\varepsilon(u) = \frac{1}{\varepsilon^2}F_\varepsilon(v),$$

where we decompose the quantity $F_\varepsilon(v)$ in terms of the powers in ε of the coefficients in the featured integrals:

$$F_\varepsilon(v) = F_\varepsilon^1(v) + \varepsilon F_\varepsilon^2(v) + \varepsilon^2 F_\varepsilon^3(v);$$

in the above identity, each contribution $F_\varepsilon^i(v)$ has coefficients of order $\mathcal{O}(1)$ as $\varepsilon \to 0$, and only the expression of $F_\varepsilon^1(v)$ will be needed for our purpose:

$$\begin{aligned}
F_\varepsilon^1(v) = \frac{1}{2}\int_\sigma \Bigg(\int_{\frac{1}{\varepsilon}(D\cap P_\sigma(p))} & 2\mu_\varepsilon \circ m_\varepsilon(1-\varepsilon|z|a\cdot n)\Big((e(v)n\cdot n)^2 + (e(v)b\cdot b)^2 + 2(e(v)n\cdot b)^2 \\
& + \frac{1}{2}(\nabla v n\cdot\tau)^2 + \frac{1}{2}(\nabla v b\cdot\tau)^2\Big)\,\mathrm{ds}(z)\Bigg)\mathrm{d}\ell(p) \\
+ \frac{1}{2}\int_\sigma \Bigg(\int_{\frac{1}{\varepsilon}(D\cap P_\sigma(p))} & \lambda_\varepsilon \circ m_\varepsilon(1-\varepsilon|z|a\cdot n)\Big(e(v)n\cdot n + e(v)b\cdot b\Big)^2 \mathrm{ds}(z)\Bigg)\,\mathrm{d}\ell(p) \\
+ \int_\sigma \Bigg(\int_{B_\sigma(p,1)} & 2(\mu_1-\mu_0)\circ m_\varepsilon(1-\varepsilon|z|a\cdot n)\Big((e(u_0)n\cdot n)(e(v)n\cdot n) + (e(u_0)b\cdot b)(e(v)b\cdot b) \\
& + (e(u_0)\tau\cdot n)(\nabla v n\cdot\tau) + (e(u_0)\tau\cdot b)(\nabla v b\cdot\tau)\Big)\,\mathrm{ds}(z)\Bigg)\mathrm{d}\ell(p) \\
+ \int_\sigma \Bigg(\int_{B_\sigma(p,1)} & (1-\varepsilon|z|a\cdot n)\,(\lambda_1-\lambda_0)\circ m_\varepsilon(\operatorname{div} u_0)\circ m_\varepsilon\Big(e(v)n\cdot n + e(v)b\cdot b\Big)\,\mathrm{ds}(z)\Bigg)\,\mathrm{d}\ell(p).
\end{aligned}$$

In the above integrals, as often in the forthcoming calculations, the mention to the integration point $p+z$ is sometimes omitted when it is clear, for the sake of brevity.

Our methodology then proceeds as in the case of Conjecture 5.8. We expect that the limiting behavior v of s_ε near the rescaled inclusion set $\omega_{\sigma,1}$ be dictated by the minimization of the energy $F_\varepsilon^1(v)$, and, in turn, by that of a simplified version $\widetilde{F}(v)$ of the latter where only the leading-order terms as $\varepsilon \to 0$ are retained. More precisely, we consider the problem:

$$\min_v \widetilde{F}(v), \tag{6.8}$$

where:

$$\begin{aligned}
\widetilde{F}(v) = \frac{1}{2}\int_\sigma \Bigg(\int_{N_{\tau(p)}} & 2\widehat{\mu}(p,z)\Big((e(v)n\cdot n)^2 + (e(v)b\cdot b)^2 + 2(e(v)n\cdot b)^2 \\
& + \frac{1}{2}(\nabla v n\cdot\tau)^2 + \frac{1}{2}(\nabla v b\cdot\tau)^2\Big)\,\mathrm{ds}(z)\Bigg)\mathrm{d}\ell(p) \\
+ \frac{1}{2}\int_\sigma \Bigg(\int_{N_{\tau(p)}} & \widehat{\lambda}(p,z)\Big(e(v)n\cdot n + e(v)b\cdot b\Big)^2 \mathrm{ds}(z)\Bigg)\,\mathrm{d}\ell(p) \\
+ \int_\sigma \Bigg(\int_{B_\sigma(p,1)} & 2(\mu_1-\mu_0)(p)\Big((e(u_0)(p)n\cdot n)(e(v)n\cdot n) + (e(u_0)(p)b\cdot b)(e(v)b\cdot b) \\
& + (e(u_0)(p)\tau\cdot n)(\nabla v n\cdot\tau) + (e(u_0)(p)\tau\cdot b)(\nabla v b\cdot\tau)\Big)\,\mathrm{ds}(z)\Bigg)\mathrm{d}\ell(p) \\
+ \int_\sigma \Bigg(\int_{B_\sigma(p,1)} & (\lambda_1-\lambda_0)(p)(\operatorname{div} u_0)(p)\Big(e(v)n\cdot n + e(v)b\cdot b\Big)\,\mathrm{ds}(z)\Bigg)\,\mathrm{d}\ell(p),
\end{aligned}$$

and we have defined, for $p \in \sigma$ and $z \in N_{\tau(p)}$,

$$\widehat{\mu}(p,z) = \begin{cases} \mu_1(p) & \text{if } |z| < 1, \\ \mu_0(p) & \text{otherwise.} \end{cases}$$

Recall that it is quite unclear what would be a rigorous framework for this minimization, and we do not elaborate on this issue.

Taking advantage of eqs. (5.8) and (5.9), the energy $\widetilde{F}(v)$ may be reformulated in terms of the normal and tangential components of v with respect to σ:

$$\begin{aligned} \widetilde{F}(v) = \frac{1}{2}\int_\sigma \int_{N_{\tau(p)}} \Big(2\widehat{\mu}(p,z)\Big(\|e_N(v_N)\|^2 + \frac{1}{2}|\nabla_N(v\cdot\tau)|^2\Big) + \widehat{\lambda}(p,z)\Big(\operatorname{tr}(e_N(v_N))\Big)^2\Big) \,\mathrm{ds}(z)\,\mathrm{d}\ell(p) \\ + \int_\sigma \int_{B_\sigma(p,1)} 2(\mu_1-\mu_0)(p)\Big(e_N(u_{0N})(p) : e_N(v_N) + e(u_0)(p)\tau\cdot\nabla_N(v\cdot\tau)\Big)\,\mathrm{ds}(z)\,\mathrm{d}\ell(p) \\ + \int_\sigma \int_{B_\sigma(p,1)} (\lambda_1-\lambda_0)(p)(\operatorname{div} u_0)(p)\operatorname{tr}(e_N(v_N))\,\mathrm{ds}(z)\,\mathrm{d}\ell(p). \quad (6.9) \end{aligned}$$

At this point, judging from the tensorized structure of the integrals and coefficients in the above expression of $\widetilde{F}(v)$, we are enticed to seek the limiting behavior v of s_ε inside the rescaled inclusion $\omega_{\sigma,1}$ under the form:

$$\forall p \in \sigma,\ z \in B_\sigma(p,1), \quad s_\varepsilon(p+z) \approx v(p,z),$$

for a certain vector field $v : \Big\{(p,z) \in \sigma \times \mathbb{R}^3,\ z \in N_{\tau(p)}\Big\} \to \mathbb{R}^3$ to be determined.

To achieve this purpose, we rely on the Euler–Lagrange equations associated to the resolution of eq. (6.8). It immediately follows from the expression eq. (6.9) of the energy $\widetilde{F}(v)$ that this minimization can be conducted in terms of the tangential and normal components $v\cdot\tau$ and v_N of the unknown function v, independently.

Let us then write down the Euler–Lagrange equations for the minimization of eq. (6.9) by considering only variations of the tangential component $v\cdot\tau$: for each point $p \in \sigma$, the function $N_{\tau(p)} \ni z \mapsto (v\cdot\tau)(p,z) \in \mathbb{R}$ turns out to satisfy the following variational problem:

$$\forall w, \quad \int_{N_{\tau(p)}} \widehat{\mu}\nabla_N(v\cdot\tau)\cdot\nabla_N w\,\mathrm{ds}(z) + \int_{B_\sigma(p,1)} 2(\mu_1-\mu_0)(p)(e(u_0)(p)\tau)\cdot\nabla_N w\,\mathrm{ds}(z) = 0. \quad (6.10)$$

The above variational problem is well-posed when the unknown and test functions v and w are chosen in the functional space $W_0^{1,-1}(\mathbb{R}^2)$ (see Remark 4.3). It exactly corresponds to the variational formulation for the $2d$ profile eq. (4.9) associated to a disk-shaped diametrically small inclusion in the conductivity setting, up to the identification of the $N_{\tau(p)}$ with $\mathbb{R}^2$; see again the proof of Conjecture 5.8, and notably the discussion immediately after eq. (5.18). More precisely, $v\cdot\tau$ equals:

$$\forall p \in \sigma, \quad \forall z \in N_{\tau(p)}, \quad (v\cdot\tau)(p,z) = \phi_{2e(u_0)(p)\tau(p)}(z),$$

where for a given vector $\xi \in \mathbb{R}^2$, the function $\phi_\xi \in W_0^{1,-1}(\mathbb{R}^2)$ is the solution to:

$$\begin{cases} -\Delta\phi_\xi = 0 & \text{in } (\mathbb{R}^2 \setminus \overline{B(0,1)}) \cup B(0,1), \\ \mu_0(p)\frac{\partial\phi_\xi^+}{\partial n} - \mu_1(p)\frac{\partial\phi_\xi^-}{\partial n} = -(\mu_0(p)-\mu_1(p))(\xi\cdot n) & \text{on } \partial B(0,1), \\ |\phi_\xi(z)| \to 0 & \text{when } |z| \to \infty; \end{cases}$$

which is exactly eq. (4.5), in which $\gamma_0(0), \gamma_1(0)$ are replaced by $\mu_0(p)$ and $\mu_1(p)$, respectively.

For further reference, we note that the 2×2 matrix $\mathcal{M}_{\tau N}(p)$ in eq. (6.2) satisfies the following identity:

$$2\mathcal{M}_{\tau N}(p)(e(u_0)(p)\tau)_N = \int_{B_\sigma(p,1)} (\mu_1(p)-\mu_0(p))(2(e(u_0)(p)\tau)_N + \nabla_N(v\cdot\tau)(p,z))\,\mathrm{ds}(z). \quad (6.11)$$

Let us now consider variations of the normal component v_N in the minimization of the energy $\widetilde{F^1_\varepsilon}(v)$ in eq. (6.9). For a fixed, arbitrary point $p \in \sigma$, the mapping $N_{\tau(p)} \ni z \mapsto v_N(p,z) \in N_{\tau(p)}$ satisfies:

$$\forall w, \quad \int_{N_{\tau(p)}} \Big(2\widehat{\mu} e_N(v_N) : e_N(w) + \widehat{\lambda}\,\mathrm{tr}(e_N(v_N))\,\mathrm{tr}(e_N(w))\Big)\,\mathrm{ds}(z) + \int_{B_\sigma(p,1)} \Big(2(\mu_1-\mu_0)(p) e_N(u_{0N})(p) : e_N(w) + (\lambda_1-\lambda_0)(p)(\mathrm{div}\,u_0)(p)\,\mathrm{tr}(e_N(w))\Big)\,\mathrm{ds}(z) = 0,$$

and we decompose $v_N(p,z)$ as:

$$v_N(p,z) = w_1(p,z) + w_2(p,z),$$

where $w_1(p,z)$ and $w_2(p,z)$ are defined as follows:

- the vector field $z \mapsto w_1(p,z)$ equals $v_{e_N(u_{0N})(p)}(z)$, where for any symmetric 2×2 matrix ξ, $v_\xi \in W_0^{1,-1}(\mathbb{R}^2)^2$ is the unique solution to the variational problem:

$$\int_{N_{\tau(p)}} \Big(2\widehat{\mu} e_N(v_\xi) : e_N(w) + \widehat{\lambda}\,\mathrm{tr}(e_N(v_\xi))\,\mathrm{tr}(e_N(w))\Big)\,\mathrm{ds}(z) + \int_{B_\sigma(p,1)} \Big(2(\mu_1-\mu_0)(p)\xi : e_N(w) + (\lambda_1-\lambda_0)(p)\,\mathrm{tr}(\xi)\,\mathrm{tr}(e_N(w))\Big)\,\mathrm{ds}(z) = 0, \quad (6.12)$$

  that is, v_ξ is exactly the profile function eq. (4.12) attached to the asymptotic expansion of the solution to the 2d linear elasticity system in the situation of a diametrically small disk-shaped inclusion.

- The vector field $z \mapsto w_2(p,z)$ equals $w_{e(u_0)(p)\tau\cdot\tau}$, where for $h \in \mathbb{R}$, w_h is the unique solution in $W_0^{1,-1}(\mathbb{R}^2)$ to the variational problem:

$$\int_{N_{\tau(p)}} \Big(2\widehat{\mu} e_N(w_h) : e_N(w) + \widehat{\lambda}\,\mathrm{tr}(e_N(w_h))\,\mathrm{tr}(e_N(w))\Big)\,\mathrm{ds}(z) + \int_{B_\sigma(p,1)} (\lambda_1-\lambda_0)(p) h\,\mathrm{tr}(e_N(w))\,\mathrm{ds}(z) = 0.$$

  By uniqueness of the solution to eq. (6.12), it holds:

$$w_h = v_{\frac{1}{2}\frac{\lambda_1-\lambda_0}{\mu_1-\mu_0+\lambda_1-\lambda_0} h\mathrm{I}}.$$

For further reference, we note that, for any symmetric 2×2 matrix ξ:

$$\mathcal{M}_{NN}(p)\xi = \int_{B_\sigma(p,1)} \Big(2(\mu_1-\mu_0)(p)(\xi + e_N(v_\xi)) + (\lambda_1-\lambda_0)(p)\,\mathrm{tr}(\xi + e_N(v_\xi))\mathrm{I}\Big)\,\mathrm{ds}(z), \quad (6.13)$$

and so:

$$\frac{1}{2}\frac{1}{\mu_1-\mu_0+\lambda_1-\lambda_0}\,\mathrm{tr}\Big(\mathcal{M}_{NN}(p)\xi\Big) = \int_{B_\sigma(p,1)} \mathrm{tr}(\xi + e_N(v_\xi))\,\mathrm{ds}(z). \quad (6.14)$$

Finally, by the same token:

$$\frac{h}{2}\frac{\lambda_1-\lambda_0}{\mu_1-\mu_0+\lambda_1-\lambda_0}\Big(\mathcal{M}_{NN}(p)\mathrm{I}\Big) = \int_{B_\sigma(p,1)} \Big(2(\mu_1-\mu_0)(p) e_N(w_h) + (\lambda_1-\lambda_0)(p)(h + \mathrm{tr}(e_N(w_h)))\mathrm{I}\Big)\,\mathrm{ds}(z). \quad (6.15)$$

Step 3: We pass to the limit in the representation formula eq. (6.5). It follows from a change of variables based on the mapping m_ε in eq. (5.14) (see also eq. (5.15)) that:

$$\begin{aligned} r_{\varepsilon,j}(x) &= \frac{1}{\varepsilon^2}\int_{\omega_{\sigma,1}} |\det(\nabla m_\varepsilon)|(A_1 - A_0)(m_\varepsilon(z))e(u_0)(m_\varepsilon(z)) : e_y(N_j(x, m_\varepsilon(z)))\,\mathrm{d}z \\ &\quad + \int_{\omega_{\sigma,1}} |\det(\nabla m_\varepsilon)|(A_1 - A_0)(m_\varepsilon(z))(e(r_\varepsilon)\circ m_\varepsilon) : e_y(N_j(x, m_\varepsilon(z)))\,\mathrm{d}z, \\ &=: I_\varepsilon^1 + I_\varepsilon^2, \end{aligned} \tag{6.16}$$

with obvious notations. It is now easy to see from the coarea formula of Proposition 5.7 that:

$$\lim_{\varepsilon\to 0} I_\varepsilon^1 = \int_\sigma \int_{B_\sigma(p,1)} (A_1 - A_0)(p)e(u_0)(p) : e_y(N_j(x,p))\,\mathrm{d}s(z)\,\mathrm{d}\ell(p). \tag{6.17}$$

As for the second integral I_ε^2, the formulas eq. (6.6), eq. (6.7) and the convergence of s_ε obtained in the first step yield:

$$\begin{aligned} \lim_{\varepsilon\to 0} I_\varepsilon^2 = \int_{\omega_{\sigma,1}} \frac{2(\mu_1-\mu_0)\circ p_\sigma}{1-\delta_\sigma(y)a(y)\cdot n(y)}\Big(&(\nabla v n\cdot\tau)(e_y(N_j(x,p_\sigma(y)))\tau\cdot n) \\ &+ (\nabla v b\cdot\tau)(e_y(N_j(x,p_\sigma(y)))\tau\cdot b) + (e(v)n\cdot n)(e_y(N_j(x,p_\sigma(y)))n\cdot n) \\ &+ (e(v)b\cdot b)(e_y(N_j(x,p_\sigma(y)))b\cdot b) + 2(e(v)n\cdot b)(e_y(N_j(x,p_\sigma(y)))n\cdot b)\Big)\,\mathrm{d}y \\ &+ \int_{\omega_{\sigma,1}} \frac{(\lambda_1-\lambda_0)\circ p_\sigma}{1-\delta_\sigma(y)a(y)\cdot n(y)}\Big(e(v)n\cdot n + e(v)b\cdot b\Big)\,\mathrm{div}_y(N_j(x,p_\sigma(y)))\,\mathrm{d}y. \end{aligned}$$

Using the coarea formula of Proposition 5.7, this rewrites:

$$\begin{aligned} \lim_{\varepsilon\to 0} I_\varepsilon^2 = \int_\sigma \int_{B_\sigma(p,1)} &2(\mu_1-\mu_0)(p)\Big(\nabla_N(v\cdot\tau)\cdot(e_y(N_j(x,p))\tau) + e_N(v_N) : e_{N_y}(N_j(x,p))\Big)\,\mathrm{d}s(z)\,\mathrm{d}\ell(p) \\ &+ \int_\sigma \int_{B_\sigma(p,1)} (\lambda_1-\lambda_0)(p)\,\mathrm{tr}(e_N(v_N))\,\mathrm{div}_y(N_j(x,p))\,\mathrm{d}s(z)\,\mathrm{d}\ell(p). \end{aligned} \tag{6.18}$$

Eventually, combining eqs. (6.17) and (6.18), we obtain:

$$\begin{aligned} \lim_{\varepsilon\to 0} r_{\varepsilon,j}(x) = &\int_\sigma \int_{B_\sigma(p,1)} (A_1 - A_0)(p)e(u_0)(p) : e_y(N_j(x,p))\,\mathrm{d}s(z)\,\mathrm{d}\ell(p) \\ &+ \int_\sigma \int_{B_\sigma(p,1)} 2(\mu_1-\mu_0)(p)\Big(\nabla_N(v\cdot\tau)\cdot(e_y(N_j(x,p))\tau) + e_N(v_N) : e_{N_y}(N_j(x,p))\Big)\,\mathrm{d}s(z)\,\mathrm{d}\ell(p) \\ &+ \int_\sigma \int_{B_\sigma(p,1)} (\lambda_1-\lambda_0)(p)\,\mathrm{tr}(e_N(v_N))\,\mathrm{div}_y(N_j(x,p))\,\mathrm{d}s(z)\,\mathrm{d}\ell(p). \end{aligned}$$

We now rewrite the above expression by bringing into play the tensors $\mathcal{M}_{NN}(p)$ and $\mathcal{M}_{\tau N}(p)$ defined in eqs. (6.2) and (6.3). To this end, expanding the first integral in the above right-hand side (and notably using eq. (5.10)), we obtain after simple, albeit tedious calculations:

$$\begin{aligned} \lim_{\varepsilon\to 0} r_{\varepsilon,j}(x) = &\int_\sigma \int_{B_\sigma(p,1)} 2(\mu_1-\mu_0)(p)(e_N(w_1) + e_N(u_0)(p)) : e_{N_y}(N_j(x,p))\,\mathrm{d}s(z)\,\mathrm{d}\ell(p) \\ &+ \int_\sigma \int_{B_\sigma(p,1)} (\lambda_1-\lambda_0)(p)\,\mathrm{tr}(e_N(w_1) + e_N(u_0)(p))\,\mathrm{tr}(e_{N_y}(N_j(x,p)))\,\mathrm{d}s(z)\,\mathrm{d}\ell(p) \\ &+ \int_\sigma \int_{B_\sigma(p,1)} 2(\mu_1-\mu_0)(p)e_N(w_2) : e_{N_y}(N_j(x,p))\,\mathrm{d}s(z)\,\mathrm{d}\ell(p) \\ &+ \int_\sigma \int_{B_\sigma(p,1)} (\lambda_1-\lambda_0)(p)(\mathrm{tr}(e_N(w_2)) + e(u_0)(p)\tau\cdot\tau)\,\mathrm{tr}(e_N(N_j(x,p)))\,\mathrm{d}s(z)\,\mathrm{d}\ell(p) \end{aligned}$$

$$
\begin{aligned}
&+ \int_\sigma \int_{B_\sigma(p,1)} 2(\mu_1-\mu_0)(p)\Big(\nabla_N(v\cdot\tau) + 2(e(u_0)\tau)_N\Big)\cdot(e_y(N_j(x,p))\tau)_N \,\mathrm{ds}(z)\,\mathrm{d}\ell(p)\\
&+ \int_\sigma \int_{B_\sigma(p,1)} (\lambda_1-\lambda_0)(p)\,\mathrm{tr}(e_N(w_1)+e_N(u_0)(p))(e_y(N_j(x,p))\tau\cdot\tau)\,\mathrm{ds}(z)\,\mathrm{d}\ell(p)\\
&+ \int_\sigma \int_{B_\sigma(p,1)} (2(\mu_1-\mu_0)(p)+(\lambda_1-\lambda_0)(p))e(u_0)(p)\tau\cdot\tau)(e_y(N_j(x,p))\tau\cdot\tau)\,\mathrm{ds}(z)\,\mathrm{d}\ell(p)\\
&+ \int_\sigma \int_{B_\sigma(p,1)} (\lambda_1-\lambda_0)(p)\,\mathrm{tr}(e_N(w_2))(e_y(N_j(x,p))\tau\cdot\tau)\,\mathrm{ds}(z)\,\mathrm{d}\ell(p)\\
=:& \sum_{j=1}^{8} \int_\sigma \int_{B_\sigma(p,1)} \alpha_j(x,p)\,\mathrm{ds}(z)\,\mathrm{d}\ell(p),
\end{aligned}
$$

with obvious notations. We now calculate the integrands $\alpha_j(x,p)$, $j=1,\dots,8$, omitting the mention to the point p when it is clear:

- Using eq. (6.13) yields:
$$(\alpha_1+\alpha_2)(x,p) = \mathcal{M}_{NN}(p)e_N(u_{0N})(p) : e_N(N_j(x,p)).$$
- Using eq. (6.15), we obtain:
$$(\alpha_3+\alpha_4)(x,p) = \frac{1}{2}\frac{\lambda_1-\lambda_0}{\mu_1-\mu_0+\lambda_1-\lambda_0}(e(u_0)\tau\cdot\tau)\,\Big(\mathcal{M}_{NN}\mathrm{I} : e_N(N_j(x,p))\Big);$$
taking advantage of the expression eq. (4.13) of the coefficients of $\mathcal{M}_{NN}$, this rewrites:
$$(\alpha_3+\alpha_4)(x,p) = \frac{\pi(\lambda_1-\lambda_0)(\lambda_0+2\mu_0)}{\mu_0+\lambda_1+\mu_1}(e(u_0)\tau\cdot\tau)\ \mathrm{tr}(e_N(N_j(x,p))).$$
- On account of eq. (6.11), one has:
$$\alpha_5(x,p) = 2\mathcal{M}_{\tau N}(2e(u_0)\tau)_N\cdot(e_y(N_j(x,p))\tau)_N = 4\mathcal{M}_{\tau N}(e(u_0)\tau)_N\cdot(e_y(N_j(x,p))\tau)_N$$
- From the relation eq. (6.14), we infer that the sixth term equals:
$$\alpha_6(x,p) = \frac{1}{2}\frac{\lambda_1-\lambda_0}{\mu_1-\mu_0+\lambda_1-\lambda_0}\,\mathrm{tr}\,\Big(\mathcal{M}_{NN}e_N(u_{0N})\Big)(e_y(N_j(x,p))\tau\cdot\tau),$$
which yields, from eq. (4.13),
$$\alpha_6(x,p) = \frac{\pi(\lambda_1-\lambda_0)(\lambda_0+2\mu_0)}{\mu_0+\lambda_1+\mu_1}\,\mathrm{tr}(e_N(u_{0N}))(e_y(N_j(x,p))\tau\cdot\tau).$$
- The term $\alpha_7(x,p)$ does not need to be reformulated.
- Using again eq. (6.14) and then eq. (4.13), $\alpha_8(x,p)$ rewrites:
$$\alpha_8(x,p) = -\pi\frac{(\lambda_1-\lambda_0)^2}{\mu_1+\lambda_1+\mu_0}(e(u_0)(p)\tau\cdot\tau)(e_y(N_j(x,p))\tau\cdot\tau).$$

This results in the desired expression.

Remark 6.2. As we have already noticed in the course of the previous calculation, the component $\mathcal{M}_{\tau N}$ of the polarization tensor $\mathcal{M}$ in eq. (6.1) coincides with the polarization tensor eq. (4.11) attached to a disk-shaped, diametrically small inclusion in the situation of the 2d conductivity equation, where the Lamé parameter μ plays the role of the conductivity coefficient. This echoes to the well-known two-dimensional reduction of the 3d linear elasticity system in the particular situation of antiplane shear; see for instance [100].

We conclude this study with the calculation of the asymptotic expansion of a quantity depending on the thickness ε via the perturbed displacement u_ε, say:

$$J_\sigma(\varepsilon) = \int_D j(u_\varepsilon)\,\mathrm{d}x,$$

where $j : \mathbb{R}^3 \to \mathbb{R}$ is smooth and satisfies the growth conditions eq. (2.8).

Proposition 6.3. *The function $J_\sigma(\varepsilon)$ admits the following asymptotic expansion:*

$$J_\sigma(\varepsilon) = J_\sigma(0) + \varepsilon^2 J'_\sigma(0) + \mathrm{o}(\varepsilon^2),$$

where the "derivative" $J'_\sigma(0)$ reads:

$$J'_\sigma(0) = \int_\sigma \mathcal{M}e(u_0) : e(p_0)\,\mathrm{d}\ell.$$

Here, $\mathcal{M}$ is the polarization tensor defined in eq. (6.1)*, and the adjoint state p_0 is the unique solution in $H^1_{\Gamma_D}(D)^3$ to the following system:*

$$\begin{cases} -\operatorname{div}(A_0 e(p_0)) = -j'(u_0) & \text{in } D, \\ p_0 = 0 & \text{on } \Gamma_D, \\ Ae(p_0)n = 0 & \text{on } \partial D \setminus \overline{\Gamma_D}. \end{cases} \tag{6.19}$$

Again, we provide a slightly different, more practical form of the "derivative" $J'_\sigma(0)$, emphasizing its dependence on the curve σ and its tangent vector τ:

$$J'_\sigma(0) = \int_\sigma P(x, \tau_1(x), \tau_2(x), \tau_3(x))\,\mathrm{d}\ell(x),$$

where at a given point $x \in \sigma$, $\tau = (\tau_1, \tau_2, \tau_3) \mapsto P(x, \tau_1, \tau_2, \tau_3)$ is the trivariate polynomial with degree 4 defined by:

$$\begin{aligned} P(x,\tau_1,\tau_2,\tau_3) &= \alpha_S \operatorname{tr} e\ \operatorname{tr} f + \beta_S e : f + \left(-2\beta_S + 8\pi\mu_0 \frac{\mu_1 - \mu_0}{\mu_1 + \mu_0}\right)(e\tau \cdot f\tau) \\ &+ \left(\pi \frac{(\lambda_1 - \lambda_0)(\lambda_0 + 2\mu_0)}{\mu_0 + \lambda_1 + \mu_1} - \alpha_S\right)(\operatorname{tr} e\,(f\tau \cdot \tau) + \operatorname{tr} f\,(e\tau \cdot \tau)) + \left(\alpha_S + \beta_S - 2\pi \frac{(\lambda_1 - \lambda_0)(\lambda_0 + 2\mu_0)}{\mu_0 + \lambda_1 + \mu_1}\right. \\ &\left. - 8\pi\mu_0 \frac{\mu_1 - \mu_0}{\mu_1 + \mu_0} + 2\pi(\mu_1 - \mu_0) + \pi(\lambda_1 - \lambda_0) - \pi \frac{(\lambda_1 - \lambda_0)^2}{\mu_1 + \lambda_1 + \mu_0}\right)(e\tau \cdot \tau)(f\tau \cdot \tau). \end{aligned}$$

In the above formula, we have taken the shortcuts $e \equiv e(u_0)$, $f \equiv e(p_0)$; the values α_S and β_S depend on μ_0, μ_1, λ_0, λ_1 via eq. (4.13) and the dependence of all the coefficients with respect to x is omitted for brevity.

7. Numerical illustrations and applications

In this illustrative section, we discuss the practical use of the asymptotic formulas eq. (1.11) for thin tubular inhomogeneities considered in this article. After verifying the numerical accuracy of these formulas in Section 7.1, we propose three different applications in shape and topology optimization. At first, in Section 7.2, we introduce a methodology for grafting a thin ligament to a shape in the course of a more "classical" optimal design process, with the aim to make the final design less sensitive to the initial guess. Secondly, Section 7.3 is devoted to an algorithm for computing an optimized set of pillars, serving as the scaffold structure of a shape during its construction by means of an additive manufacturing technique. Eventually, in Section 7.4, we present a strategy for the computation of a judicious initial design in view of the optimization of a truss-like structure.

Before proceeding, let us already emphasize that these numerical methods are proposed as preliminary "proofs of concept", rather than as fully mature techniques. In particular, several algorithmic aspects have not been paid much attention in the present article; see in particular Remark 7.1 and Section 8 for several criticisms and leads towards improving their computational efficiency which will be considered in a future work.

7.1. **Numerical validation**

In this first example section, we appraise numerically the validity of our asymptotic formulas for thin tubular inhomogeneities in the 2d and 3d conductivity and linear elasticity settings.

The physical configurations at stake are depicted in Figure 7.1: in two space dimensions, the hold-all domain D is the rectangle $D = (-1, 1) \times (0, 1)$, Γ_D is defined as the left-hand side of ∂D and Γ_N is its right-hand side. The base curve $\sigma \subset D$ of the considered tubular inclusions is the straight segment $\sigma = (-\frac{1}{2}, \frac{1}{2}) \times \left\{\frac{1}{2}\right\}$. In three space dimensions, D is the unit cube $D = (0, 1)^3$ and the regions Γ_D and Γ_N are the left-hand side and the right-hand side of ∂D, respectively; the base curve σ is defined by $\sigma = \left\{\frac{1}{2}\right\} \times (\frac{1}{2}, \frac{3}{4}) \times \left\{\frac{1}{2}\right\}$.

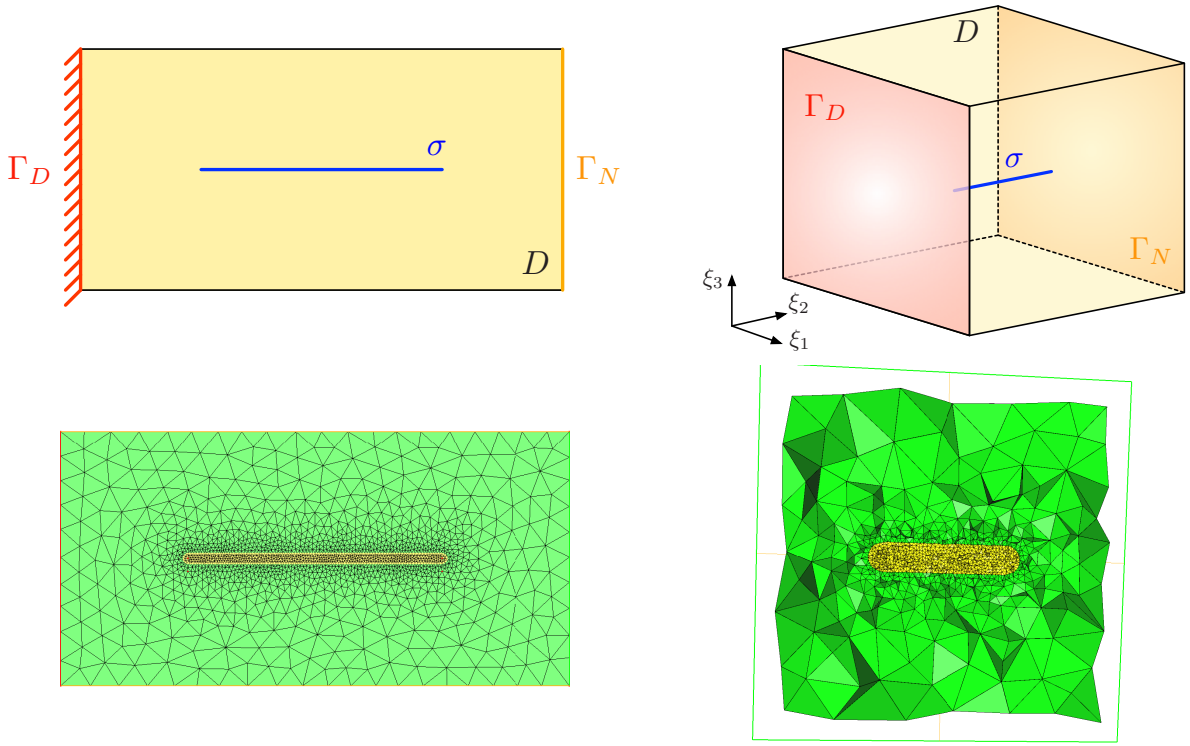

Figure 7.1. Numerical evaluation of the asymptotic formulas for thin tubular inhomogeneities in Section 7.1; (top) common physical setting of the test cases (left) in 2d, (right) in 3d; (bottom) computational mesh where the inclusion $\omega_{\sigma,\varepsilon}$ is explicitly discretized (left) in 2d for $\varepsilon = 0.02$, (right) in 3d for $\varepsilon = 0.05$.

7.1.1. *The case of the conductivity equation in 2d and 3d*

In the "background" situation, the domain D is filled by a material with conductivity $\gamma_0 \equiv 1$; a flux $g = -1$ is applied on Γ_N and volumic sources f are omitted for simplicity. In the perturbed

situation, several values of the thickness ε are considered for the tubular inclusion $\omega_{\sigma,\varepsilon}$, as well as for the (constant) conductivity γ_1 inside the latter.

On the one hand, we evaluate the compliance of the domain D in the perturbed situation, that is, the quantity:

$$C_\sigma(\varepsilon) := \int_{\Gamma_N} g u_\varepsilon \, \mathrm{d}s = \int_D \gamma_\varepsilon \nabla u_\varepsilon \cdot \nabla u_\varepsilon \, \mathrm{d}x,$$

where u_ε is the solution to eq. (2.4). The numerical computation relies on the use of the Lagrange $\mathbb{P}_1$ finite element method on a conforming mesh of D where the inclusion $\omega_{\sigma,\varepsilon}$ is meshed explicitly – i.e. a mesh of $\omega_{\sigma,\varepsilon}$ appears as a submesh of that of D; see Figure 7.1, (bottom). We rely on the remeshing library `mmg` (see [52, 53]) for the construction of such a mesh, and on the `FreeFem` environment [71] for the finite element calculations.

On the other hand, we compute the approximation of $C_\sigma(\varepsilon)$ predicted by the asymptotic expansion of Theorem 2.1 and Conjecture 5.8:

$$C_\sigma(0) + \varepsilon^{d-1} C'_\sigma(0).$$

The solution u_0 to the background conductivity equation eq. (2.2) and all the depending quantities involved in the expressions eq. (2.37) (in 2d) and eq. (5.20) (in 3d) of the derivative $C'_\sigma(0)$ are calculated on a fixed reference mesh of D.

The values of both expressions, associated to different conductivities $\gamma_1 = 10, 100$, or 1000 and different thicknesses ε for the inclusion set are reported on Figure 7.2 in the two-dimensional case, and on Figure 7.3 in the three-dimensional case.

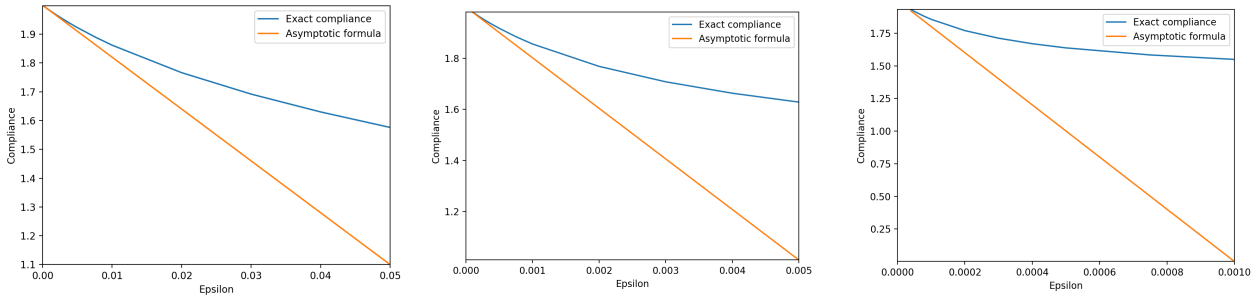

Figure 7.2. Evaluation of the asymptotic formula for tubular inhomogeneities in the 2d conductivity case of Section 7.1.1: comparison between $C_\sigma(\varepsilon)$ and the formula $C_\sigma(0) + \varepsilon C'_\sigma(0)$ for $\gamma_0 = 1$ and (left) $\gamma_1 = 10$, (middle) $\gamma_1 = 100$ and (right) $\gamma_1 = 1000$.

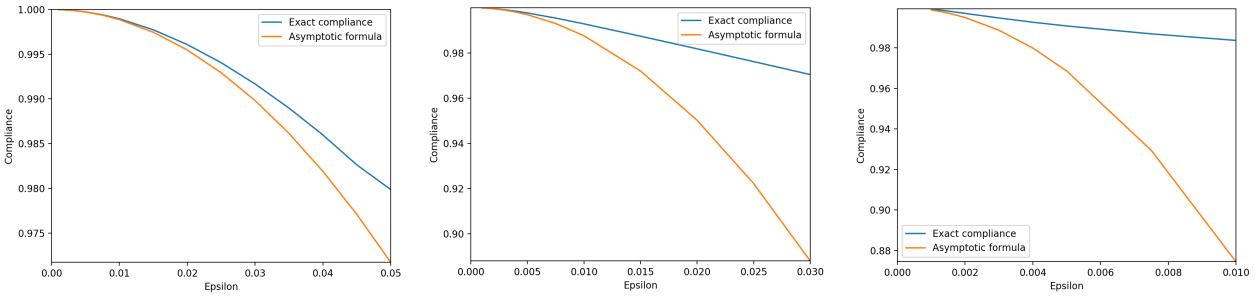

Figure 7.3. Evaluation of the asymptotic formula for tubular inhomogeneities in the 3d conductivity case of Section 7.1.1: comparison between $C_\sigma(\varepsilon)$ and $C_\sigma(0) + \varepsilon^2 C'_\sigma(0)$ for $\gamma_0 = 1$ and (left) $\gamma_1 = 10$, (middle) $\gamma_1 = 100$ and (right) $\gamma_1 = 1000$.

As expected, the asymptotic formula $C_\sigma(0) + \varepsilon^{d-1} C'_\sigma(0)$ provides a fairly good approximation of the exact, perturbed compliance $C_\sigma(\varepsilon)$ when ε is sufficiently small (especially in 3d). Let us notice however that, for a given value of the thickness ε, the quality of the approximation deteriorates as the conductivity γ_1 inside $\omega_{\sigma,\varepsilon}$ (thus the contrast γ_1/γ_0) gets larger. This observation is in line with the conclusions of [46, 47, 54], according to which the asymptotic formulas eqs. (2.5) and (5.11) for u_ε cannot hold uniformly with respect to the contrast γ_1/γ_0, i.e. the remainders $o(\varepsilon)$ and $o(\varepsilon^2)$ in there depend on γ_1/γ_0. Actually, it turns out that the limit of u_ε itself may differ from the background potential u_0 when the contrast γ_1/γ_0 degenerates to 0 or ∞ as $\varepsilon \to 0$. It would be interesting to appraise the use of the asymptotic formulas for u_ε established in these articles, which hold uniformly with respect to the ratio γ_1/γ_0 (and are unfortunately much more difficult to derive and compute numerically) to get more robust approximation formulas for u_ε and $C_\sigma(\varepsilon)$ with respect to the values of γ_1.

7.1.2. *The case of the linear elasticity system in 2d and 3d*

We perform a similar analysis in the context of the linearized elasticity system: now, u_0 is the solution to the background elasticity system eq. (3.3), where the Hooke's tensor A_0 in eq. (3.1) is characterized by the Lamé coefficients $\lambda_0 = 0.5769$ and $\mu_0 = 0.3846$. In the perturbed situation, the displacement u_ε is the solution to the system eq. (3.4), and several values are considered for the thickness ε of the inclusion set $\omega_{\sigma,\varepsilon}$ and the Lamé coefficients λ_1, μ_1 of its constituent material A_1. In all cases, body forces f are omitted; the surface load reads $g = (0, -1)$ in 2d and $g = (0, 0, -1)$ in 3d.

On the one hand, we calculate the perturbed displacement u_ε, and the corresponding compliance

$$C_\sigma(\varepsilon) := \int_{\Gamma_N} g \cdot u_\varepsilon \, \mathrm{d}s = \int_D A_\varepsilon e(u_\varepsilon) : e(u_\varepsilon) \, \mathrm{d}x \tag{7.1}$$

on a confoming mesh of D where $\omega_{\sigma,\varepsilon}$ is explicitly discretized; see Figure 7.1 (bottom row).

On the other hand, we evaluate the asymptotic formula

$$C_\sigma(0) + \varepsilon^{d-1} C'_\sigma(0) \tag{7.2}$$

on a fixed mesh of D. The results associated to different values of the thickness ε, and different values of the Lamé coefficients λ_1, μ_1 are displayed on Figure 7.4 in the 2d case, and on Figure 7.5 in the 3d case.

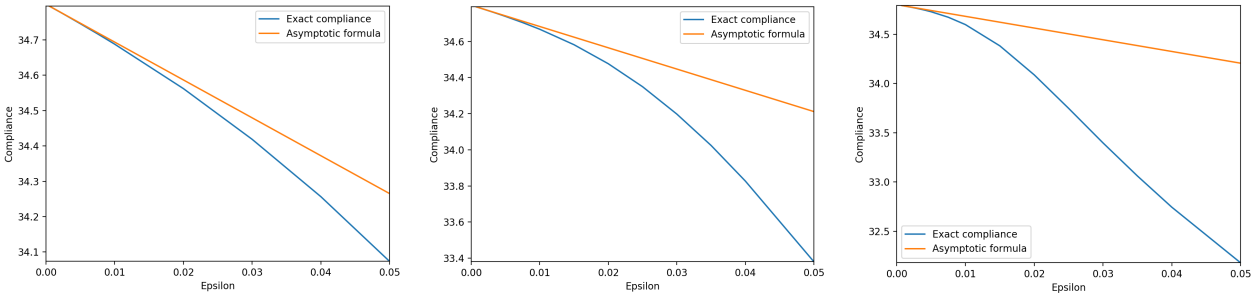

Figure 7.4. Evaluation of the asymptotic formula for tubular inhomogeneities in the 2d elasticity case of Section 7.1.2: comparison between $C_\sigma(\varepsilon)$ and $C_\sigma(0) + \varepsilon C'_\sigma(0)$ for values of the ratio $\frac{\mu_1}{\mu_0} = \frac{\lambda_1}{\lambda_0}$ equal to (left) 10, (middle) 100 and (right) 1000.

Again, a fine matching is observed between both quantities eqs. (7.1) and (7.2), which is, perhaps a little surprisingly, better than in the case of the conductivity equation. As can be expected from the discussion in the previous Section 7.1.1, for a fixed value of ε, this correspondance deteriorates as the ratios $\frac{\mu_1}{\mu_0}$ and $\frac{\lambda_1}{\lambda_0}$ increase (again, to a lesser extent than in the case of the conductivity equation).

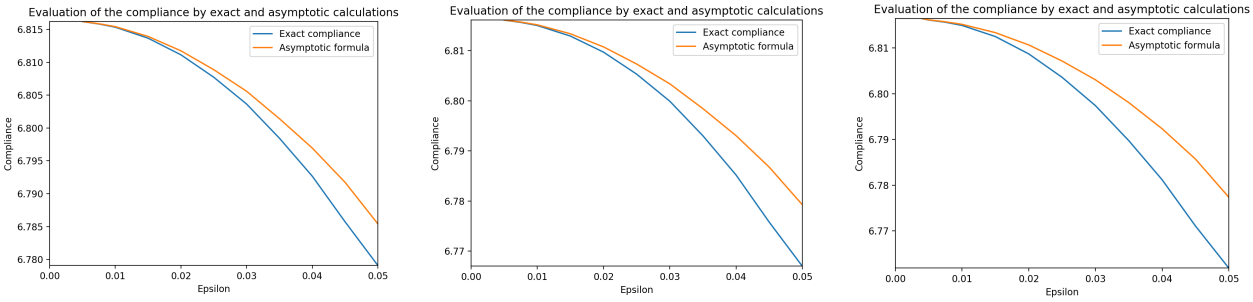

FIGURE 7.5. Evaluation of the asymptotic formula for tubular inhomogeneities in the 3d elasticity case of Section 7.1.2: comparison between $C_\sigma(\varepsilon)$ and $C_\sigma(0) + \varepsilon^2 C'_\sigma(0)$ for values of the ratio $\frac{\mu_1}{\mu_0} = \frac{\lambda_1}{\lambda_0}$ equal to (left) 10, (middle) 100 and (right) 1000.

7.2. **Topological ligament for elastic structures**

The first application context of our asymptotic expansion formulas for thin tubular inhomogeneities is also our initial motivation for the work of this article (see Section 1.1): we intend to use them in the course of a structural optimization process, as a guide to insert now and then bars of material between distant regions of the shape, in an optimal way with respect to a function of the domain.

7.2.1. *Shape and topology optimization of elastic structures using the boundary variation method of Hadamard*

We deal with the optimization of an elastic structure $\Omega \subset \mathbb{R}^d$ $(d = 2, 3)$, whose boundary $\partial\Omega$ is composed of three disjoint parts: $\partial\Omega = \Gamma_D \cup \Gamma_N \cup \Gamma$. The structure is clamped on Γ_D, and surface loads $g : \Gamma_N \to \mathbb{R}^d$ are applied on Γ_N; both regions are imposed by the context, so that the remaining, traction-free region Γ is the only one subject to optimization. Omitting body forces for simplicity, the displacement $u_\Omega : \Omega \to \mathbb{R}^d$ of the structure in these circumstances is the solution to the linear elasticity system

$$\begin{cases} -\operatorname{div}(Ae(u_\Omega)) = 0 & \text{in } \Omega, \\ u_\Omega = 0 & \text{on } \Gamma_D, \\ Ae(u_\Omega)n = g & \text{on } \Gamma_N, \\ Ae(u_\Omega)n = 0 & \text{on } \Gamma, \end{cases} \tag{7.3}$$

where the Hooke's law A of the material reads:

$$\forall e \in \mathcal{S}_d(\mathbb{R}), \quad Ae = 2\mu e + \lambda \operatorname{tr}(e)\mathrm{I}, \text{ with Lamé coefficients } \lambda = 0.5769,\ \mu = 0.3846. \tag{7.4}$$

Our purpose is to solve the shape optimization problem

$$\min_\Omega C(\Omega) \text{ s.t. } \operatorname{Vol}(\Omega) = V_T, \tag{7.5}$$

where $C(\Omega)$ is the elastic compliance of Ω (or the work of external loads), namely:

$$C(\Omega) = \int_\Omega Ae(u_\Omega) : e(u_\Omega)\,\mathrm{d}x = \int_{\Gamma_N} g \cdot u_\Omega\,\mathrm{d}s, \tag{7.6}$$

and $\operatorname{Vol}(\Omega) = \int_\Omega \mathrm{d}x$ is the volume, which is expected not to exceed the threshold value V_T. Note that the choice of the compliance and the volume as the objective and constraint in eq. (7.5) is only a matter of simplicity, and that other functionals could be considered instead without much change to the forthcoming discussion: least-square difference functions over the displacement, stress-based criteria, etc.

Our numerical resolution of eq. (7.5) relies on the boundary variation method of Hadamard, which we have already evoked in Section 1.1, and whose salient features are now briefly recalled for the convenience of the reader; see e.g. [12, 72, 86, 102] for further mathematical details and [8, 96] about implementation issues.

Variations of a given shape Ω are considered under the form

$$\Omega_\theta := (\mathrm{Id} + \theta)(\Omega), \quad \text{where } \theta \in W^{1,\infty}(\mathbb{R}^d, \mathbb{R}^d), \quad \|\theta\|_{W^{1,\infty}(\mathbb{R}^d,\mathbb{R}^d)} < 1,$$

is a "small" vector field encoding the deformation of Ω; see Figure 1.1 (top, right). The *shape derivative* of, say, $C(\Omega)$ is the Fréchet derivative $C'(\Omega)$ of the underlying mapping $\theta \mapsto C(\Omega_\theta)$ at $\theta = 0$:

$$C(\Omega_\theta) = C(\Omega) + C'(\Omega)(\theta) + \mathrm{o}(\theta), \quad \text{where } \frac{\mathrm{o}(\theta)}{\|\theta\|_{W^{1,\infty}(\mathbb{R}^d,\mathbb{R}^d)}} \xrightarrow{\theta\to 0} 0. \tag{7.7}$$

The shape derivatives of $C(\Omega)$ and $\mathrm{Vol}(\Omega)$ are well-known to be (see e.g. [11]):

$$C'(\Omega)(\theta) = -\int_\Gamma Ae(u_\Omega) : e(u_\Omega)\, \theta \cdot n \,\mathrm{ds}, \quad \text{and} \quad \mathrm{Vol}'(\Omega)(\theta) = \int_\Gamma \theta \cdot n \,\mathrm{ds}. \tag{7.8}$$

This allows to calculate a so-called (negative) "shape gradient" $\theta_C : \mathbb{R}^d \to \mathbb{R}^d$ for $C(\Omega)$ (and similarly, a shape gradient θ_V for $\mathrm{Vol}(\Omega)$): θ_C is a vector field such that the deformed version $\Omega_{t\theta_C}$ of Ω achieves a lesser value $C(\Omega_{t\theta_C}) < C(\Omega)$ of the compliance for $t > 0$ small enough. One such possibility, among others, is such that:

$$\theta_C = Ae(u_\Omega) : e(u_\Omega) n \text{ on } \Gamma,$$

as follows readily from eqs. (7.7) and (7.8). This information is the main ingredient of shape optimization algorithms based on the method of Hadamard, a generic sketch of which is provided in Algorithm 1.

Algorithm 1 Resolution of Problem eq. (7.5) using the method of Hadamard.

Initialization: Initial shape Ω^0, intial values α_C^0, α_V^0 of the optimization parameters.
for $n = 0, \ldots,$ until convergence **do**

(1) Calculate the elastic displacement u_{Ω^n} of Ω^n.

(2) Calculate negative shape gradients θ_C^n and θ_V^n for the functionals $C(\Omega)$ and $\mathrm{Vol}(\Omega)$, respectively.

(3) Calculate the deformation

$$\theta^n = \alpha_C^n \theta_C^n + \alpha_V^n \theta_V^n.$$

(4) Deform Ω^n along θ^n:

$$\Omega^{n+1} := (\mathrm{Id} + \tau^n \theta^n)(\Omega^n),$$

where the pseudo-time step τ^n is chosen small enough so that:

$$\alpha_C^n C(\Omega^{n+1}) + \alpha_V^n \mathrm{Vol}(\Omega^{n+1}) < \alpha_C^n C(\Omega^n) + \alpha_V^n \mathrm{Vol}(\Omega^n).$$

(5) Update the optimization parameters α_C^n and α_V^n.

end for
return Ω^n

In Algorithm 1, the optimization parameters α_C^n, α_V^n are updated so that the volume constraint is gradually enforced, while decreasing the value of the compliance, insofar as possible. Several strategies are available to this end, and in our practical implementation, we rely on the constrained optimization algorithm from [60]. As far as the numerical representation of shapes and their evolution are

concerned, we rely on the level set based mesh evolution method from [6, 7] (see also [59, 61] for recent developments). Grossly speaking, this method couples a level set representation of the shape on a fixed computational domain D [11, 105] (see also [94] for the seminal reference about the level set method) with remeshing operations using the open source library `mmg` [52, 53] to ensure that the shape is meshed explicitly at each stage of the process: no ersatz material approximation is needed in our numerical realization of Algorithm 1. Again, all the finite element calculations considered in this article rely on the `FreeFem` environment [71].

One drawback of the method of Hadamard is that it does not, in theory, leave the room for topological changes between iterations; indeed, the mappings $(\mathrm{Id}+\theta)$ driving the update process are homeomorphisms. As a result, the quality of the optimized design strongly depends on that of the initial guess Ω^0. In practice, a little abuse of the above framework authorizes certain topological changes: for instance, two separate holes can merge, but no hole can appear inside the bulk of the shape. To alleviate this problem, classical shape optimization algorithms based on the method of Hadamard are often complemented with the use of topological derivatives, as a mechanism to nucleate holes inside the optimized shape in an "optimal" way; see again Section 1.1, and [9, 40].

In the next section, we present another mechanism to enrich the topology of a shape in the course of its optimization via the method of Hadamard, namely the addition of a thin bar.

7.2.2. *Insertion of a material bar*

In this section, we explain how a thin bar can be added to a shape Ω arising in the course of Algorithm 1; for notational simplicity, we drop the mention ^{n} to the particular iteration in the present discussion.

To achieve our purpose, we approximate the mechanical behavior of Ω by the displacement u_0 supplied by the ersatz material method; the latter is the solution to the following system, posed on the whole computational domain D:

$$\begin{cases} -\operatorname{div}(A_0 e(u_0)) = 0 & \text{in } D, \\ u_0 = 0 & \text{on } \Gamma_D, \\ A_0 e(u_0) n = g & \text{on } \Gamma_N, \\ A_0 e(u_0) n = 0 & \text{on } \partial D \setminus (\overline{\Gamma_D} \cup \overline{\Gamma_N}), \end{cases} \quad \text{where } A_0(x) = \begin{cases} A & \text{if } x \in \Omega, \\ \eta A & \text{otherwise,} \end{cases} \tag{7.9}$$

and $\eta \ll 1$ is a very small parameter (in all our examples, we take $\eta = 10^{-3}$). Accordingly, the variation $\Omega_{\sigma,\varepsilon} = \Omega \cup \omega_{\sigma,\varepsilon}$ where the thin tube $\omega_{\sigma,\varepsilon}$ is grafted to Ω is described by the solution u_ε to:

$$\begin{cases} -\operatorname{div}(A_\varepsilon e(u_\varepsilon)) = 0 & \text{in } D, \\ u_\varepsilon = 0 & \text{on } \Gamma_D, \\ A_\varepsilon e(u_\varepsilon) n = g & \text{on } \Gamma_N, \\ A_\varepsilon e(u_\varepsilon) n = 0 & \text{on } \partial D \setminus (\overline{\Gamma_D} \cup \overline{\Gamma_N}), \end{cases} \quad \text{where } A_\varepsilon(x) = \begin{cases} A & \text{if } x \in \Omega \cup \omega_{\sigma,\varepsilon}, \\ \eta A & \text{otherwise.} \end{cases} \tag{7.10}$$

The compliance $C(\Omega_{\sigma,\varepsilon})$ of the perturbed shape $\Omega \cup \omega_{\sigma,\varepsilon}$ is then approximated by the quantity:

$$C_\sigma(\varepsilon) := \int_D A_\varepsilon e(u_\varepsilon) : e(u_\varepsilon) \, \mathrm{d}x = \int_{\Gamma_N} g \cdot u_\varepsilon \, \mathrm{d}s;$$

in particular, $C_\sigma(0)$ is the approximation of $C(\Omega)$ supplied by the ersatz material method. Relying on Proposition 3.3 and Proposition 6.3, this quantity has the following expansion as $\varepsilon \to 0$:

$$C_\sigma(\varepsilon) = C_\sigma(0) + \varepsilon^{d-1} C'_\sigma(0) + \mathrm{o}(\varepsilon^{d-1}); \tag{7.11}$$

note that the adjoint state p_0 in eqs. (3.25) and (6.19) featured in those formulas for $C'_\sigma(0)$ is simply $p_0 = -u_0$ in the present context where the compliance functional is considered; see also Remark 2.12.

On the other hand, the expansion of the volume $\mathrm{Vol}(\Omega_{\sigma,\varepsilon})$ of the perturbed shape is easily calculated as:

$$\mathrm{Vol}(\Omega \cup \omega_{\sigma,\varepsilon}) = \mathrm{Vol}(\Omega) + \varepsilon^{d-1}|\sigma| + \mathrm{o}(\varepsilon^{d-1}), \tag{7.12}$$

where $|\sigma|$ is the length of σ.

The sensitivities eqs. (7.11) and (7.12) lead to a simple methodology to add a bar with thickness ε (of the order of the mesh size in our applications) to the shape Ω in order to optimize its behavior with respect to Problem eq. (7.5). The proposed procedure is summarized in Algorithm 2.

Algorithm 2 Optimal insertion of a bar in the course of one particular iteration of Algorithm 1.

Initialization: Shape Ω, optimization parameters α_C, α_V, thickness parameter ε.

(1) Calculate the solution u_0 to eq. (7.10) in D.

(2) Calculate $C'_\sigma(0)$ for all the segments of the form $\sigma = [x^1, x^2]$, with $x^1, x^2 \in \partial\Omega$.

(3) Retain the segment σ where the quantity

$$\alpha_C \left(C_\sigma(0) + \varepsilon^{d-1} C'_\sigma(0) \right) + \alpha_V \left(\mathrm{Vol}(\Omega) + \varepsilon^{d-1}|\sigma| \right) \tag{7.13}$$

is the most negative.

return $\Omega_{\sigma,\varepsilon} := \Omega \cup \omega_{\sigma,\varepsilon}$.

Remark 7.1.

(i) For simplicity, we have only considered the graft of straight bars to a shape Ω, while in principle, the strategy of Algorithm 2 could feature quite arbitrary base curves σ. It is expected, however, that the search for such a curve minimizing the quantity eq. (7.13) would be difficult to parametrize and implement.

(ii) The strategy of Algorithm 2, running through all segments of the form $[x^1, x^2]$, where x^1, x^2 belong to (a discretization of) $\partial\Omega$ is admittedly naive: even though the evaluation of the asymptotic formula eq. (7.11) for $C'_\sigma(0)$ is cheap (the background displacement u_0 needs only to be computed once and for all, independently of σ), we expect that this procedure could become computationally expansive when the size of the mesh gets larger, thus raising the need for a more clever strategy (e.g. a randomized procedure); see Section 8 for further comments about this point.

Remark 7.2. In the strategy of Algorithm 2, the specifications of the base curve σ of the new bar to be added to Ω are inferred so as to minimize the quantity eq. (7.13), which amounts to assuming that the inserted bar has an infinitesimal thickness. In practice, we rely on a "small" (but not infinitesimal) value ε for the thickness, of the order of the mesh size. Therefore, it might happen that the inserted bar, with thickness ε, is not exactly the optimal bar to be inserted with this value of the thickness. Note that the same issue occurs when using topological derivative formulas (see Section 1.1 for a glimpse), which are, in principle, relevant only when infinitesimally small holes are considered.

Remark 7.3. In all the considered examples where Algorithm 2 is intertwined with steps of the boundary variation Algorithm 1, the minimized quantity eq. (7.13) is evaluated before and after insertion of the bar predicted by Algorithm 2. The insertion of this bar is then retained only if this value has decreased in the process. In practice, especially when more sensitive functions of the domain than the compliance are considered, it may be desirable to allow a small tolerance over a possible (slight) increase of eq. (7.13) as a result of the insertion of the bar.

7.2.3. *An example in 2d: the benchmark cantilever test case*

The first numerical illustration of our topological ligament approach features the benchmark 2d cantilever test case, whose details are reported on Figure 7.6 (top, left): the shapes Ω of interest are contained inside a box D with size 2×1; they are clamped on their left-hand side Γ_D, and a unit vertical load $g = (0, -1)$ is applied on the region Γ_N in the middle of their right-hand side. Starting from the initial design of Figure 7.6 (top, left), we solve the shape optimization problem eq. (7.5) with a value $V_T = 0.8$ for the volume target, while imposing symmetry of shapes with respect to the ξ_2 direction.

In a first attempt, we rely on Algorithm 1, which solely uses the boundary variation method of Hadamard. We intentionally select update rules for the optimization parameters α_C, α_V so that the volume constraint is very rapidly enforced. It turns out that the optimized shape develops very early a trivial topology and the optimization path ends in a local minimum with a quite simple topology and poor structural performance: the compliance of the final shape equals 3.09; see Figure 7.6 where several intermediate shapes are represented.

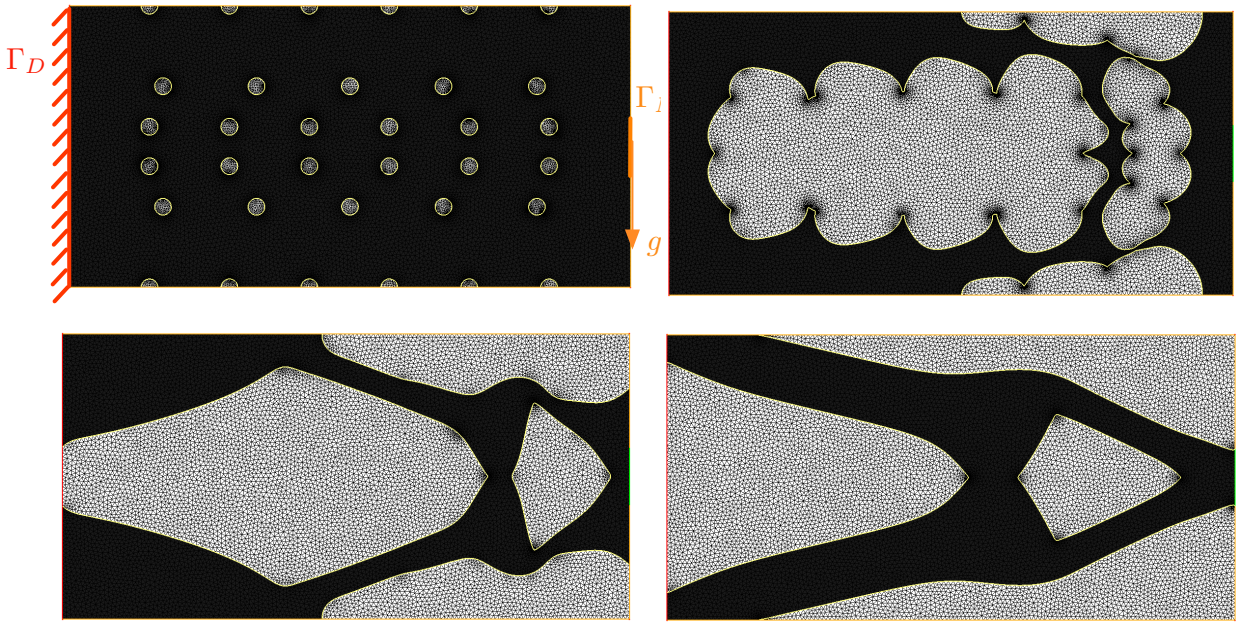

Figure 7.6. (From left to right, top to bottom) Iterations 0 (with details of the test case), 20, 40 and 200 in the 2d cantilever test case of Section 7.2.3 solved by using the boundary variation Algorithm 1.

We then conduct the same experiment, up to an additional ingredient: the optimization process of Algorithm 1 is periodically interrupted every 10 iteration, from iteration 40 to iteration 100, in order to try and graft a bar to the optimized shape, according to Algorithm 2. Several snapshots of this process are depicted on Figure 7.7, and the related convergence histories are reported on Figure 7.8: obviously, the final shape has a richer topology, showing a larger number of holes, and the compliance of the final shape equals 2.61, a lower value than in the previous situation.

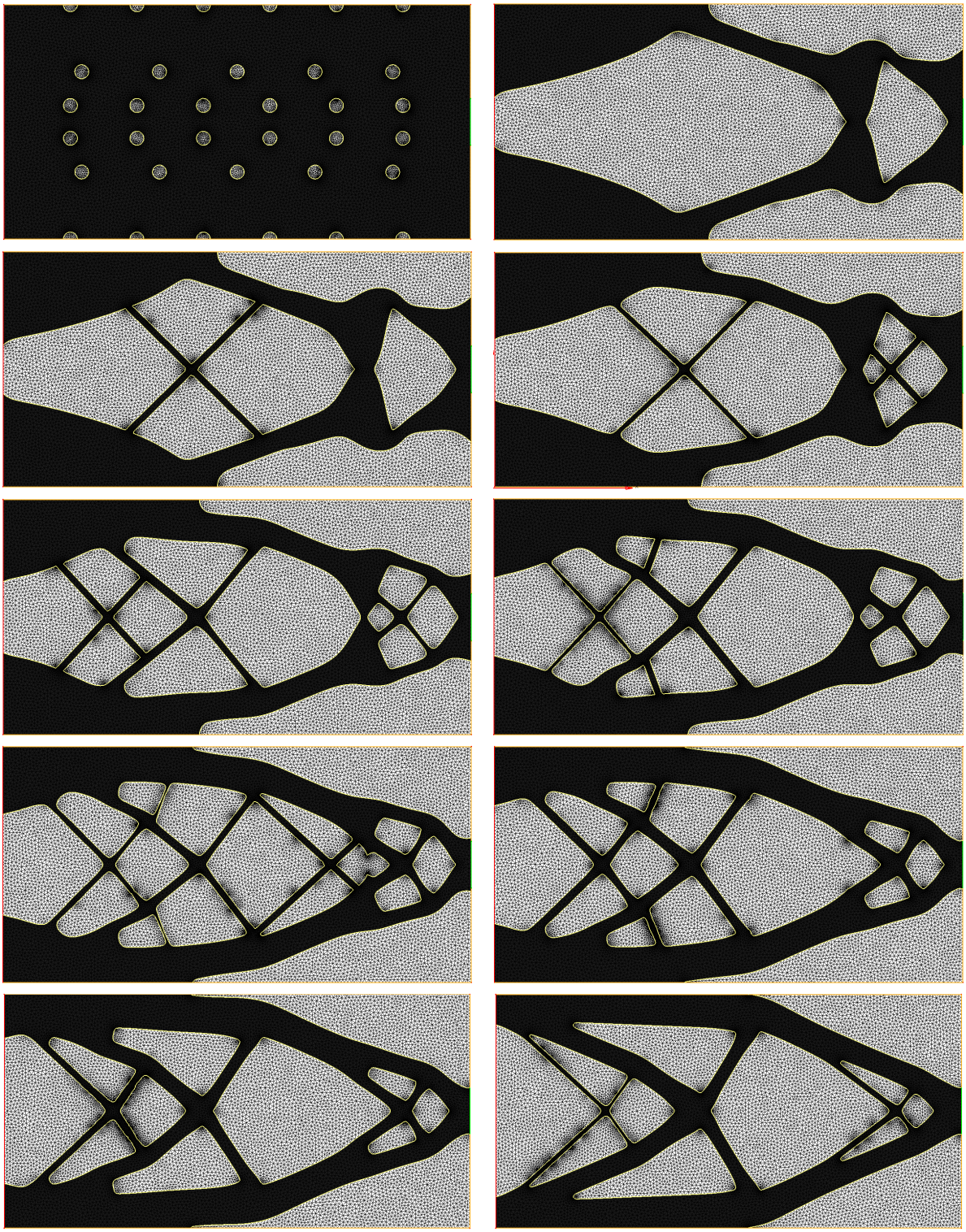

Figure 7.7. Iterations 0, 40, 41, 51, 61, 71, 81, 90, 100 and 200 in the 2d cantilever test case of Section 7.2.3 solved by using a coupling of Algorithm 1 with periodic insertion of bars owing to Algorithm 2.

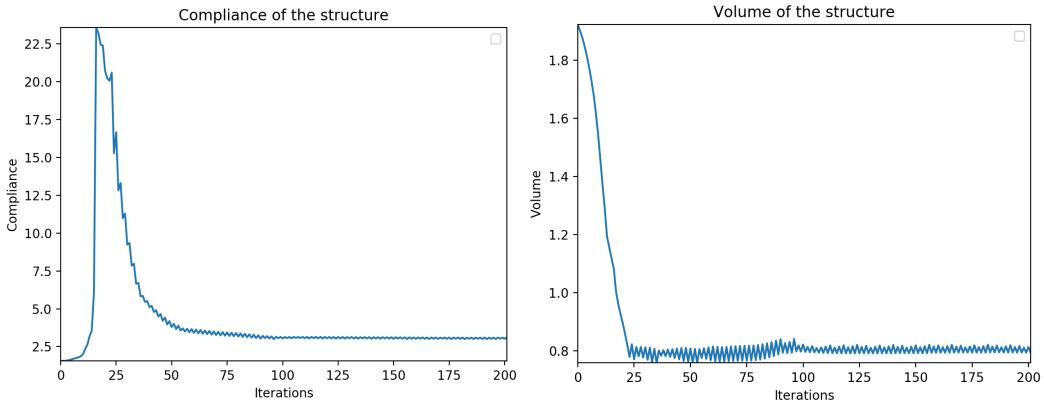

FIGURE 7.8. (Left) Evolution of the compliance in the course of the optimization of the 2d cantilever in Section 7.2.3 with a combined use of Algorithms 1 and 2; (right) evolution of the volume of the structure.

7.2.4. *Optimization of the shape of a three-dimensional bridge*

A similar experiment is conducted in the context of the optimization of a 3d bridge. As depicted on Figure 7.9, the shapes are contained inside a trapezoid D with dimensions $4 \times 1 \times 1$. They are clamped on the reunion Γ_D of four disjoint regions located on the side and bottom parts of their boundary, while a unit vertical load $g = (0, 0, -1)$ is distributed on their upper side Γ_N. Starting from the initial shape of Figure 7.10 (top, left), we solve the problem eq. (7.5), with the value $V_T = 0.12$ for the volume constraint, while imposing symmetry of shapes with respect to the ξ_2 direction.

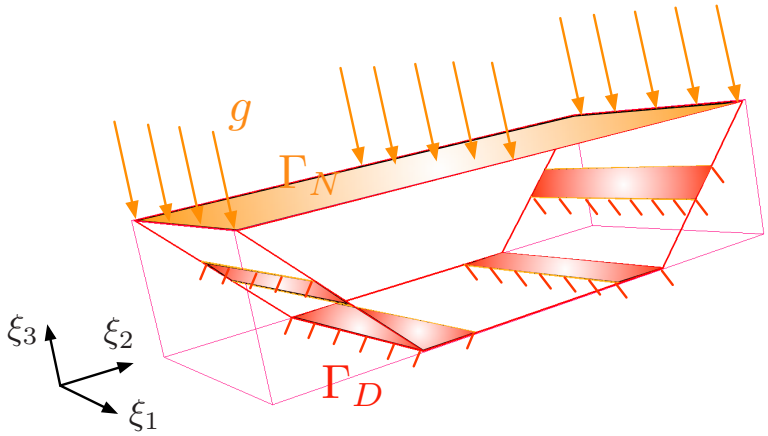

FIGURE 7.9. Setting of the three-dimensional bridge example of Section 7.2.4.

We rely first on the boundary variation Algorithm 1, where we use an awkward rule for the update of the optimization parameters α_C, α_V. Again, the volume constraint is imposed very rapidly, so that the shape accidentally gets disconnected from two of the four clamping regions which compose ∂D. The optimized shape in this case has a poor structural performance, as reflected by the large value $C(\Omega) = 29.66$ of its compliance; see Figure 7.10 for several snapshots of the process.

In a second time, we perform the same experiment, up to the use of our topological ligament approach: every 10 iteration from iteration 40 to iteration 100 of the procedure in Algorithm 1, we apply Algorithm 2 to try and add a bar to Ω, which either connects two points $x^1, x^2 \in \partial\Omega$, or one

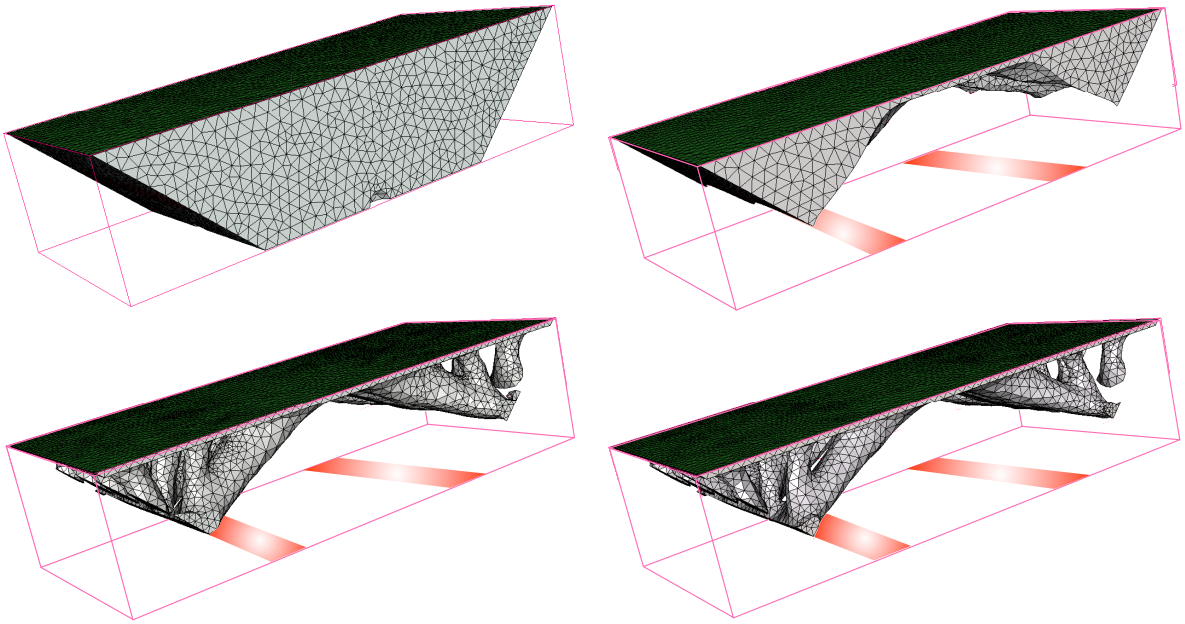

Figure 7.10. Iterations 0, 40, 100 and 200 in the three-dimensional bridge test case of Section 7.2.4 solved by using the boundary variation Algorithm 1.

point $x^1 \in \partial\Omega$ and a point $x^2 \in \Gamma_D$. Several intermediate shapes of the process are represented on Figure 7.11, and the convergence histories are reported on Figure 7.12. Obviously, the algorithm is able to detect that it is beneficial to insert bars between the shape and the isolated components of the clamping region Γ_D; the resulting shape from this procedure has a much lower compliance value $C(\Omega) = 8.34$ than in the previous situation.

7.3. **Optimal design of supports for additive manufacturing.**

In this section, we apply our asymptotic formulas for thin tubular inhomogeneities to the computation of an optimized collection of vertical pillars, serving as the support structure for a fixed shape Ω in the course of its construction by an additive manufacturing technique.

We refer to [65] for a general overview of additive manufacturing techniques, and to the survey article [81] for a description of the new issues and challenges they raise in connection with the field of shape and topology optimization. Briefly, additive manufacturing (or 3d printing) is a common label for a whole range of fabrication processes, which have in common that they begin with a subdivision of the constructed shape into a series of horizontal slices; these layers are then constructed one atop the other, according to the selected technology (Fused Filament Fabrication, Electron Beam melting, etc.). These additive manufacturing methodologies have recently become very popular in engineering since they are allegedly capable of assembling arbitrarily complex shapes, such as the lattice structures whose optimality is predicted in a wide variety of situations by the homogenization theory. Unfortunately, additive manufacturing methods also impose limitations of their own on the constructed design Ω; in particular, for various reasons, they all experience difficulties when Ω shows large *overhangs*, i.e. nearly horizontal regions hanging over void. One possible solution to cope with the presence of such features is to erect a support structure S at the same time as Ω (possibly made of a different, cheaper material) so as to anchor them to the build table; see [41, 57] among other contributions.

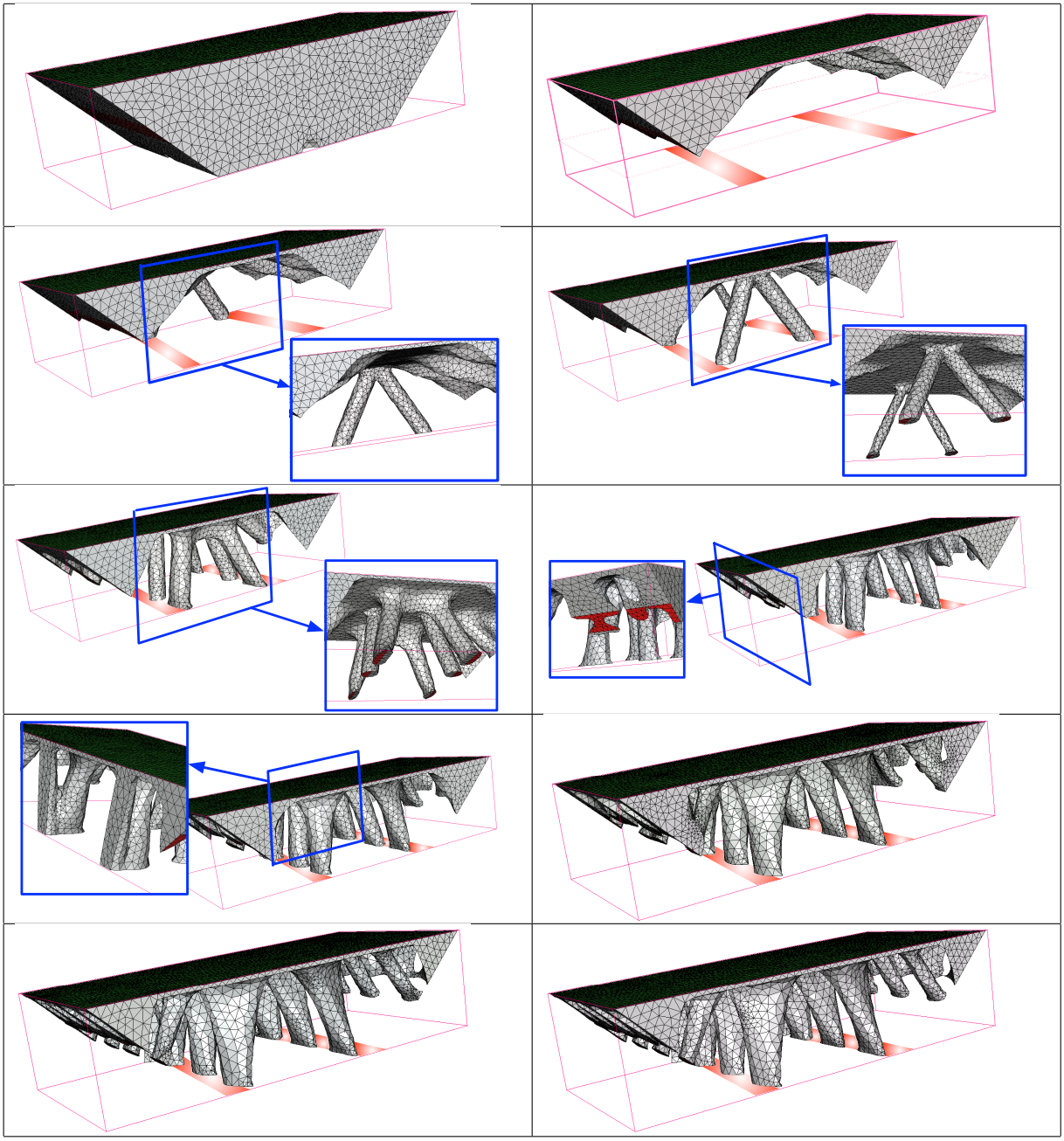

FIGURE 7.11. Iterations 0, 40, 41, 51, 61, 71, 81, 100, 150 and 200 in the three-dimensional bridge test case of Section 7.2.4 solved by using a combination of Algorithms 1 and 2.

In this section, we aim to optimize the design of a support structure S for a given shape Ω containing large overhangs. The optimized supports S should ease the construction of the total structure $\Omega \cup S$, for a minimum weight, so as to limit material consumption.

We rely on the model introduced in [3] for the fabrication process. The structure Ω to be assembled, together with all the possible designs for the supports S are contained in a fixed computational domain D of the form $D = [0, M_1] \times \ldots \times [0, M_d]$, which stands for the build chamber. Since Ω is

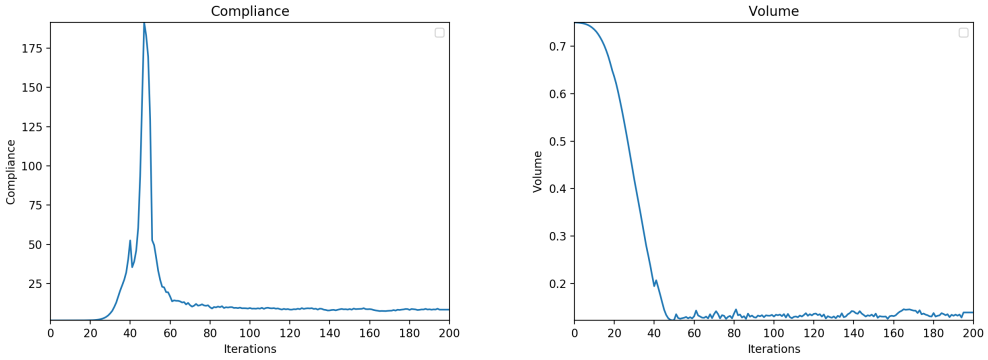

FIGURE 7.12. (Left) Evolution of the compliance in the course of the optimization of the three-dimensional bridge of Section 7.2.4 with a combined use of Algorithms 1 and 2; (right) evolution of the volume of the structure.

fixed throughout this section, the dependences of the various considered quantities with respect to Ω are omitted for brevity. The physical behavior of $\Omega \cup S$ during the construction stage is accounted for by the linearized elasticity system, in the situation where $\Omega \cup S$ is clamped on the ground $\Gamma_0 := \{x = (x_1, \cdots, x_d) \in D, \quad x_d = 0\}$, and is submitted to gravity loads, represented by a body force $f : \mathbb{R}^d \to \mathbb{R}^d$. The displacement u_S of $\Omega \cup S$ in these circumstances is the solution to:

$$\begin{cases} -\operatorname{div} A_S e(u_S) = \rho f & \text{in } \Omega \cup S, \\ u_S = 0 & \text{on } \Gamma_0, \\ A e(u_S) n = 0 & \text{on } \partial(\Omega \cup S) \setminus \overline{\Gamma_0}. \end{cases} \tag{7.14}$$

Here ρ is the density of material, which equals 1 inside the structure Ω, and 0 inside the supports for simplicity; the value of the Hooke's tensor A_S inside Ω is that A in eq. (7.4), as used in the previous section; inside the support structure, A_S takes the weaker value $A_1 = \eta_S A$ (in practice, we use $\eta_S = 0.4$).

We aim to solve the problem

$$\min_{S \subset D} \operatorname{Vol}(S) \text{ s.t. } C(S) \leq C_T, \tag{7.15}$$

where $\operatorname{Vol}(S) := \int_S \mathrm{d}x$ is the volume of the support structure, and the compliance of the structure during its manufacturing,

$$C(S) := \int_{\Omega \cup S} A_S e(u_S) : e(u_S) \, \mathrm{d}x = \int_{\Omega \cup S} f \cdot u_S \, \mathrm{d}x \tag{7.16}$$

is required not to exceed the user-defined threshold C_T.

Remark 7.4.

- This model for the physical behavior of a shape Ω and the companion scaffold structure S during the fabrication process was proposed in [3]. It is a simplified version of the layer-by-layer approach introduced in [4, 5, 15], where the compliance of each intermediate shape $\Omega_h := \{x \in \Omega, \quad x_d < h\}$ (corresponding to the stage where Ω is assembled up to the level $x_d = h$) is involved.

- Other physical criteria than the compliance eq. (7.16) could be used for evaluating the performance of the structure S, such as criteria based on the steady-state heat equation, as a means to measure the rapidity of heat evacuation or the accumulation of residual stress (see

e.g. [10, 37]). The application of the strategy described below to create an optimized set of pillars in view of Problem eq. (7.15) in this other context governed by the conductivity equation could make use of the asymptotic formulas derived in Sections 2 and 5.

The optimal design problem eq. (7.15) of a suitable support structure for Ω was treated by means of a boundary variation algorithm very similar to Algorithm 1 in [3]. In many practical situations, however, it is desirable that the scaffold structure S resemble as much as possible a collection of vertical pillars (at the very least, S itself should not feature overhang regions!) One idea in this direction is to rely on the asymptotic formulas in this article to devise an optimized set of vertical pillars with respect to Problem eq. (7.15).

To achieve this, as in Sections 1.2 and 7.2.2, we approximate the solution u_S to eq. (7.14) by that u_0 to the approximate counterpart supplied by the ersatz material method:

$$\begin{cases} -\operatorname{div} A_0 e(u_0) = \rho f & \text{in } D, \\ u_0 = 0 & \text{on } \Gamma_0, \\ A_0 e(u_0) n = 0 & \text{on } \partial D \setminus \overline{\Gamma_0}, \end{cases} \quad \text{where } A_0(x) = \begin{cases} A & \text{if } x \in \Omega, \\ \eta_S A & \text{if } x \in S, \\ \eta A & \text{otherwise,} \end{cases} \tag{7.17}$$

and the small parameter for the ersatz material equals $\eta = 10^{-3}$. Likewise, the mechanical behavior $u_{S \cup \omega_{\sigma,\varepsilon}}$ of the total structure when a thin bar $\omega_{\sigma,\varepsilon}$ is added to the supports S is approximated by the solution u_ε to:

$$\begin{cases} -\operatorname{div} A_\varepsilon e(u_\varepsilon) = \rho f & \text{in } D, \\ u_\varepsilon = 0 & \text{on } \Gamma_0, \\ A_\varepsilon(u_\varepsilon) n = 0 & \text{on } \partial D \setminus \overline{\Gamma_0}, \end{cases} \quad \text{where } A_\varepsilon(x) = \begin{cases} A & \text{if } x \in \Omega, \\ \eta_S A & \text{if } x \in S \cup \omega_{\sigma,\varepsilon}, \\ \eta A & \text{otherwise,} \end{cases} \tag{7.18}$$

We now replace the compliance $C(S \cup \omega_{\sigma,\varepsilon})$ in eq. (7.16) by the quantity

$$C_\sigma(\varepsilon) = \int_D A_\varepsilon e(u_\varepsilon) : e(u_\varepsilon) \, \mathrm{d}x = \int_D \rho f \cdot u_\varepsilon \, \mathrm{d}x,$$

whose asymptotic expansion

$$C_\sigma(\varepsilon) = C_\sigma(0) + \varepsilon^{d-1} C'_\sigma(0) + \mathrm{o}(\varepsilon^{d-1})$$

is supplied by Proposition 3.3 in 2d and by Proposition 6.3 in 3d.

Starting from an empty support structure $S^0 = \emptyset$, we repeatedly apply an easy adaptation of Algorithm 2 to insert a vertical bar with thickness $\varepsilon > 0$ and material properties A_1, connecting one point $x \in \partial\Omega$ with its projection $\tilde{x} := (x_1, \dots, x_{d-1}, 0)$ on the base table Γ_0 in an optimal way. This procedure is repeated until the performance of the support structure S, as measured by the compliance $C(S)$ of $\Omega \cup S$ in eq. (7.16) gets below the threshold C_T. In concrete applications the thickness ε of the inserted pillars should be set according to the capabilities of the machine tool; for simplicity, however, in the model examples of this article, we simply choose ε of the order of the mesh size.

Depending on the capabilities of the machine tool, it may be possible to construct more general shapes of supports than just pillars. In such a case, the optimized collection of pillars S_{temp} resulting from the previous procedure may serve as a "good" initial guess for a subsequent resolution of eq. (7.15) by means of a more classical boundary variation algorithm, such as Algorithm 1 up to some minor adaptations, as in the article [3].

These considerations lead to a two-stage optimal design process for the support structure S, which is summarized in Algorithm 3.

Remark 7.5.

- In practice, in the first stage of Algorithm 3, bars are inserted, regardless of their volume, until the compliance constraint is fulfilled, before the true constrained optimization Algorithm 1,

Algorithm 3 Optimization of the support structure S for the construction of Ω by 3d printing

Initialization: Shape Ω, intial support structure $S^0 = \emptyset$, thickness parameter ε.
Step 1:
while $C(S) \geq C_T$ **do**

(1) Calculate the ersatz material approximation u_0 to the solution u_S of eq. (7.14).

(2) For all point $x \in \partial\Omega$, calculate the quantity $C'_\sigma(0)$, where $\sigma = [x, \widetilde{x}]$ connects x with its projection $\widetilde{x} = (x_1, \ldots, x_{d-1}, 0)$ on Γ_0. and retain the segment achieving the most negative value.

(3) Update S by $S \cup \omega_{\sigma,\varepsilon}$.

end while
Intermediate result: Optimized collection of vertical pillars S_{temp}.
Step 2: Solve the shape optimization problem eq. (7.15) by using (an adapted version of) the boundary variation algorithm Algorithm 1, starting from S_{temp}.
return Optimized support structure S.

based on the method of Hadamard, is used. Of course, it would be possible to rely on a constrained optimization algorithm since the beginning.

- We sometimes interrupt the first stage when the compliance of the support structure S reaches a slightly larger value than the imposed threshold C_T: we indeed observe that at some point, it is no longer optimal to insert bars, but a better design is more easily obtained by switching to a boundary variation algorithm such as Algorithm 1.

7.3.1. *Optimization of the support structure of a 2d MBB beam*

We first consider a 2d example where the shape Ω to be produced is the MBB Beam of Figure 7.13 (top), which has been optimized with respect to its elastic compliance; see Figure 7.13 (top) (the details of this optimization are not reported for brevity). Obviously, Ω presents large overhangs, and we solve Problem eq. (7.15) so as to calculate a suitable support structure S, which eases its construction by additive manufacturing. We use Algorithm 3 to achieve our purpose, while imposing symmetry of the structure S in the direction ξ_1. The numerical value $f = (0, -9.8)$ is used for the body force representing gravity effects in eq. (7.14), and we select the threshold $C_T = 67$ for the compliance constraint.

The optimized structures resulting from both stages are represented on Figure 7.13 and the associated convergence histories are in Figure 7.14. The compliance $C(S)$ decreases very rapidly in the course of the first stage, and only 20 iterations are needed to obtain an intermediate structure S_{temp} such that $C(S_{\text{temp}}) < C_T$. The second stage of Algorithm 3 proves also quite efficient in delivering a final support structure S which uses a lesser amount of material for about the same compliance value as S_{temp}. Interestingly, S resembles much the intermediate design S_{temp} resulting from the first, bar insertion stage.

7.3.2. *Optimization of the support structure for a 3d chair*

We apply the same methodology on a three-dimensional example, similar to one of those tackled in [3]. The constructed structure Ω is a chair, enclosed in a box D with size $0.7 \times 0.5 \times 1$, which results from a preliminary shape optimization process; see Figure 7.15 (top, left) below.

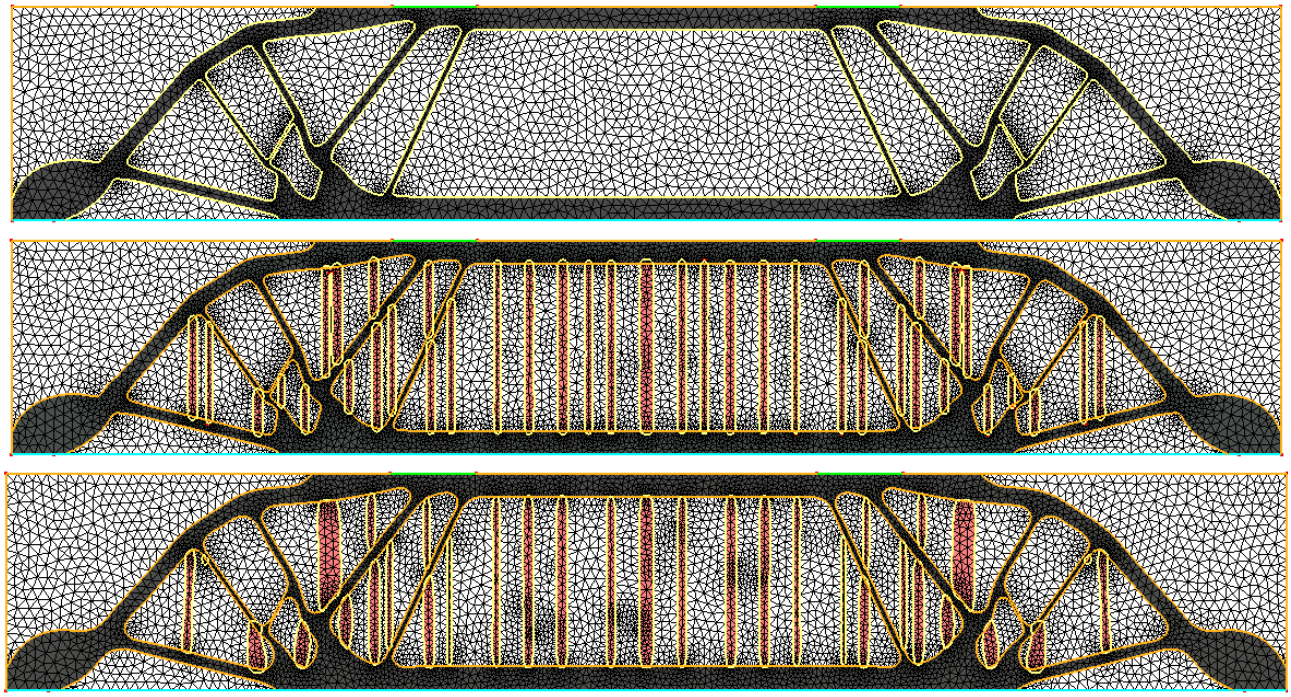

FIGURE 7.13. (Top) Optimized design Ω of an MBB Beam in terms of is structural compliance; (middle) optimized collection of pillars S_{temp} resulting from the first stage of Algorithm 3 (in red); (bottom) optimized support structure S resulting from the second stage of Algorithm 3.

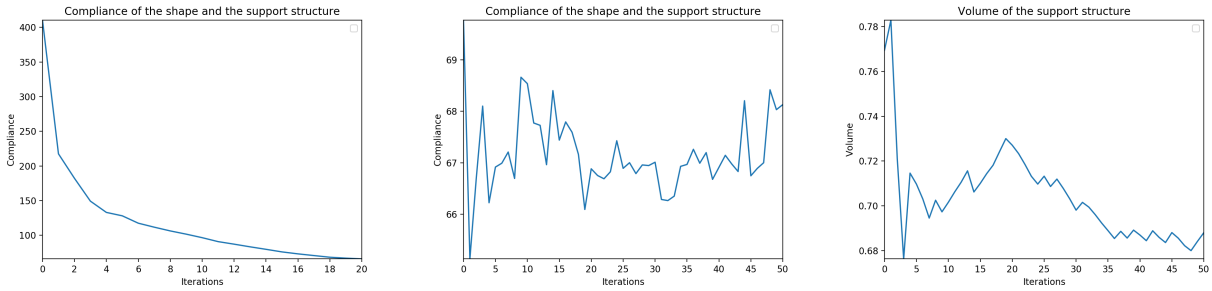

FIGURE 7.14. (Left) Evolution of the compliance $C(S)$ in eq. (7.16) of the support structure for the MBB beam example of Section 7.3.1, during the first stage of Algorithm 3; (middle) evolution of $C(S)$ during the second stage of Algorithm 3; (right) evolution of the volume $\text{Vol}(S)$ during the second stage.

The body force f modeling gravity effects equals $f = (0, 0, -9.8)$, and the threshold value for the compliance constraint is $C_T = 1$. No particular symmetry is imposed on the support structure S. We apply Algorithm 3, and several snapshots of the optimization process are displayed on Figure 7.15; the associated convergence histories are reported on Figure 7.16.

As in the example of Section 7.3.1, very few iterations of the first stage are needed to deliver a support structure S_{temp} whose compliance satisfies the desired inequality in eq. (7.15). The second stage also offers a significant improvement of this intermediate design.

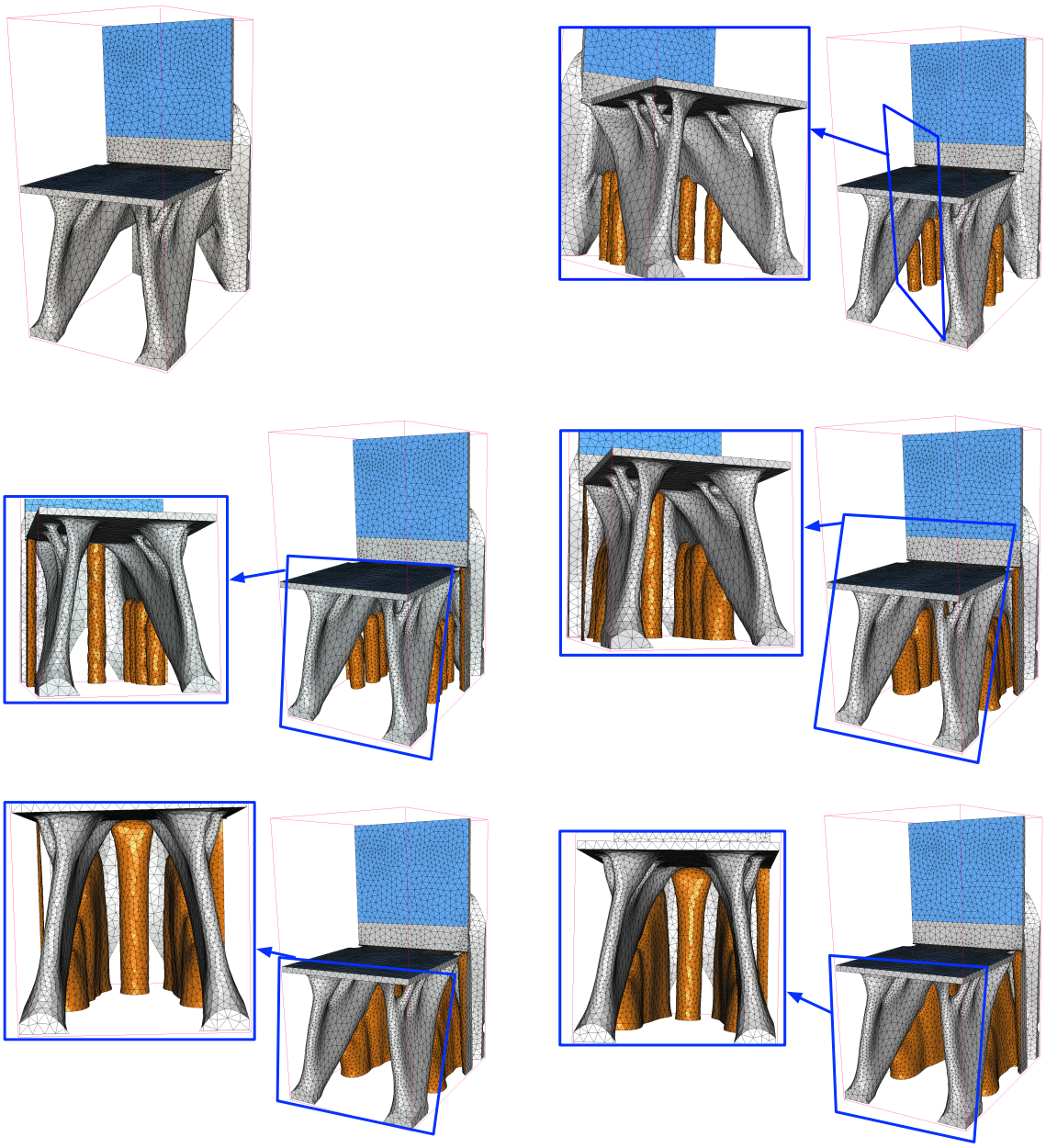

FIGURE 7.15. (From top to bottom, left to right) Iterations 0, 5, 10 of the first phase, followed by iterations $7, 19, 30$ of the second phase of Algorithm 3 in the scaffold structure optimization example of Section 7.3.2. The fixed shape Ω to be fabricated is represented in grey, and the support structure S is displayed in orange.

7.4. **An incremental algorithm for the optimization of truss structures.**

Although we have hitherto focused on the optimization of continuous structures in this example section, one promising application of asymptotic formulas for thin tubular inhomogeneities concerns the optimization of trusses, that is, structures that are collections of straight members, connected at joints. Most often, the optimal design of such structures is conducted by means of combinatorial,

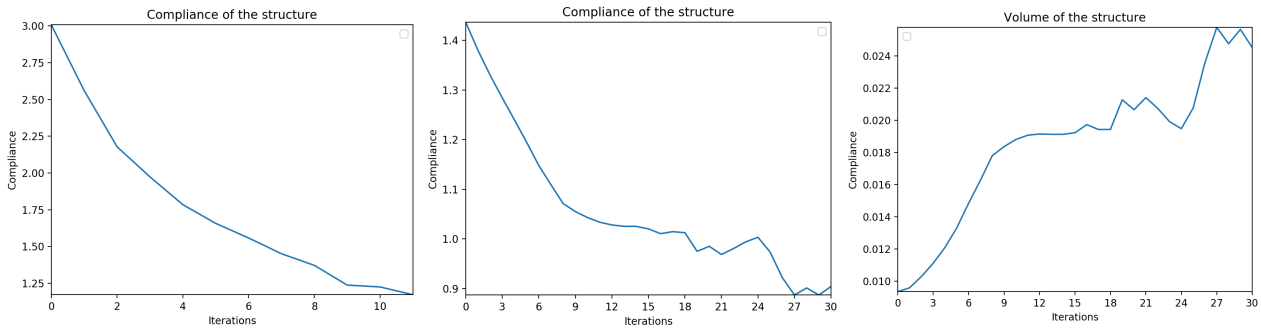

FIGURE 7.16. (Left) Evolution of the compliance $C(S)$ of the support structure for the 3d chair example of Section 7.3.2, during the first stage of Algorithm 3; (middle) evolution of $C(S)$ during the second stage of Algorithm 3; (right) evolution of the volume $\mathrm{Vol}(S)$ during the second stage.

or sizing optimization algorithms. One popular approach is the so-called "ground structure" method (see [56] for the seminal article), where the optimized structure is initialized with a very large amount of bars, connecting all the nodes of a user-defined set. The thickness of each bar is optimized with respect to a given measure of the mechanical performance of the structure, and a vanishing thickness for a bar indicates that it should be removed from the structure. One obvious drawback of the resulting optimal control formulation is that it typically features a very large number of variables. Quite differently, truss-like structures have also been optimized by means of modern continuous shape optimization methods (see e.g. [11]), with the risk that the resulting structure might be too "bulky", and lose its "truss-like" character. We refer to [29] for a general overview of the question of truss optimization.

In this section, we propose a fairly simple variation of the bar insertion methodology of Section 7.2.2 to address the model structural optimization problem

$$\min_{\Omega} \mathrm{Vol}(\Omega) \text{ s.t. } C(\Omega) \leq C_T, \tag{7.19}$$

in a context where the structure Ω is expected to resemble a truss. Here, as before, $C(\Omega)$ stands for the elastic compliance eq. (7.6) of the structure Ω, whose mechanical behavior is characterized by the elastic displacement u_Ω in eq. (7.10), and C_T is a user-defined threshold.

Contrary to the "ground structure" approach, our algorithm starts with an empty structure Ω. A set $\mathcal{N} = \left\{x^1, \dots, x^N\right\}$ of nodes is defined once and for all by the user within the computational domain D; we then rely on the methodology of Algorithm 3 in Section 7.2.2 to iteratively try and enrich Ω with bars: the ersatz material method is used to produce an approximation $C_\sigma(\varepsilon)$ of the compliance $C(\Omega_{\sigma,\varepsilon})$, where variations of the actual structure Ω are of the form $\Omega_{\sigma,\varepsilon} = \Omega \cup \omega_{\sigma,\varepsilon}$, involving segments $\sigma = [x^i, x^j]$ with endpoints in $\mathcal{N}$. Relying on the asymptotic expansion of $C_\sigma(\varepsilon)$ supplied by Proposition 3.3 and Proposition 6.3, we iteratively try and insert bars to decrease the value of the compliance until it gets below the threshold C_T.

As a complement to this bar insertion algorithm, and depending on whether the optimized structure Ω is required to be exactly a collection of bars, or this assumption might be relaxed slightly, it is interesting to try and optimize further the resulting design Ω_{temp} from this first stage by means of the more classical boundary variation Algorithm 1.

This optimal design methodology for truss-like structures is summarized in Algorithm 4.

Algorithm 4 Optimization of a truss-like structure Ω

Initialization: Initial shape $\Omega = \emptyset$, set of nodes $\mathcal{N} = \left\{x^1, \ldots, x^N\right\} \subset D$, thickness parameter ε.
Step 1:
while $C(S) \geq C_T$ **do**

(1) Calculate the ersatz material approximation u_0 to the solution u_Ω of eq. (7.10).

(2) For all pairs of nodes $x^i, x^j \in \mathcal{N}$, calculate the quantity $C'_\sigma(0)$, for $\sigma = [x^i, x^j]$, and retain the segment achieving the most negative value.

(3) Update Ω by $\Omega \cup \omega_{\sigma,\varepsilon}$.

end while
Intermediate result: Optimized collection of bars Ω_{temp}.
Step 2: Solve the shape optimization problem eq. (7.19) by using (an adapted version of) the boundary variation algorithm Algorithm 1, starting from Ω_{temp}.
return Optimized truss-like structure Ω.

7.4.1. *Optimization of the layout of a crane in 2d*

Our first optimization example of a truss-like structure is that of a two-dimensional crane, as depicted on Figure 7.17 (top, left). The considered shapes are enclosed in a box with size 5×4; two vertical loads $g = (0, -1)$ are applied on the front and rear parts Γ_N of the crane, mimicking the weight of the lifted object and the counterweight, respectively. The optimization problem eq. (7.19) is considered, with a value $C_T = 120$ for the imposed threshold on the compliance of shapes.

We apply Algorithm 4 to the resolution of this problem. Several iterates of the optimization process are depicted on Figure 7.17, and the associated convergence histories are reported on Figure 7.18. Interestingly, the optimized shape resembles very much a truss and its outline is very reminiscent of the intermediate collection of bars Ω_{temp} resulting from the first, bar insertion stage.

7.4.2. *Optimization of the layout of a mast in 3d*

We now turn to a three-dimensional example, that of the optimization of an electric mast. The physical situation is represented on Figure 7.19 (top, left): shapes are enclosed in a $3 \times 1 \times 3$ T-shaped domain D and they are clamped at their bottom side; surface loads $g = (0, 0, -1)$ are applied at the end of both arms. Here, symmetry is imposed with respect to the ξ_2 direction, and the considered threshold for the compliance is $C_T = 100$.

Several intermediate shapes arising in the course of the optimization process are represented on Figure 7.19, and the associated convergence histories are reported on Figure 7.20. Note that the resulting collection of bars Ω_{temp} from the first stage is connected, while no particular effort was paid during the optimization to enforce this property.

8. **Conclusions and perspectives**

The investigations of the present article lie halfway between the fields of asymptotic analysis and shape and topology optimization.

From the theoretical point of view, we have focused on the asymptotic expansion of the solution to a "background" partial differential equation (particularly, the conductivity equation and the linear elasticity system in 2d and 3d) when the ambient medium is perturbed inside a tube with vanishing thickness. Our main contribution in this direction was to propose a simple, heuristic argument to

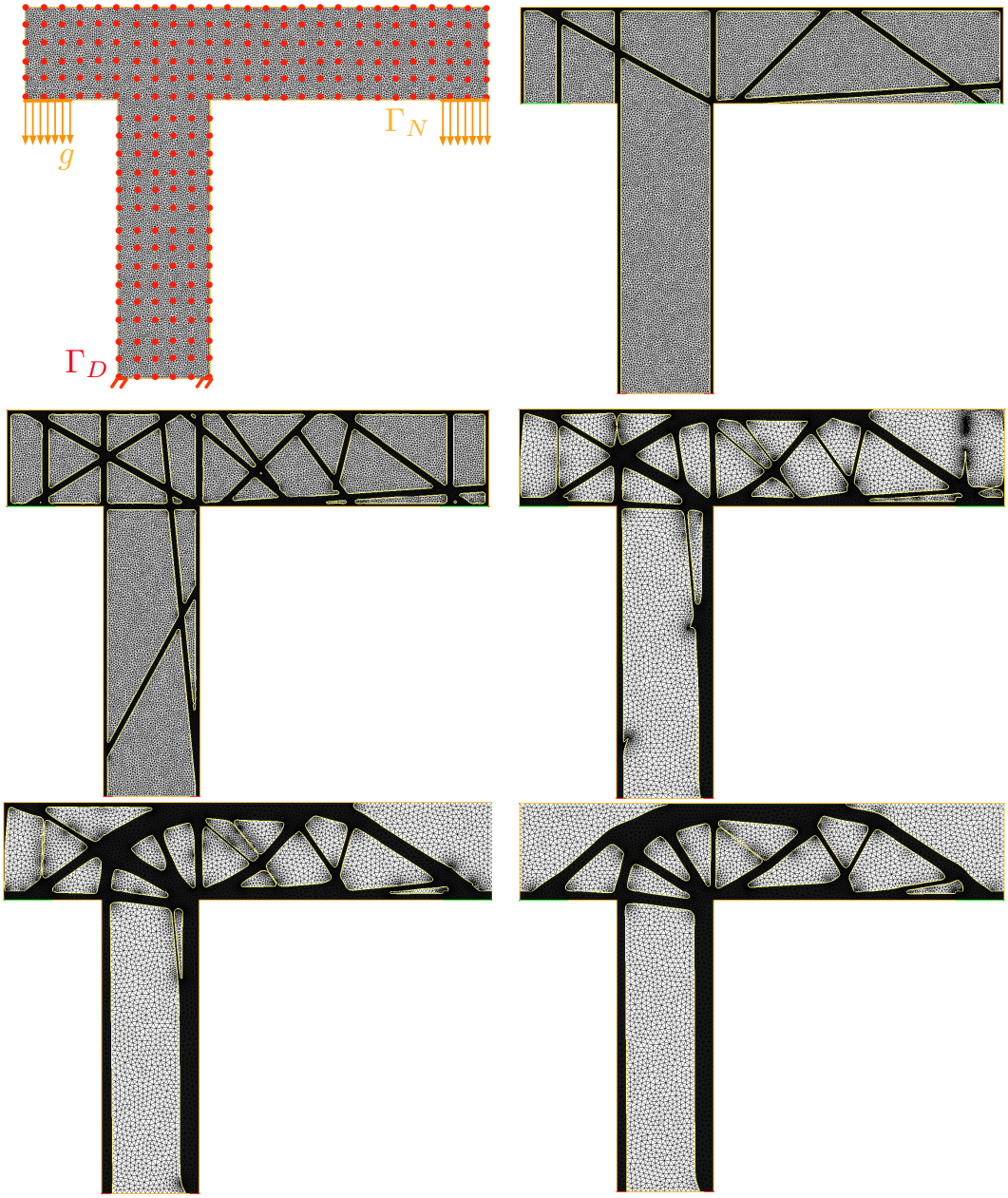

FIGURE 7.17. (Top) Iterations 0, 4 and 9 of the first phase; (bottom) Iterations 11, 91 and 200 of the second phase in the crane optimization example with design of a truss-like initial guess, as considered in Section 7.4.1.

conduct the analysis. Albeit not perfectly rigorous, it allows to retrieve quite effortlessly existing formulas and also to deal with settings which have not yet been addressed in the literature, to the best of our knowledge.

As regards applications, we have proposed a formal use of these asymptotic formulas for thin tubular inhomogeneities in order to graft a bar to a shape in an "optimal" way. We approximate the sensitivity of a function of the domain with respect to the addition of a ligament between two distant regions of the shape – a question which was investigated in [87, 88, 89] from a different perspective. Taking advantage

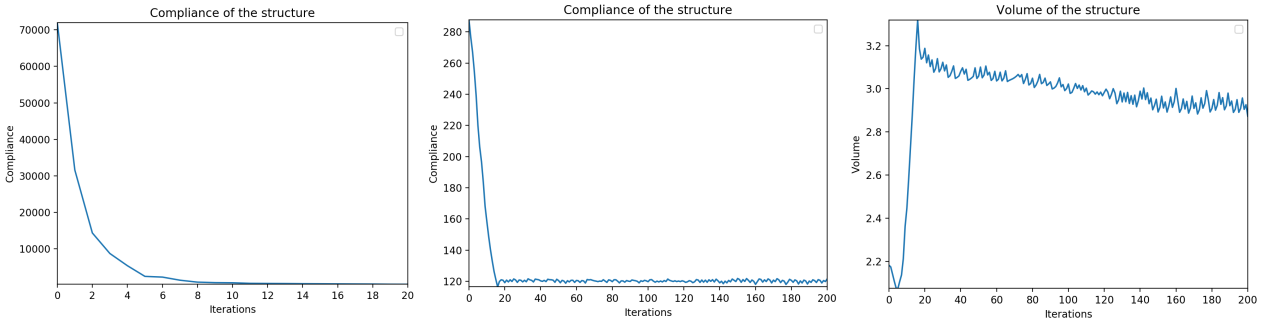

Figure 7.18. (Left) Evolution of the compliance in the course of the first stage; (middle) evolution of the compliance during the second step; (right) evolution of the volume during the second step in the crane optimization example of Section 7.4.1

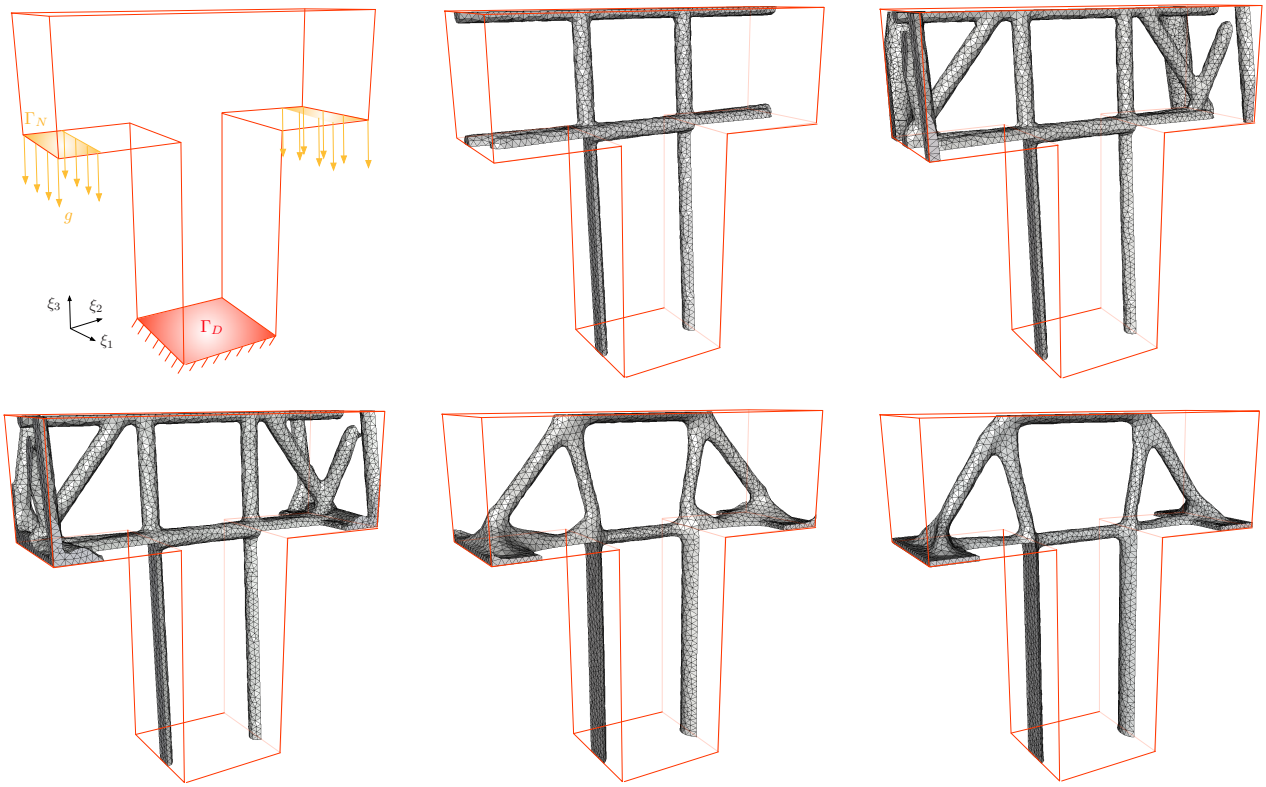

Figure 7.19. (Top) Iterations 0, 3 and 7 of the first phase; (bottom) Iterations 0, 20 and 100 of the second phase in the T-shaped mast optimization example with design of a truss-like initial guess considered in Section 7.4.2.

of the popular adjoint method from optimal control theory, our approximate sensitivities can be given a very convenient structure for numerical calculations. We have exemplified how this strategy may serve various purposes in the field of shape and topology optimization with three different applications: it supplies a complementary means to enrich the topology of a shape in the course of its optimization within the framework of Hadamard's method; it is also a natural ingredient in the optimization of

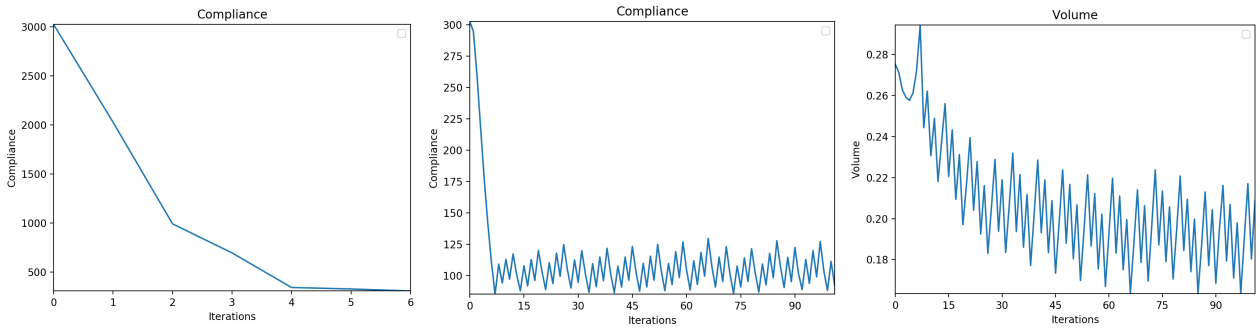

FIGURE 7.20. (Left) Evolution of the compliance in the course of the first stage; (middle) evolution of the compliance during the second step; (right) evolution of the volume during the second step in the mast optimization example of Section 7.4.2.

the support structure of a shape constructed by additive manufacturing, or in the optimization of truss-like structures.

The present work opens the way to various perspectives, at first regarding the mathematical analysis. One first lead for future work arises from the observations made in Section 7.1: it is natural to wonder in which capacity our asymptotic analyses can be made uniform with respect to the contrast between the material properties outside and inside the vanishing ligament $\omega_{\sigma,\varepsilon}$ (γ_0 and γ_1, A_0 and A_1 in the conductivity and elasticity settings, respectively). This is interesting for our applications, where these asymptotic formulas are used with "very soft" background properties γ_0 or A_0. This may also help to make the connection between our formal topological ligament approach and the rigorous expansions derived in [87, 88, 89]. In this direction, let us mention that, in the conductivity setting, such asymptotic expansions of the potential u_ε which are uniform with respect to this contrast have been derived in [91] in the context of diametrically small inclusions and in [46, 47, 54] in the context of thin inhomogeneities.

On a different note, it would be interesting to conduct the investigations of this article in other physical contexts, and notably that of fluid mechanics, as described by, e.g., the Stokes equations. We expect that our formal energy argument would have to be adapted in a non trivial way to handle such situations, where the physical partial differential equations at stake are no longer elliptic.

As far as applications are concerned, besides those described in Sections 7.2 to 7.4, we believe that the approximate sensitivity formulas considered in this article could be adapted to deal with a wide variety of tasks, such as the following ones:

- Besides its mathematical interest, the extension of the present work to the context of fluid mechanics would allow to optimize the outline of the cooling channels conveying the refrigerating liquid within molds; indeed, these intrinsically take the form of tubes, although their base curve may not be a straight segment; see for instance [106] and the references therein for more details about this problem.

- The techniques developed in this article naturally allow to address another requirement imposed on a shape Ω constructed by means of a powder-based additive manufacturing process, such as Electron Beam Melting (EBM) or Selective Laser Sintering (SLS): the powder used for construction has to be removed at the end of the process, lest that it cause unnecessary material loss and potential health hazard. Much of the effort in this direction has been directed towards designing structures Ω which are free from internal voids. As such, the article [80] introduces the so-called "virtual temperature method" to enforce the simple connectedness of the optimized design. In a different spirit, and following [104], our asymptotic formulas could

help in identifying one channel connecting an internal void of a structure Ω to its outer surface, which can be pierced as a post-processing of the construction stage and which is "optimal" in the sense that it degrades as little as possible the mechanical performance of Ω.

- Still about applications related to powder-based additive manufacturing, the techniques introduced in this article could be used to optimize the path of the laser in charge of fusing the processed metallic powder, in order to e.g. evacuate heat as fast as possible; we refer to [37] for further details about this question, where a totally different method is used.

- The thin tubular inhomogeneities considered in this article find another interesting application in the optimization of cylindrical geometries in 3d, that is, structures that are described by a midsurface $\mathcal{S}$ and with given thickness function in the normal direction. Such structures are ubiquitous in nature, since they encompass elastic plates or shells (see e.g. [98]) or, for instance, micro-chip devices such as those used in nanophotonics (see e.g. [79] and the references therein). The optimization of such devices is often carried out as a 2d optimization on the midsurface, and so the calculation of topological derivatives in the 2d midsurface boils down to a topological ligament asymptotic expansion for the underlying, three-dimensional partial differential equation.

- Beyond the work of this article, and quite in the same spirit, it would be interesting to use "thin" inhomogeneities (that is, sets which shrink to a hypersurface in $\mathbb{R}^d$, as in eq. (1.14)) to add "walls" of material to a three-dimensional shape.

Let us finally highlight a few potential algorithmic improvements of the methods presented in this article:

- One obvious improvement direction of the proposed method, which is crucial for realistic applications, is the device of a procedure for locating the "optimal" bar to be inserted, which does not incur an exhaustive search as in Algorithm 2. We believe that gradient methods based on the minimization of the expansion $\sigma \mapsto C_\sigma(0) + \varepsilon^{d-1} C'_\sigma(0)$ with respect to the endpoints of σ, however cheap, would be prone to end up in local minima with poor structural performance. One interesting alternative might be to use stochastic optimization algorithms.

- Although the approximate sensitivities derived in this article account for the addition of not only bars, but also curved ligaments to shapes, the optimization of such geometric entities is certainly a more challenging algorithmic topic.

Acknowledgements

This work was partly supported by the project ANR-18-CE40-0013 SHAPO, financed by the French Agence Nationale de la Recherche (ANR). The author is very grateful to G. Allaire for the multiple discussions related to possible implementations of topological ligaments which initially motivated this work. This article has also benefitted from the essential advice (and encouragements!) of E. Oudet, Y. Privat, N. Lebbe, M. Albertelli and G. Michailidis. The author is finally thankful to A. Froelhy for her constant help in the development of the `mmg` remeshing library. Finally, special thanks are in order for the two anonymous referees, whose careful reading and judicious suggestions have greatly contributed to improve the quality of the manuscript.

Appendix A. The coarea formula

For the reader's convenience, we recall the following avatar of the coarea formula (a curved version of the Fubini theorem), which is used in several different contexts in the present article; see [48]:

Lemma A.1. *Let X, Y be two smooth Riemannian manifolds with respective dimensions $m \geq n$, and $f : X \to Y$ be a surjective mapping of class $\mathcal{C}^1$, whose differential $d_x f : T_x X \to T_{f(x)} Y$ is surjective for almost every $x \in X$. Then, for any function $\varphi \in L^1(X)$, it holds:*

$$\int_X \varphi(x) \mathrm{d}x = \int_Y \left(\int_{z \in f^{-1}(y)} \varphi(z) \frac{1}{\mathrm{Jac}(f)(z)} \, \mathrm{d}z \right) \mathrm{d}y,$$

where the Jacobian $\mathrm{Jac}(f)$ *is defined by* $\mathrm{Jac}(f)(x) := \sqrt{\det(\nabla f(x) \, \nabla f(x))^T}$.

Appendix B. Technical results

The following lemma gathers convergence results of the solution u_ε to the perturbed conductivity equation eq. (2.4) to the background potential u_0 in eq. (2.2); we handle both cases $d = 2, 3$ at the same time.

Lemma B.1. *Let $\sigma \Subset D$ be a (open or close) smooth curve which is not self-intersecting; let u_ε be the perturbed potential in eq.* (2.4)*, and u_0 be the solution to the background equation eq.* (2.2)*. Then, for $\varepsilon > 0$ small enough,*

(i) *There exists a constant $C > 0$, depending only on u_0, such that $\|u_\varepsilon - u_0\|_{H^1(D)} \leq C \varepsilon^{\frac{d-1}{2}}$.*

(ii) *For any exponent $1 \leq p < 2$, there exists $C > 0$ depending on u_0 and p only such that:*

$$\left\| \frac{u_\varepsilon - u_0}{\varepsilon^{d-1}} \right\|_{L^p(D)} \leq C,$$

where the constant $C > 0$ is independent of ε.

(iii) *The sequence of functions $\frac{1}{\varepsilon^{d-1}}(u_\varepsilon - u_0)$ is uniformly integrable, i.e. for any real number $\eta > 0$, there exists $\delta > 0$ such that:*

$$\text{For all Borel subset } E \subset D \text{ with } |E| < \delta, \text{ for all } \varepsilon > 0, \quad \int_E \left| \frac{u_\varepsilon - u_0}{\varepsilon^{d-1}} \right| \mathrm{d}x < \eta.$$

Proof. Proof of (i). The difference $r_\varepsilon := u_\varepsilon - u_0$ is the unique solution in $H^1_{\Gamma_D}(D)$ to the variational problem:

$$\forall v \in H^1_{\Gamma_D}(D), \quad \int_D \gamma_\varepsilon \nabla r_\varepsilon \cdot \nabla v \, \mathrm{d}x = - \int_{\omega_{\sigma,\varepsilon}} (\gamma_1 - \gamma_0) \nabla u_0 \cdot \nabla v \, \mathrm{d}x.$$

Hence, taking $v = r_\varepsilon$ as a test function and using the Cauchy–Schwarz inequality, we obtain:

$$\|\nabla r_\varepsilon\|_{L^2(D)^d} \leq C \left(\int_{\omega_{\sigma,\varepsilon}} |\nabla u_0|^2 \, \mathrm{d}x \right)^{\frac{1}{2}},$$

and the result follows from the Poincaré inequality and the smoothness of u_0 on a neighborhood of $\omega_{\sigma,\varepsilon}$ (see again [38, 66]).

Proof of (ii). This is a variation of the classical Aubin–Nitsche duality argument; see [28, 92] for the original references, and [49] in the context of the finite element method.

At first, the remainder $s_\varepsilon := \frac{u_\varepsilon - u_0}{\varepsilon^{d-1}}$ is the unique solution in $H^1_{\Gamma_D}(D)$ to the variational problem:

$$\forall v \in H^1_{\Gamma_D}(D), \quad \int_D \gamma_\varepsilon \nabla s_\varepsilon \cdot \nabla v \, \mathrm{d}x = - \frac{1}{\varepsilon^{d-1}} \int_{\omega_{\sigma,\varepsilon}} (\gamma_1 - \gamma_0) \nabla u_0 \cdot \nabla v \, \mathrm{d}x.$$

The conclusion of (i) immediately implies that:

$$\|\nabla s_\varepsilon\|_{L^2(D)^d} \leq C\varepsilon^{-\frac{d-1}{2}}. \tag{B.1}$$

Let now $q > 2$ be defined by the relation $\frac{1}{p} + \frac{1}{q} = 1$ and $z \in L^q(D)$ be arbitrary; we introduce the unique solution $v_0 \in H^1_{\Gamma_D}(D)$ to the problem:

$$\forall v \in H^1_{\Gamma_D}(D), \quad \int_D \gamma_0 \nabla v_0 \cdot \nabla v \,\mathrm{d}x = \int_D zv \,\mathrm{d}x. \tag{B.2}$$

Classical interior elliptic regularity theory implies that there exists an open subset $\mathcal{V} \Subset D$ containing $\omega_{\sigma,\varepsilon}$ for ε small enough, as well as a constant $C > 0$ such that $v_0 \in W^{2,q}(\mathcal{V})$ and:

$$\|v_0\|_{H^1(D)} + \|v_0\|_{W^{2,q}(\mathcal{V})} \leq C\|z\|_{L^q(D)}. \tag{B.3}$$

A simple calculation then yields:

$$\begin{aligned}
\int_D zs_\varepsilon \,\mathrm{d}x &= \int_D \gamma_0 \nabla v_0 \cdot \nabla s_\varepsilon \,\mathrm{d}x \\
&= \int_D \gamma_\varepsilon \nabla v_0 \cdot \nabla s_\varepsilon \,\mathrm{d}x + \int_D (\gamma_0 - \gamma_\varepsilon)\nabla v_0 \cdot \nabla s_\varepsilon \,\mathrm{d}x \\
&= -\frac{1}{\varepsilon^{d-1}} \int_{\omega_{\sigma,\varepsilon}} (\gamma_1 - \gamma_0)\nabla v_0 \cdot \nabla u_0 \,\mathrm{d}x + \int_{\omega_{\sigma,\varepsilon}} (\gamma_0 - \gamma_1)\nabla v_0 \cdot \nabla s_\varepsilon \,\mathrm{d}x.
\end{aligned} \tag{B.4}$$

Now since $\|\nabla u_0\|_{L^\infty(\mathcal{V})} \leq C$ as a result of classical interior elliptic regularity, and $\|\nabla v_0\|_{L^\infty(\mathcal{V})^d} \leq C\|z\|_{L^q(D)}$ owing to eq. (B.3) and the Sobolev embedding theorem (see e.g. [1]), the first term in the above right-hand side is estimated by:

$$\left| \frac{1}{\varepsilon^{d-1}} \int_{\omega_{\sigma,\varepsilon}} (\gamma_1 - \gamma_0)\nabla v_0 \cdot \nabla u_0 \,\mathrm{d}x \right| \leq C\|\nabla u_0\|_{L^\infty(\mathcal{V})^d}\|\nabla v_0\|_{L^\infty(\mathcal{V})^d} \leq C\|z\|_{L^q(D)}. \tag{B.5}$$

As for the second term in the right-hand side of eq. (B.4), we obtain:

$$\begin{aligned}
\left| \int_{\omega_{\sigma,\varepsilon}} (\gamma_0 - \gamma_1)\nabla v_0 \cdot \nabla s_\varepsilon \,\mathrm{d}x \right| &\leq C\|\nabla v_0\|_{L^2(\omega_{\sigma,\varepsilon})^d}\|\nabla s_\varepsilon\|_{L^2(D)^d}, \\
&\leq C\varepsilon^{\frac{d-1}{2}}\|\nabla v_0\|_{L^\infty(\mathcal{V})^d}\varepsilon^{-\frac{d-1}{2}}, \\
&\leq C\|z\|_{L^q(D)},
\end{aligned} \tag{B.6}$$

where we have used eq. (B.1) to pass from the first line to the second one.
Eventually, combining eqs. (B.4) to (B.6), we obtain the desired result.

Proof of (iii). Let $\varepsilon > 0$ be given; we still use the notation $s_\varepsilon := \frac{u_\varepsilon - u_0}{\varepsilon^{d-1}}$. For an arbitrary Borel subset $E \subset D$, we define the function $z = \mathrm{sgn}(s_\varepsilon)\mathbb{1}_E \in L^\infty(D)$, where

$$\forall s \in \mathbb{R}, \quad \mathrm{sgn}(s) := \begin{cases} 1 & \text{if } s > 0, \\ 0 & \text{if } s = 0, \\ -1 & \text{if } s < 0. \end{cases}$$

Introducing the function $v_0 \in H^1_{\Gamma_D}(D)$ defined by eq. (B.2) and re-using eqs. (B.4) to (B.6), we obtain:

$$\int_E |s_\varepsilon| \,\mathrm{d}x = \int_D zs_\varepsilon \,\mathrm{d}x \leq C\|z\|_{L^q(D)} = C|E|^{\frac{1}{q}},$$

whence the desired uniform integrability follows immediately. ∎

References

[1] Robert A. Adams and John Fournier. *Sobolev spaces*, volume 140. Academic Press Inc., 2003.

[2] Grégoire Allaire. *Shape optimization by the homogenization method*, volume 146. Springer, 2002.

[3] Grégoire Allaire and Beniamin Bogosel. Optimizing supports for additive manufacturing. *Struct. Multidiscip. Optim.*, 58(6):2493–2515, 2018.

[4] Grégoire Allaire, Charles Dapogny, Rafael Estevez, Alexis Faure, and Georgios Michailidis. Structural optimization under overhang constraints imposed by additive manufacturing technologies. *J. Comput. Phys.*, 351:295–328, 2017.

[5] Grégoire Allaire, Charles Dapogny, Alexis Faure, and Georgios Michailidis. Shape optimization of a layer by layer mechanical constraint for additive manufacturing. *C. R. Math. Acad. Sci. Paris*, 355(6):699–717, 2017.

[6] Grégoire Allaire, Charles Dapogny, and Pascal Frey. Topology and geometry optimization of elastic structures by exact deformation of simplicial mesh. *C. R. Math. Acad. Sci. Paris*, 349(17-18):999–1003, 2011.

[7] Grégoire Allaire, Charles Dapogny, and Pascal Frey. Shape optimization with a level set based mesh evolution method. *Comput. Methods Appl. Mech. Eng.*, 282:22–53, 2014.

[8] Grégoire Allaire, Charles Dapogny, and François Jouve. Shape and topology optimization. In *Geometric partial differential equations, part II*, volume 22 of *Handbook of Numerical Analysis*, pages 1–132. Elsevier, 2021.

[9] Grégoire Allaire, Frédéric De Gournay, François Jouve, and Anca-Maria Toader. Structural optimization using topological and shape sensitivity via a level set method. *Control Cybern.*, 34(1):59, 2005.

[10] Grégoire Allaire and Lukas Jakabčin. Taking into account thermal residual stresses in topology optimization of structures built by additive manufacturing. *Math. Models Methods Appl. Sci.*, 28(12):2313–2366, 2018.

[11] Grégoire Allaire, François Jouve, and Anca-Maria Toader. Structural optimization using sensitivity analysis and a level-set method. *J. Comput. Phys.*, 194(1):363–393, 2004.

[12] Grégoire Allaire and Marc Schoenauer. *Conception optimale de structures*, volume 58. Springer, 2007.

[13] Luigi Ambrosio and Carlo Mantegazza. Curvature and distance function from a manifold. *J. Geom. Anal.*, 8(5):723–748, 1998.

[14] Luigi Ambrosio and H Mete Soner. Level set approach to mean curvature flow in arbitrary codimension. *J. Differ. Geom.*, 43:693–737, 1994.

[15] Oded Amir and Yoram Mass. Topology optimization for staged construction. *Struct. Multidiscip. Optim.*, 57(4):1679–1694, 2018.

[16] Habib Ammari, Elena Beretta, and Elisa Francini. Reconstruction of thin conductivity imperfections. *Appl. Anal.*, 83(1):63–76, 2004.

[17] Habib Ammari, Elena Beretta, and Elisa Francini. Reconstruction of thin conductivity imperfections, II. The case of multiple segments. *Appl. Anal.*, 85(1-3):87–105, 2006.

[18] Habib Ammari and Hyeonbae Kang. *Reconstruction of small inhomogeneities from boundary measurements*. Springer, 2004.

[19] Habib Ammari and Hyeonbae Kang. *Polarization and moment tensors: with applications to inverse problems and effective medium theory*, volume 162. Springer, 2007.

[20] Habib Ammari, Hyeonbae Kang, and Hyundae Lee. A boundary integral method for computing elastic moment tensors for ellipses and ellipsoids. *J. Comput. Math.*, pages 2–12, 2007.

[21] Habib Ammari, Hyeonbae Kang, Gen Nakamura, and Kazumi Tanuma. Complete asymptotic expansions of solutions of the system of elastostatics in the presence of an inclusion of small diameter and detection of an inclusion. *J. Elasticity*, 67(2):97–129, 2002.

[22] Habib Ammari, Shari Moskow, and Michael S. Vogelius. Boundary integral formulae for the reconstruction of electric and electromagnetic inhomogeneities of small volume. *ESAIM, Control Optim. Calc. Var.*, 9:49–66, 2003.

[23] Habib Ammari and Jin Keun Seo. An accurate formula for the reconstruction of conductivity inhomogeneities. *Adv. Appl. Math.*, 30(4):679–705, 2003.

[24] Habib Ammari, Michael S. Vogelius, and Darko Volkov. Asymptotic formulas for perturbations in the electromagnetic fields due to the presence of inhomogeneities of small diameter II. The full Maxwell equations. *J. Math. Pures Appl.*, 80(8):769–814, 2001.

[25] Samuel Amstutz. Sensitivity analysis with respect to a local perturbation of the material property. *Asymptotic Anal.*, 49(1-2):87–108, 2006.

[26] Samuel Amstutz and Heiko Andrä. A new algorithm for topology optimization using a level-set method. *J. Comput. Phys.*, 216(2):573–588, 2006.

[27] Samuel Amstutz, Charles Dapogny, and Àlex Ferrer. A consistent relaxation of optimal design problems for coupling shape and topological derivatives. *Numer. Math.*, pages 1–60, 2016.

[28] Jean Pierre Aubin. Behavior of the error of the approximate solutions of boundary value problems for linear elliptic operators by Galerkin's and finite difference methods. *Ann. Sc. Norm. Super. Pisa, Cl. Sci.*, 21(4):599–637, 1967.

[29] Martin P. Bendsøe, Aharon Ben-Tal, and Jochem Zowe. Optimization methods for truss geometry and topology design. *Structural optimization*, 7(3):141–159, 1994.

[30] Martin Philip Bendsoe and Ole Sigmund. *Topology optimization: theory, methods, and applications*. Springer, 2013.

[31] Elena Beretta, Eric Bonnetier, Elisa Francini, and Anna L. Mazzucato. Small volume asymptotics for anisotropic elastic inclusions. *Inverse Probl. Imaging*, 6(1):1–23, 2012.

[32] Elena Beretta, Yves Capdeboscq, Frédéric De Gournay, and Elisa Francini. Thin cylindrical conductivity inclusions in a three-dimensional domain: a polarization tensor and unique determination from boundary data. *Inverse Probl.*, 25(6):065004, 2009.

[33] Elena Beretta and Elisa Francini. An asymptotic formula for the displacement field in the presence of thin elastic inhomogeneities. *SIAM J. Math. Anal.*, 38(4):1249–1261, 2006.

[34] Elena Beretta, Elisa Francini, and Michael S. Vogelius. Asymptotic formulas for steady state voltage potentials in the presence of thin inhomogeneities. A rigorous error analysis. *J. Math. Pures Appl.*, 82(10):1277–1301, 2003.

[35] Elena Beretta, Arup Mukherjee, and Michael S. Vogelius. Asymptotic formulas for steady state voltage potentials in the presence of conductivity imperfections of small area. *Z. Angew. Math. Phys.*, 52(4):543–572, 2001.

[36] Vladimir I. Bogachev. *Measure theory*, volume 1. Springer, 2007.

[37] Mathilde Boissier, Grégoire Allaire, and Christophe Tournier. Scanning path optimization using shape optimization tools. to appear in *Structural and Multidisciplinary Optimization*; `https://hal.archives-ouvertes.fr/hal-0241048v1`, 2020.

[38] Haim Brezis. *Functional analysis, Sobolev spaces and partial differential equations*. Springer, 2010.

[39] Martin Brühl, Martin Hanke, and Michael S. Vogelius. A direct impedance tomography algorithm for locating small inhomogeneities. *Numer. Math.*, 93(4):635–654, 2003.

[40] Martin Burger, Benjamin Hackl, and Wolfgang Ring. Incorporating topological derivatives into level set methods. *J. Comput. Phys.*, 194(1):344–362, 2004.

[41] F. Calignano. Design optimization of supports for overhanging structures in aluminum and titanium alloys by selective laser melting. *Materials & Design*, 64:203–213, 2014.

[42] Piermarco Cannarsa and Pierre Cardaliaguet. Representation of equilibrium solutions to the table problem of growing sandpiles. *J. Eur. Math. Soc.*, 6(4):435–464, 2004.

[43] Yves Capdeboscq, Roland Griesmaier, and Marvin Knöller. An asymptotic representation formula for scattering by thin tubular structures and an application in inverse scattering. *Multiscale Model. Simul.*, 19(2):846–885, 2021.

[44] Yves Capdeboscq and Michael S. Vogelius. A general representation formula for boundary voltage perturbations caused by internal conductivity inhomogeneities of low volume fraction. *ESAIM, Math. Model. Numer. Anal.*, 37(1):159–173, 2003.

[45] Donna J. Cedio-Fengya, Shari Moskow, and Michael S. Vogelius. Identification of conductivity imperfections of small diameter by boundary measurements. Continuous dependence and computational reconstruction. *Inverse Probl.*, 14(3):553, 1998.

[46] Matthew Charnley and Michael S. Vogelius. A uniformly valid model for the limiting behaviour of voltage potentials in the presence of thin inhomogeneities I. The case of an open mid-curve. to appear in *Asymptotic Analysis*, 2019.

[47] Matthew Charnley and Michael S. Vogelius. A uniformly valid model for the limiting behaviour of voltage potentials in the presence of thin inhomogeneities II. A local energy approximation result. to appear in *Asymptotic Analysis*, 2019.

[48] Isaac Chavel. *Riemannian geometry: a modern introduction*, volume 98. Cambridge University Press, 2006.

[49] Philippe G. Ciarlet. *The finite element method for elliptic problems*, volume 40. Society for Industrial and Applied Mathematics, 2002.

[50] Marc Dambrine and Djalil Kateb. On the ersatz material approximation in level-set methods. *ESAIM, Control Optim. Calc. Var.*, 16(3):618–634, 2010.

[51] Charles Dapogny. A connection between topological ligaments in shape optimization and thin tubular inhomogeneities. `https://arxiv.org/abs/1912.11810`, 2019.

[52] Charles Dapogny, Cécile Dobrzynski, and Pascal Frey. Three-dimensional adaptive domain remeshing, implicit domain meshing, and applications to free and moving boundary problems. *J. Comput. Phys.*, 262:358–378, 2014.

[53] Charles Dapogny, Cécile Dobrzynski, Pascal Frey, and Algiane Froelhy. `mmg`, 2019. `https://www.mmgtools.org`.

[54] Charles Dapogny and Michael S. Vogelius. Uniform asymptotic expansion of the voltage potential in the presence of thin inhomogeneities with arbitrary conductivity. *Chin. Ann. Math., Ser. B*, 38(1):293–344, 2017.

[55] Michel C. Delfour and Jean-Paul Zolésio. *Shapes and geometries: metrics, analysis, differential calculus, and optimization*. Society for Industrial and Applied Mathematics, 2011.

[56] W. Dorn. Automatic design of optimal structures. *J. Méc., Paris*, 3:25–52, 1964.

[57] Jérémie Dumas, Jean Hergel, and Sylvain Lefebvre. Bridging the gap: automated steady scaffoldings for 3D printing. *ACM Trans. Graph.*, 33(4):1–10, 2014.

[58] Lawrence Craig Evans and Ronald F. Gariepy. *Measure theory and fine properties of functions*. CRC Press, 2015.

[59] Florian Feppon, Grégoire Allaire, Felipe Bordeu, Julien Cortial, and Charles Dapogny. Shape optimization of a coupled thermal fluid–structure problem in a level set mesh evolution framework. *SeMA J.*, pages 1–46, 2019.

[60] Florian Feppon, Grégoire Allaire, and Charles Dapogny. Null space gradient flows for constrained optimization with applications to shape optimization. submitted, `https://hal.archives-ouvertes.fr/hal-01972915/`, 2019.

[61] Florian Feppon, Grégoire Allaire, Charles Dapogny, and Pierre Jolivet. Topology optimization of thermal fluid–structure systems using body-fitted meshes and parallel computing. *J. Comput. Phys.*, page 109574, 2020.

[62] Gerald B. Folland. *Introduction to partial differential equations*. Princeton University Press, 1995.

[63] Avner Friedman and Michael S. Vogelius. Identification of small inhomogeneities of extreme conductivity by boundary measurements: a theorem on continuous dependence. *Arch. Ration. Mech. Anal.*, 105:299–326, 1989.

[64] Stéphane Garreau, Philippe Guillaume, and Mohamed Masmoudi. The topological asymptotic for PDE systems: the elasticity case. *SIAM J. Control Optimization*, 39(6):1756–1778, 2001.

[65] Ian Gibson, David W Rosen, Brent Stucker, et al. *Additive manufacturing technologies*, volume 17. Springer, 2014.

[66] David Gilbarg and Neil S. Trudinger. *Elliptic partial differential equations of second order*. Springer, 2015.

[67] Roland Griesmaier. Reconstruction of thin tubular inclusions in three-dimensional domains using electrical impedance tomography. *SIAM J. Imaging Sci.*, 3(3):340–362, 2010.

[68] Roland Griesmaier. A general perturbation formula for electromagnetic fields in presence of low volume scatterers. *ESAIM, Math. Model. Numer. Anal.*, 45(6):1193–1218, 2011.

[69] Xu Guo, Weisheng Zhang, and Wenliang Zhong. Doing topology optimization explicitly and geometrically–a new moving morphable components based framework. *J. Appl. Mech.*, 81(8), 2014.

[70] Wolfgang Hackbusch. *Integral equations: theory and numerical treatment*, volume 120. Birkhäuser, 2012.

[71] Frédéric Hecht. New development in FreeFem++. *J. Numer. Math.*, 20(3-4):251–266, 2012.

[72] Antoine Henrot and Michel Pierre. *Shape Variation and Optimization*, volume 28 of *EMS Tracts in Mathematics*. European Mathematical Society, 2018.

[73] Hesaneh Kazemi, Ashkan Vaziri, and Julián A Norato. Topology optimization of structures made of discrete geometric components with different materials. *Journal of Mechanical Design*, 140(11), 2018.

[74] Abdessatar Khelifi and Habib Zribi. Asymptotic expansions for the voltage potentials with two-dimensional and three-dimensional thin interfaces. *Math. Methods Appl. Sci.*, 34(18):2274–2290, 2011.

[75] Marcelo H. Kobayashi, Robert A. Canfield, and Raymond M. Kolonay. On a cellular developmental method for layout optimization via the two-point topological derivative. *Struct. Multidiscip. Optim.*, 64(4):2343–2360, 2021.

[76] Rainer Kress. Inverse scattering from an open arc. *Math. Methods Appl. Sci.*, 18(4):267–293, 1995.

[77] Rainer Kress. *Linear integral equations*, volume 82. Springer, 2012.

[78] Ohin Kwon, Jin Keun Seo, and Jeong-Rock Yoon. A real time algorithm for the location search of discontinuous conductivities with one measurement. *Commun. Pure Appl. Math.*, 55(1):1–29, 2002.

[79] Nicolas Lebbe, Charles Dapogny, Edouard Oudet, Karim Hassan, and Alain Gliere. Robust shape and topology optimization of nanophotonic devices using the level set method. *J. Comput. Phys.*, 395:710–746, 2019.

[80] Quhao Li, Wenjiong Chen, Shutian Liu, and Liyong Tong. Structural topology optimization considering connectivity constraint. *Struct. Multidiscip. Optim.*, 54(4):971–984, 2016.

[81] Jikai Liu, Andrew Gaynor, Shikui Chen, Zhan Kang, Krishnan Suresh, Akihiro Takezawa, Lei Li, Junji Kato, Jinyuan Tang, Charlie Wang, et al. Current and future trends in topology optimization for additive manufacturing. *Struct. Multidiscip. Optim.*, 57:2457–2483, 2018.

[82] Carlo Mantegazza and Andrea Carlo Mennucci. Hamilton-Jacobi Equations and Distance Functions on Riemannian Manifolds. *Appl. Math. Optim.*, 47(1), 2003.

[83] William Charles Hector McLean. *Strongly elliptic systems and boundary integral equations*. Cambridge University Press, 2000.

[84] Dorina Mitrea. *Distributions, partial differential equations, and harmonic analysis*. Springer, 2013.

[85] Dietrich Morgenstern and István Szabó. *Vorlesungen über theoretische Mechanik*, volume 112. Springer, 2013.

[86] F. Murat and J. Simon. Sur le contrôle par un domaine géométrique. Pré-publication du Laboratoire d'Analyse Numérique (76015), 1976.

[87] Serguei A. Nazarov, Andrey Slutskij, and Jan Sokołowski. Topological derivative of the energy functional due to formation of a thin ligament on a spatial body. *Folia Math.*, 12:39–72, 2005.

[88] Serguei A. Nazarov and Jan Sokołowski. The topological derivative of the Dirichlet integral due to formation of a thin ligament. *Sib. Math. J.*, 45(2):341–355, 2004.

[89] Serguei A. Nazarov and Jan Sokołowski. Self-adjoint extensions of differential operators and exterior topological derivatives in shape optimization. *Control Cybern.*, 34:903–925, 2005.

[90] Jean-Claude Nédélec. *Acoustic and electromagnetic equations: integral representations for harmonic problems*, volume 144. Springer, 2001.

[91] Hoai-Minh Nguyen and Michael S. Vogelius. A representation formula for the voltage perturbations caused by diametrically small conductivity inhomogeneities. Proof of uniform validity. *Ann. Inst. Henri Poincaré, Anal. Non Linéaire*, 26(6):2283–2315, 2009.

[92] Joachim Nitsche. Ein kriterium für die quasi-optimalität des ritzschen verfahrens. *Numer. Math.*, 11(4):346–348, 1968.

[93] Antonio André Novotny and Jan Sokołowski. *Topological derivatives in shape optimization*. Springer, 2012.

[94] Stanley Osher and James A Sethian. Fronts propagating with curvature-dependent speed: algorithms based on Hamilton-Jacobi formulations. *J. Comput. Phys.*, 79(1):12–49, 1988.

[95] Claus Pedersen and Peter Allinger. Industrial implementation and applications of topology optimization and future needs. In *IUTAM Symposium on Topological Design Optimization of Structures, Machines and Materials*, pages 229–238. Springer, 2006.

[96] Olivier Pironneau. *Optimal shape design for elliptic systems*. Springer, 1982.

[97] Lalaina Rakotondrainibe, Grégoire Allaire, and Patrick Orval. Topology optimization of connections in mechanical systems. *Struct. Multidiscip. Optim.*, pages 1–17, 2020.

[98] Junuthula Narasimha Reddy. *Theory and analysis of elastic plates and shells*. CRC Press, 2006.

[99] Ole Sigmund and Kurt Maute. Topology optimization approaches. *Struct. Multidiscip. Optim.*, 48(6):1031–1055, 2013.

[100] William S Slaughter. *The linearized theory of elasticity*. Springer, 2012.

[101] Jan Sokołowski and Antoni Zochowski. On the Topological Derivative in Shape Optimization. *SIAM J. Control Optimization*, 37(4):1251–1272, 1999.

[102] Jan Sokołowski and Jean-Paul Zolésio. *Introduction to shape optimization*. Springer, 1992.

[103] Michael Spivak. *A comprehensive introduction to differential geometry, Vol. 1, 2nd Edition*. Publish or Perish Inc., 1979.

[104] Daniel Stojanov, Xinhua Wu, Brian G. Falzon, and Wenyi Yan. Axisymmetric structural optimization design and void control for selective laser melting. *Struct. Multidiscip. Optim.*, 56(5):1027–1043, 2017.

[105] Michael Yu Wang, Xiaoming Wang, and Dongming Guo. A level set method for structural topology optimization. *Comput. Methods Appl. Mech. Eng.*, 192(1-2):227–246, 2003.

[106] Xi Zhao, Mingdong Zhou, Ole Sigmund, and Casper Schousboe Andreasen. A "poor man's approach" to topology optimization of cooling channels based on a Darcy flow model. *Int. J. Heat Mass Transfer*, 116:1108–1123, 2018.